ELSEVIER

Nanotribology: Microscopic mechanisms of friction

O.M. Braun*, A.G. Naumovets[1]

Institute of Physics, National Academy of Sciences of Ukraine, 03028 Kiev, Ukraine

Abstract

Friction is one of the oldest problems in physics with a huge practical significance. However, during the last decade this problem gets strong acceleration due to the development of new experimental techniques (surface-force apparatus, quartz-crystal microbalance technique, friction-force microscopy) and essentially due to the great progress in molecular dynamics (MD) simulation of tribological systems. In the present review we describe the modern state of the problem from the point of view of surface science physicists. The main accent is devoted to recent MD results in their connection with experiments.
© 2005 Elsevier B.V. All rights reserved.

Contents

* Corresponding author. Tel.: +380 44 5301850; fax: +380 44 5251589.
E-mail addresses: obraun@iop.kiev.ua (O.M. Braun), naumov@iop.kiev.ua (A.G. Naumovets).
[1] Tel.: +380 44 5250927; fax: +380 44 5251589.

1. Introduction

Tribology is the science of surfaces in relative motion. It is of great theoretical interest and huge practical significance.

First of all, one has to distinguish two physically different frictional phenomena: the static friction and the kinetic friction. The *static* frictional force f_s is defined as a minimal force needed to initiate sliding. Its value is determined by the atomic structure of the sliding interface and the adhesion interactions. To initiate the sliding, one has either to break interatomic bonds or to initiate a plastic flow at an interface, and it is clear that this process will occur first at some "weak" places.

The *kinetic* frictional force f_k is the force needed to keep two substrates sliding. Actually, the kinetic friction has to be considered as a mechanism to convert the energy of translational motion into heat. Therefore, the value of f_k is determined by the rate of excitation of various degrees of freedom of the system due to sliding; the energy of these excitations is eventually transformed into heat.

Both static and kinetic frictions are highly important in applications, and in different situations either a high or low value of friction is desired. Without static friction we would not be able to walk and cars to move. A high static friction is necessary to keep stable mechanical constructions connected by bolts and nuts. A low static friction is desired in moving parts of machines, e.g., car engines, and the zero value of f_s achievable with liquid lubricants would be the best solution. While the kinetic friction cannot be avoided, in most machines we prefer to have it as low as possible. Persson [1,2] presented the following impressive estimation: in the USA friction takes away 6% of the gross national product, that is >$700 billion per year. However, in some cases we need a high kinetic friction, e.g., between the road and the tyres when braking the car, or when lighting a fire by rubbing wood on wood as ancient people did (the latter is in fact an example of a tribochemical reaction).

It is not surprising that the main friction laws, the famous Amontons' laws (see below Section 2), belong to the oldest physical laws and are known already for more than three hundred years. However, a physical explanation of the empirical Amontons' laws was given by Bowder and Tabor [3] as late as the middle of the 20th century. A new era in tribology began at the end of the 20th century, when this science approached a microscopic and even atomic level in the study of the contacts themselves. This approach rapidly expanded due to the development of new experimental techniques such as the atomic-force microscope (AFM), the friction-force microscope (FFM), the surface-force apparatus (SFA), and the quartz-crystal microbalance (QCM) able to perform experiments on well-characterized model systems at the nanoscale. At the same time, the evolution of powerful computers allowed detailed simulations of friction processes on the atomic scale.

One should distinguish between two different regimes, the hydrodynamic (liquid) friction and the boundary lubrication. In the former case, the substrates are separated by a thick (e.g., $\gtrsim 0.01$ mm) liquid lubricant film. The physical problem in this case reduces to solution of the Navier–Stokes equation of hydrodynamics with appropriate boundary conditions and geometry of the contact, and the kinetic friction is determined mainly by the viscosity of the liquid lubricant (Reynolds, 1886). In the present article we discuss only the case of boundary lubrication, when the substrates are separated by a thin (a few atomic diameters) lubricant film. The case of "dry friction" also belongs to this class. The boundary lubrication is obviously the most important in micromachines. However, even in the macromachines where the hydrodynamic friction operates typically, the boundary lubrication is also important at stop/start moments, when the lubricant is squeezed out from the contact area and the surfaces come into direct contact.

Because tribology is an extremely important branch of material science, at least several review papers are published every year. We mention only some of them, such as Refs. [1,2,4–13], but this list is far from a complete one. Some of the works are devoted mainly to tribological experiments [3–6,9,11–13], others are more concentrated on theoretical or simulation aspects of the problem [1,2,7,8,10]. In any case we cannot claim to present a whole picture of the problem. Our goal in this work is to give sight into the problem from physicists working in surface science and, moreover, mainly on theoretical approaches based on molecular dynamics (MD) simulations and using simple physical models. In the present work we discuss and try to answer the following questions:

- How to model friction and why should we use Langevin equations for this aim?
- How does the frictional force depend on system parameters, in particular,
  - on the interaction between the atoms or molecules, the external damping in Langevin equations;
  - on the geometry of the contact, the lubricant thickness and its structure,
  - on temperature?
- Where do the energy losses occur and what is the mechanism of the losses?
- When could one expect a minimal friction?
- How does the kinetic frictional force depend on the sliding velocity, in particular, what is a minimally possible velocity for smooth sliding?
- What is the mechanism of stick–slip motion and of the transition to smooth sliding?
- Which common features exist between the behavior of lubricating films and surface diffusion mechanisms?
- Which knowledge from surface phase transitions and surface nonequilibrium self-organization can be used to understand friction processes?

One of the main aims of this review is to emphasize the existence of many far-reaching analogies between phenomena in the lubricant films and in the diffusing or drifting adsorbed layers. Actually it is not surprising, because the case of boundary friction involves two interfaces separated by an oligolayer lubricant film. In modern terms, this system represents a kind of quantum well which is operating in strongly nonequilibrium conditions.

The paper is organized as follows. We begin Section 2 with brief discussion of basic experimental techniques used in tribological studies and a summary of well-established facts and laws. Then we also describe qualitative theories of friction such as the Bowden and Tabor theory (Section 2.2) and the phenomenological theory of the transition from stick–slip motion to smooth sliding (Section 2.3). A short Section 2.4 is devoted to low-dimensional models such as the Tomlinson model, the Frenkel–Kontorova model and their combinations. These simplified models allow a qualitative explanation of many tribological phenomena, at the same time being analytically tractable. Then in Section 3 we present in a brief form some useful information from surface physics to demonstrate similarities of adsorbed and lubricant films. In particular, we describe different mechanisms of interaction between adsorbed particles and crystalline structures of adlayers. Special attention is given to collective mechanisms of surface diffusion. Section 4 summarizes theoretical results on static friction, while Section 5 is devoted to problems of kinetic friction. The latter consists of several subsections. First, in Section 5.1 we give a rather detailed description of the model used in MD simulations of friction. Melting of a thin confined film is described in Section 5.2. The simulation shows that the friction mechanisms are determined mainly by an interplay of the substrate–lubricant and lubricant–lubricant interactions. When the substrate–lubricant interaction is stronger than the lubricant–lubricant one, the lubricant film melts during sliding. This case (termed below as the "soft" lubricant) is described in Section 5.3. An opposite case of the "hard" lubricant, which may lead to the smallest friction coefficients (the so-called "perfect sliding"), is discussed in Section 5.4. The mechanism of self-ordering of the lubricant film, which provides its "self-organization" and minimizes the friction, is discussed in Section 5.5. Finally, in Section 5.6 we present a possible phenomenological approach which explains analytically the simulation data. Section 6 is devoted to the important problem of stick–slip motion and the transition to smooth sliding. We discuss both the microscopic mechanism of smooth sliding (i.e., the problem of the minimal velocity when the sliding remains smooth, see Section 6.1) and the macroscopic mechanism of smooth sliding, which is explained with the help of the earthquakelike model (Section 6.2). The last Section 7 concludes the paper with the summary of known results and discussion of the most important questions, from our point of view, which still remain unsolved.

2. Basic experimental techniques, tribological facts and laws

2.1. Techniques and major observations

Let us first briefly describe typical experimental techniques used in tribology. A standard experimental setup to study macroscopic friction is shown schematically in Fig. 1 (see [3,14], and also more recent experiments with paper on paper due to Heslot et al. [15]). The control parameters in the experiments are the pulling velocity v_{spring}, the machine stiffness k_{spring}, the loading force F_{load}, and the temperature T. In most tribological experiments the only measured parameter is the spring force $F_{spring} = F_{friction}$, and this is a serious problem, because it is not simple to extract much information on the physics of system
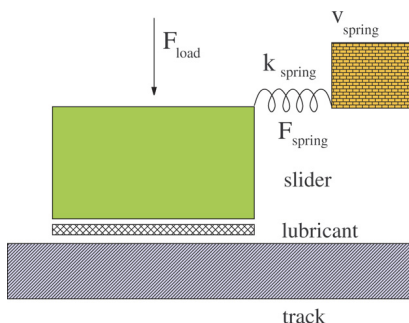
Fig. 1. A standard experimental setup for tribology studies. A top solid substrate (slider) is put on the bottom substrate (track). The slider and track may be separated by a thin lubricant film and compressed together by a loading force F_{load} (e.g., due to the mass M of the top block, $F_{\text{load}} = Mg$, where g is the earth acceleration). The slider is connected with the base moving with a constant velocity v_{spring} through a spring of the elastic constant k_{spring} (in a real system, the role of the spring may be played by the elasticity of the top block itself). The output (measured) parameter is the spring force F_{spring}.

behavior from a single measured characteristic. Then the "tribological" friction coefficient is defined as

$$\mu \equiv F_{\text{friction}}/F_{\text{load}}. \tag{1}$$

A more precise technique, known as the surface-force apparatus (SFA), was developed by Israelachvili and coworkers [16,17]. In this technique the solids can have a well defined structure as, e.g., in the case of atomically flat mica plates glued to two crossed cylinders. The separation between the surfaces may be controlled with the help of optical interferometry by studying multiple beam interference fringes, so that an accuracy to within ~1 Å may be achieved [17,18,4]. The SFA technique was modified for rheological experiments by Granick and coworkers [19–21] [in rheological experiments an ac ("alternating current", i.e. oscillating) force is applied to the slider, in contrast to the dc ("direct current", i.e. constant valued) force in tribological experiments].

The quartz-crystal microbalance (QCM) technique was developed by Widom and Krim [22–24]. In this case gas atoms, such as Kr, Xe, or Ar, are condensed onto the surface of a quartz-crystal oscillator covered by, e.g., a (111) oriented noble-metal film such as Au or Ag. The added mass of the adsorbate and the dissipation due to *slip* of the layer over the substrate shift and broaden the microbalance resonance peak. By measuring these changes, information about the magnitude of the friction force can be obtained. Such experiments can be done in ultrahigh vacuum. However, this technique allows one to measure not the friction between two solids, but that between a solid and a film one or two monolayers thick.

Finally, an outstanding role belongs to techniques that use the tip-based scanning microscopies: the scanning tunnelling microscope (STM, Binnig et al. [25]) useable for conducting surfaces and the atomic-force microscope (AFM, Binnig et al. [26]) useable for dielectric surfaces — both measure surface topography, and the friction-force microscope (FFM, Mate et al. [27,5]) which measures forces transverse to the surface. Application of the FFM technique to tribology studies may be found, e.g., in Refs. [6,9]. We only mention its main characteristics: the experiments can be done in ultrahigh vacuum; a typical tip radius is 10–100 nm; typical load forces F_{load} are of order 10–150 nN; typical measured friction forces are $F \lesssim 10^{-11}$ N; and available sliding velocities are typically quite low, $v \sim 1$ nm/s to 1 μm/s. Therefore, the FFM technique mainly gives information on the static friction between the tip and surface, i.e., the friction for a single asperity. An important aspect of these experiments is that while

the whole tip has a macroscopic-scale size (e.g., 1 mm), the contact area is very small, and is comprised of one or a few atoms only. Special care must also be taken to determine the real contact area [28,29]. Moreover, in analyzing experimental dependences the mechanical characteristics of the device such as the tip mass and its stiffness should properly be taken into account [30].

Now let us describe the tribological laws and properties that are already well established experimentally. First of all, two famous Amontons' laws dating to 1699 state:

The first Amontons law: The frictional force is directly proportional to the load. This law is also known as the Coulomb friction law.

The second Amontons law: The tribological friction coefficient (1) is independent of the contact area and the loading force, i.e. μ is approximately a constant $\lesssim 1$.

A qualitative explanation of these laws was given by Bowden and Tabor (see Section 2.2). It should be emphasized that both laws work for static as well as kinetic friction, although the static coefficient μ_s and the kinetic coefficient μ_k are determined by different mechanisms. The following results are also well established for the solid-on-solid friction:

1. *Kinetic versus static friction.* In most cases μ_k is less or much less than μ_s, and the kinetic friction μ_k is approximately independent of the driving velocity v. The inequality $\mu_k < \mu_s$ naturally leads to a stick–slip motion at low velocities (see below Section 2.3).
2. *Forces.* The forces in the contacts are of atomic-scale values — close to the plasticity threshold. The forces can be estimated as follows. A typical force per atom is $f \sim 1$ eV/1 Å $= 10^{-19}$ J/10^{-10} m $= 10^{-9}$ N. In the case of STM–AFM–FFM devices, where the area of one contact is $A \sim 5$ Å^2, taking for the plasticity threshold $P_{\text{yield}} \approx 0.2$ GPa (gold) to $P_{\text{yield}} \approx 100$ GPa (diamond), we obtain $F \sim P_{\text{yield}} A \sim 10^{-11}$ N to 5×10^{-9} N. Note also that the hardness of the contacts is typically much larger than that of the material itself, because there are no dislocations in the (very small) stressed volume; therefore, a deformation (either elastic or plastic) always occurs at the contacts. Namely this fact is used to explain the Amontons laws (see Section 2.2).
3. *Contacts, junctions, asperities.* The area of a real atomic contact A_{real} between two solids is very small in comparison with the geometrical (visible) area A_{visible}. The contacts are randomly distributed in space over the area of apparent contact, and their typical sizes are 1–10 μm (these results follow from optical experiments). Persson [1,2] has given the following estimation: for a steel cube of $10 \times 10 \times 10$ cm^3 put on a steel table, taking $P_{\text{load}}^{(\text{real})} \sim P_{\text{yield}} \approx 10^9$ Pa (the penetration hardness of steel), from the relation $F_{\text{load}} = Mg = P_{\text{load}}^{(\text{real})} A_{\text{real}}$, where M is the block mass and g is the earth acceleration, we obtain $A_{\text{real}} \sim 0.1$ mm^2. Thus, $A_{\text{real}}/A_{\text{visible}}$ is $\sim 10^{-5}$, and $\sim 10^3$–10^5 junctions are expected at the interface.
4. *Memory (age) effects.* Numerous experiments show that in fact the frictional forces are not constant but slowly change depending on the previous dynamical history of the solid–solid contacts, e.g., $\mu_s(t) \approx a_s + b_s \ln(t)$ and $\mu_k(v) \approx \mu_s(a_\phi/v)$ with a characteristic length $a_\phi \sim 1$ μm. This effect can be explained by thermally activated plasticity of the system [1,2,31,32].
5. *Stick–slip motion and smooth sliding.* If the static frictional force is nonzero and the system dynamics exhibits hysteresis, its motion can proceed via the stick–slip mechanism. The stick–slip motion is observed for soft systems and/or low velocities, while the smooth sliding, for stiff machines and/or high velocities. A phenomenological theory of this effect is given below in Section 2.3, while a more detailed discussion is presented in Section 6.

For the boundary lubrication, when the surfaces are separated by a thin lubricant film a few nm wide, the friction measured experimentally is typically much higher, e.g., by a factor of 10^2 or even 10^5–10^7, comparing with the hydrodynamic lubrication. It depends mainly not on lubricant viscosity but on the chemical composition of the lubricant. Usually a good lubricant is a substance that is adsorbed by the solid substrates, because this prevents the squeezing of the lubricant from the contact area. The following well established facts should be mentioned in this context:

- Almost always there is a *lubricant* between the solids (called "*the third bodies*" by tribologists) — either a specially chosen lubricant film, or a grease (oil), or dust, or wear debris produced by sliding, or water or/and a thin layer of hydrocarbons, etc. adsorbed from air. Thus, the frictional force is almost entirely determined by the force required to shear the lubricant film itself.
- The lubricant and the solids are almost always "*incommensurate*", because their lattice constants do not coincide in a general case, and/or the direction of sliding is generally at some angle to the surface lattice, so that the two surface lattices are not generally in registry. However, the situation is not so simple. Most often are used the lubricants whose molecules are "glued" ("grafted") to the substrates, because this helps to avoid the squeezing of the lubricant out from the contact region. As a result, we may actually have the sliding interface between the "glued" lubricant layer and other lubricant layers, which may appear commensurate.
- A thin film (e.g., less than 10 molecules wide) is always *layered*, i.e., the substrate surfaces induce some ordering in the film [33–39,18,40–42]. Moreover, when the width is less than 3 to 5 layers, most films behave like a solid. This effect is known as *solidification*, or *freezing* of the lubricant [18,43, 44]); see also [4,7] and references therein).
- Finally, large-scale MD simulations show that the lubricant structure may be either *liquid* (with low kinetic friction and $f_s = 0$), or *amorphous* (with high friction), or *crystalline* (with very low kinetic friction).

2.2. Bowden and Tabor theory

An explanation of the Amontons law that μ is a constant $\lesssim 1$, was first given by Bowden and Tabor [3]. It is based on the assumption that the surfaces in contact are rough, therefore the real (actual) contact area is very small and proportional to the load, $A_{\text{real}} \propto F_{\text{load}}$. The area A_{real} should grow until the external loading force will be balanced by the counteracting contact pressure integrated over A_{real}. Namely, let $P_{\text{load}}^{(\text{real})} = P_{\text{load}} A / A_{\text{real}}$ be the real pressure at the contact. Then at low loading pressure, $P_{\text{load}}^{(\text{real})} < P_{\text{yield}}$, when the substrates are in the elastic regime, the area of each contact is approximately constant, while the number of contacts increases with load. At the high load, $P_{\text{load}}^{(\text{real})} > P_{\text{yield}}$ (i.e., in the plastic regime), the area of one contact should increase linearly with the load because of its plastic deformation. In this way we obtain that $\mu \sim F_{\text{yield}}^{(\text{shear})} / F_{\text{yield}}^{(\text{plastic})}$ so that $\mu \sim 1$ and is independent of the surface area.

More rigorously, let us assume that the yield stress τ_s at the contact is linearly coupled with the *local* pressure p,

$$\tau_s(p) = \tau_0 + \alpha p, \tag{2}$$

where τ_0 is the yield stress at zero external pressure. Then, integrating over the area of real contact, we obtain

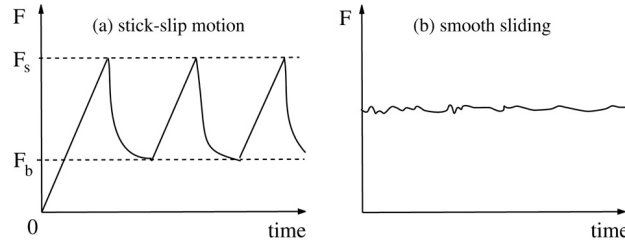$$F_{\text{friction}} = \tau_0 A_{\text{real}} + \alpha P_{\text{load}} \tag{3}$$

Fig. 2. Friction force as a function of time in the stick–slip (a) and smooth sliding (b) regimes (schematically).

and

$$\mu = \alpha + \tau_0/\langle p \rangle, \tag{4}$$

where $\langle p \rangle = F_{\text{load}}/A_{\text{real}}$. Thus, the Amontons law operates when either $\langle p \rangle \gg \tau_0$, or $\langle p \rangle$ is constant, the latter holds both for plastic and elastic surfaces. In the case of the ideally plastic surfaces $\langle p \rangle$ is constant, $\langle p \rangle = P_{\text{yield}}$. For the elastic surfaces the real surfaces are self-affine fractals (see [45] for details). Therefore, when P_{load} increases, the old contacts are expanding and new contacts are created, that leads to $\langle p \rangle \approx$ const too [46,45]. Finally, when the real area of contact becomes equal to the apparent area, the Amontons law does not operate anymore. However, this regime may be achieved for rubber but not for steel — a machine will be destroyed earlier.

2.3. Stick–slip and smooth sliding: Phenomenology

In a typical tribological experiment a spring is attached to the slider, and its end is connected to a base moving with a constant velocity v_{spring} as shown in Fig. 1. The same is true for real machines, where the elasticity of the moving parts plays the same role. Let us assume that initially the system is in rest and the spring has its natural length. When the base begins to move, the spring stretches, F increases until it reaches the threshold value F_s corresponding to the static frictional force, and the block starts to move. Then due to inertia, the slider accelerates to catch the base. If v_{spring} is small, F decreases down to the "backward" threshold force F_b, and the slider stops. Then the process repeats, so the stick–slip motion occurs as shown in Fig. 2(a); otherwise, when v_{spring} is large, smooth sliding takes place as in Fig. 2(b).

Numerous experiments agree that the behavior depends on the values v_{spring} and k_{spring}: the smooth sliding is observed if the spring is stiff and/or the velocity is high; otherwise, the stick–slip motion is observed (see Fig. 3, left panel). During stick, the elastic energy is pumped into the system by the driving; during slip, this elastic energy is released into kinetic energy, which eventually must be dissipated as heat.

If the frictional force is dependent on the instantaneous velocity only, $F_{\text{fric}} = f(v)$, then the boundary separating two regimes would correspond to the vertical line on the $(v_{\text{spring}}, k_{\text{spring}})$ plane (i.e., the critical velocity is independent of k_{spring}) [1,2], which contradicts the experiments. Thus, "memory" effects must be incorporated to explain this behavior.

A phenomenological theory of the transition from stick–slip motion to smooth sliding has been developed by Heslot et al. [15], Baumbergeret al. [47,48], and Persson [31,49]. The model is based on the assumption that the static frictional force depends on the time of stationary contact. For example, if the sliding-to-locked transition occurred at $t = 0$, then the static frictional force should grow as

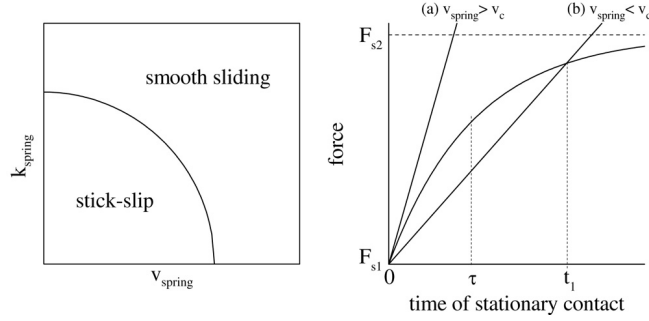$$F_s(t) = F_{s1} + (F_{s2} - F_{s1})(1 - e^{-t/\tau}), \tag{5}$$

Fig. 3. Left panel: phase diagram on the $(v_{\text{spring}}, k_{\text{spring}})$ plane showing regions with stick–slip and smooth sliding regimes. Right panel: growing of f_s with the time of stationary contact and increasing of the spring constant $f = k_{\text{spring}} v_{\text{spring}} t$ at high (a) and low (b) driving velocities.

so that just after the locking the force is $F_s(0) = F_{s1}$, but later, at $t \to \infty$, it approaches the value $F_s(\infty) = F_{s2} > F_{s1}$.

Following Persson [1,2,31], let us draw in Fig. 3 the dependence (5) and the spring force $F_{\text{spring}}(t) = k_{\text{spring}} v_{\text{spring}} t$ as functions of the contact time for two different driving velocities. In case (a) the spring force increases faster with t than the initial linear increase of the static frictional force; hence the motion of the slider will not stop and no stick–slip motion will occur. In case (b) the spring force will be smaller than the static frictional force until t reaches the value t_1 at which time slip starts, hence stick–slip motion will occur. Thus, the critical velocity is determined by the initial slope of the dependence (5), $v_c \sim k_{\text{spring}}^{-1} \mathrm{d} F_s(t)/\mathrm{d} t|_{t=0}$.

The phenomenological model, in its simplest version, includes two differential equations. The motion of the sliding block is described by the equation

$$M \ddot{x}(t) + M \eta \dot{x}(t) + F_{\text{fric}}[x(t)] = F_{\text{drive}}[x(t)] = k_{\text{spring}}[v_{\text{spring}} t - x(t)], \tag{6}$$

where $x(t)$ is the coordinate of the sliding block, M is its mass, and η is a phenomenological coefficient describing the viscous damping when the block slides over the bottom block. The second equation has to describe the frictional force $F_{\text{fric}}[x(t)]$. The idea is to introduce some artificial variable called the "*contact-age function*" $\phi(t)$ which depends on the *prehistory* of the system, and is defined by the following differential equation,

$$\dot{\phi}(t) = 1 - \dot{x}(t)\phi(t)/a_\phi, \tag{7}$$

where a_ϕ is some characteristic distance of microscopic-scale order, e.g., the substrate lattice constant a. Then one assumes that $F_{\text{fric}}[x(t)]$ in Eq. (6) is determined by Eq. (5) where, however, one has to substitute the contact-age function ϕ instead of time, the backward force F_b instead of F_{s1}, and the static frictional force F_s instead of F_{s2}, so that

$$F_{\text{fric}}[x(t)] = F_b + (F_s - F_b)\left(1 - \exp\{-\phi[x(t)]/\tau\}\right). \tag{8}$$

Thus, for the stationary contact, $\dot{x}(t) = 0$, we have $\phi(t) = t$ and recover the dependence (5). On the other hand, for the steady sliding regime the contact-age function $\phi = a_\phi/v_{\text{spring}} \equiv \tau_v(v_{\text{spring}})$ does not depend on time (here τ_v is the average time a junction survives before being broken by the sliding motion). The force $F_{\text{fric}}(v) = F_b + (F_s - F_b)\left[1 - \exp(-a_\phi/v_{\text{spring}}\tau)\right]$ is constant, but its value depends

on v_{spring}. The friction force is large at low velocities, $F_{\text{fric}} = F_s$ for $v_{\text{spring}} \to 0$, and it is small at high velocities, $F_{\text{fric}} = F_b$ for $v_{\text{spring}} \to \infty$.

The set of equations (6)–(8) leads to smooth sliding at large v_{spring} and to stick–slip motion at low velocities. The boundary curve in the (v_{spring}, k_{spring}) phase diagram separating the steady smooth sliding from the stick–slip motion, can be found by linear stability analysis [49] by substituting

$$x(t) = v_{\text{spring}}t - \left[F_{\text{fric}}(v_{\text{spring}}) + M\eta v_{\text{spring}} \right]/k_{\text{spring}} + \Delta x \, e^{\kappa t}$$

and $\phi(t) = \tau_v(v_{\text{spring}}) + \Delta\phi \, e^{\kappa t}$ into Eqs. (6)–(8) and linearizing over small Δx and $\Delta\phi$.

Using the parameters M, k_{spring} and v_{spring} corresponding to an experimental setup, taking reasonable values for the forces F_b and F_s, and playing with the phenomenological parameters τ, η and a_ϕ, one can achieve an excellent agreement with experimental results, especially if one takes a more complicated form for the dependence (8), e.g., one with a few characteristic times. However, while the dependence (5) can be explained with the help of a physical model, the phenomenological dependence (8) has no good physical background, because it does not follow from simulation. However, in Section 6.2 we show that these ideas being combined with an earthquakelike model, do explain the experiments.

A more involved model was developed by Aranson et al. [50]. It is based on the hydrodynamic equation for flow coupled to a dynamic order parameter field $\rho(\mathbf{r}, t)$. The dynamics of the latter is governed by the Ginzburg–Landau equation like in phenomenological approaches to the phase transition problem. Therefore, such a model accounts for the shear- or sliding-induced melting/freezing of the confined film. With an appropriate (but reasonable) choice of the model parameters, it successfully describes stick–slip and smooth sliding, and even predicts new effects such as nucleation of liquid droplets in the overheated lubricant film, and ultrasound generation at stick–slip.

Finally, a large attention was paid recently to a mesoscopic approach based on a generalization of the "shear transformation zone" theory [51]. In this theory, the plastic deformation of the substrates or the lubricant at the interface is represented by a population of mesoscopic regions which may undergo nonaffine (plastic) deformations in response to stress. The theory of this class claims to fill a gap between microscopic MD simulations and macroscopic phenomenological theories.

2.4. Low-dimensional models

Many tribological phenomena can be explained with the help of quite simple models. In these models one usually assumes that the substrates are rigid and the driving force is applied to the top substrate or even directly to the lubricant. Two different algorithms are typically used: the constant-force algorithm, when the driving force changes adiabatically, and the constant-velocity algorithm (or the algorithm with an attached spring), when the top block is driven through a spring whose end moves with a constant velocity (as an everyday analogy, one may think about driving a car with a constant acceleration or with a constant speed). Both algorithms are useful in different situations.

The best known among simple models are the Tomlinson model [53] and the Frenkel–Kontorova model [54,55]. However, even the simplest model of a single atom placed into the external sinusoidal potential and driven by the dc force applied directly to the atom (see Fig. 4) can explain the essential physics of friction in terms of the Langevin motion equation in the *underdamped* limit. This model allows a rigorous treatment as summarized in the monograph by Risken [56]. At zero system temperature, $T = 0$, the average velocity $\langle v \rangle$ of the particle as a function of the driving dc force F exhibits hysteresis. Namely, let us consider a particle of mass M placed into the external sinusoidal potential $V(x)$ of the
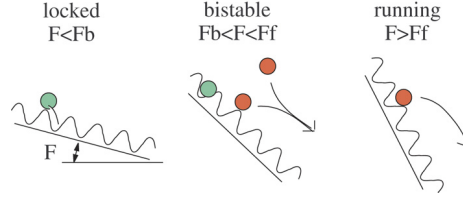
Fig. 4. Bistability of a single driven atom in the periodic substrate potential. The atom is either locked in the minimum of the potential at $F < F_b$, or it is in the running (sliding) state if $F > F_s$ when the minima are degraded. For intermediate forces, $F_b < F < F_s$, the system is bistable, and its behavior depends on the initial state.

height $\mathcal{E} = \max V(x) - \min V(x)$ and the period a, and let it be driven by the dc force F. Then the forward locked-to-running transition takes place at the force $F = F_s = \pi \mathcal{E}/a$, while the backward transition, as is shortly shown, at the threshold force $F = F_b = (2\sqrt{2}/\pi)\eta \sqrt{M\mathcal{E}}$ (here η is the viscous damping coefficient). Thus, in the underdamped case, $\eta < \eta_c \equiv (\pi^2/2\sqrt{2})\sqrt{\mathcal{E}/Ma^2} = (\pi/4)\,\omega_s$, we have $F_b < F_s$, and the system has to exhibit hysteresis due to the inertia of the particle [here $\omega_s = (2\pi/a)\sqrt{\mathcal{E}/2M}$ is the frequency of small-amplitude oscillation of the particle at the bottom of the external potential]. In the simplest model of friction the force F_s corresponds to the static frictional force, while the threshold force F_b, to the kinetic frictional force, and the inequality $F_b < F_s$ is just the necessary condition for the existence of stick–slip motion.

The threshold force F_b can be found from calculation of energy gain and loss. When the particle moves for the distance a (one period of the external potential), it gains the energy $E_{\text{gain}} = Fa$ and loses an energy E_{loss}. In the regime of steady motion these energies must be equal to each other, $E_{\text{gain}} = E_{\text{loss}}$. Thus, the backward threshold force for the transition from the sliding (running) motion to the locked (pinned) state is determined by $F_b = \min(E_{\text{loss}})/a$. The energy losses are caused by the external frictional force $F_{\text{fric}} = M\eta v$,

$$E_{\text{loss}} = \int_0^\tau \mathrm{d}t\, F_{\text{fric}}(t)\, v(t) = \int_0^\tau \mathrm{d}t\, M\eta v^2(t) = M\eta \int_0^a \mathrm{d}x\, v(x), \tag{9}$$

where τ is the "washboard period" (the time of motion for the distance a). The minimal losses are achieved when the particle has zero velocity on top of the total external potential $V_{\text{tot}}(x) = V(x) - Fx$.

In the limit $\eta \to 0$ and $F \to 0$, the minimal energy losses can easily be found analytically. From the energy conservation law, $\frac{1}{2}Mv^2 + \frac{1}{2}\mathcal{E}[1 - \cos(2\pi x/a)] = \mathcal{E}$, we can find the particle velocity $v(x)$. Substituting it into Eq. (9), we obtain

$$F_b = \frac{M\eta}{a}\left(\frac{\mathcal{E}}{M}\right)^{1/2}\int_0^a \mathrm{d}x\left[1 + \cos\left(\frac{2\pi x}{a}\right)\right]^{1/2} = C\eta\,(\mathcal{E}M)^{1/2}, \tag{10}$$

where the numerical constant $C \equiv (2\pi)^{-1}\int_0^{2\pi}\mathrm{d}y(1 + \cos y)^{1/2} = 2\sqrt{2}/\pi \approx 0.9$ depends on the shape of the external potential only. Eq. (10) can be rewritten as

$$F_b = M\eta\bar{v} = (2/\pi)M\eta v_m,$$

where $\bar{v} = a^{-1}\int_0^a \mathrm{d}x v(x)$, and $v_m = (2\mathcal{E}/M)^{1/2} = \pi\bar{v}/2$ is the maximum velocity achieved by the particle when it moves at the bottom of the external potential. Note that the average particle velocity, $\langle v \rangle = \tau^{-1}\int_0^\tau \mathrm{d}t v(t) = a/\tau$, continuously tends to zero when $F \to F_b$, because $\tau \to \infty$ in this limit.
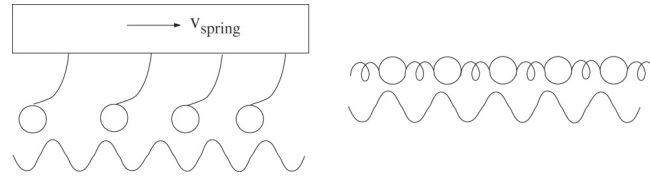
Fig. 5. The Tomlinson model (left panel) and the Frenkel–Kontorova model (right panel).

The characteristic velocity of the transition, however, depends on the mass of the moving block. As shown above, it may be estimated as $v_m \propto (\mathcal{E}/M)^{1/2}$, where $\mathcal{E} = N_s\varepsilon$, N_s is the number of atoms at the interface, and ε is the barrier per one surface atom. When the sliding block is considered as a *rigid* one, then $M = N_s N_\perp m$, where m is the atomic mass and $N_\perp$ is the number of atomic layers in the block. Thus, for a macroscopically large block, $N_\perp \to \infty$, the velocity at the transition may be made as small as desired, $v_m \propto N_\perp^{-1/2}$, e.g., such as that observed experimentally. This picture, however, is wrong as was first mentioned by Persson [57]. The reason is that for a *nonrigid* substrate, only the first (closest to the interface) atomic layer stops at the transition, so that $M = mN_s$, and v_m should be of atomic-scale value (see Section 6.1 below for a more detailed discussion).

Now, if we attach a spring to the atom instead of driving it directly, we observe either the stick–slip or smooth sliding depending on the driving velocity, and the transition between these two regimes [58]). In fact, in this way we just come to the famous Prandtl and Tomlinson model [52,53] shown in Fig. 5 (left panel). This model is, probably, the most widely used in interpretation of tribological experiments due to its simplicity and incorporation of main physics. It clearly shows that a nonzero static friction emerges due to multistability of the system. The system is locked in one of the minima of the potential energy landscape until the increasing elastic stress allows overcoming the barrier. After that the slider is accelerated. The potential energy of the elastic stress is converted into the kinetic energy of the slip (which then must be converted into heat, although this process may be included into the model only artificially). Then, the system rapidly drops to the next nearest minimum, where it is locked again. The Tomlinson model is described in detail in many surveys, e.g., in Refs. [7,8,10]. The physics of this model is quite simple: when the stage moves with a constant velocity v, the "kinetic friction" corresponds in fact to f_s and, therefore, it does not depend on the velocity in agreement with many experiments. A long list of applications of the Tomlinson model to concrete systems can be found in the review paper of Robbins and Müser [8]. However, this simple model can provide only a qualitative description of the problem. Note also that it is more applicable to tip motion in tip-based devices than to a contact between two macroscopic solids.

Another model widely used in tribology is the Frenkel–Kontorova (FK) model [54,55] (see also [75,76] and references therein). The FK model describes a chain of interacting atoms (with harmonic interaction in the simplest case) placed into a periodic (e.g., sinusoidal) substrate potential (Fig. 5, right panel). First introduced to describe dislocations in solids, the FK model found then a wide area of applications, in particular, in surface physics, where it is used to describe adsorbed monolayers. The most important object in the FK model is the so-called kink. Let us consider the simplest case of the trivial ground state (GS) when the number of atoms N coincides with the number of minima of the substrate potential M so that the dimensionless concentration $\theta = N/M$ (often termed coverage) is $\theta = 1$. Then the kink (or antikink) describes a configuration with one extra atom (or vacancy) inserted into the chain,

$N = M \pm 1$. After relaxation, the minimum-energy configuration corresponds to a local compression (or extension in the antikink case) of the chain. The reason why kinks are so important, is that they can move along the chain much easier than the atoms themselves. The activation energy for kink motion, the so-called Peierls–Nabarro (PN) barrier, is typically always smaller or much smaller than the amplitude of the substrate potential. Because the kinks (antikinks) correspond to extra atoms (vacancies), their motion provides a mechanism for mass transport along the chain. Therefore, namely kinks are responsible for mobility, conductivity, diffusivity, etc. in such systems. The higher is the concentration of kinks, the higher will be the system mobility. In the case when the GS is trivial (i.e., $\theta = 1$), the first step in system motion is the creation of a kink–antikink pair. When the chain is finite, kinks are generated at one of the chain's free ends and then propagate along the chain until disappearing at the other free end. Each run of the kink (antikink) through the chain results in the shift of the whole chain by the distance of one lattice constant. In the case of a finite film confined between two solids, one may expect that the onset of sliding is initiated by the emerging of a local compression (kink, misfit dislocation) at the boundary of the contact, while a kink's motion is just the mechanism of sliding.

The most important concept of the FK model is the so-called incommensurability and the Aubry transition connected with it. Namely, let N and M be "incommensurate" (more rigorously, let the substrate period $a_s = L/M$ and the natural period of the chain $a_A = L/N$ be such that in the limit of infinite chain's length $L \to \infty$, their ratio a_A/a_s is an irrational number). Then for a stiff enough chain, $g > g_{\text{Aubry}}$ (here g is the elastic constant of the chain), the chain becomes "free" from the substrate. In the sliding state, the static frictional force is zero, $f_s = 0$, so that any small applied force f leads to the chain's motion. However, the motion is still not absolutely free: the kinetic frictional force is nonzero, because the motion results in the creation of phonons in the chain, although with a quite subtle mechanism. The threshold value g_{Aubry} nonanalytically depends on the atomic concentration θ and takes the minimum value for the golden-mean ratio $a_A/a_s = (\sqrt{5} - 1)/2$. A simple explanation of the $f_s = 0$ sliding state is the following: in this state, for every atom going up over the barrier, there is another going down, and these two processes exactly compensate one another. On the other hand, below the Aubry transition the two incommensurate 1D surfaces are locked together due to creation of local regions of common periodicity. Note also that a *finite* FK chain is always pinned, even in the truly incommensurate case of $g > g_{\text{Aubry}}$, because of the pinning of free ends of the chain. The pinning force in this case, however, does not depend on the chain length, $F_s \propto N^0$.

For the quasiperiodic substrate potential, qualitatively the same scenario is observed, if one uses the spiral-mean concentration (a cubic irrational) instead of the golden-mean one (a quadratic irrational) [59]. The case of the random substrate potential was studied by Cule and Hwa [60] for the 1D system, and then it was generalized to the 2D model in [61].

The FK model and especially its generalized versions are naturally applicable to the description of a contact of two solid surfaces (i.e., the case of "dry" friction), and especially to QCM experiments, where a 1D or 2D system of interacting atoms slides over the periodic substrate potential. Another important point is that the FK model allows a more or less accurate investigation of the transient behavior at the onset (or stop) of sliding, which is quite difficult to study in realistic 3D models.

There are also several combined models used in tribology, such as:

1. The model with two periodic substrates with an atom in between, when the top substrate is driven through an attached spring [62–65];

2. The "train" FK model, where the driving force acts on the end atom of the chain only [66]. This model demonstrates an avalanche-like behavior at the onset of sliding;
3. The combined FK–Tomlinson model [67,68];
4. The model consisting of two coupled FK chains [69];
5. The model describing the FK chain between two sinusoidal potentials [70–73];
6. The two-dimensional Tomlinson model [74];
7. The two-dimensional "springs and balls" FK model describing a 2D layer of harmonically interacting atoms in the 2D periodic substrate (see [75,76] and references therein);
8. The *scalar anisotropic* 2D FK model treating a system of coupled 1D FK chains (see [75] and references therein);
9. The *vector anisotropic* 2D FK model (e.g., the zigzag FK model; see [75] and references therein);
10. The *vector isotropic* 2D FK model (see [77–79,57], and also [75] and references therein);
11. The two-dimensional tribology model [80,81].

It should be noted, however, that simplified low-dimensional models, being very useful in understanding some physical aspects of friction, may claim on qualitative explanations only. The static friction is determined by the atomic structure of the interface, and clearly any low-dimensional model cannot reproduce this structure adequately. A situation is even worse with kinetic friction: as we already mentioned, the kinetic friction is due to conversion of the kinetic energy into heat. This process must pass through the stage of excitation of phonons at the interface, but the rate of this process is first of all determined by the density of phonon states, which can be correctly described only in a three-dimensional model.

3. An adsorbed film: Structure, energy exchange, diffusion

As stated above, it is now recognized that in the case of boundary friction the lubricant film confined between the "hills" of rubbing surfaces is no more than a few monomolecular layers thick. It is thus not surprising that many problems in tribology should be, and actually are, closely related to problems studied in surface physics and chemistry, in particular to surface diffusion and migration processes. Although surface phenomena are generally distinguished by their complexity (according to W. Pauli, "Surface was invented by the devil"), anyhow "open" surfaces are evidently more accessible to experimental investigations with powerful modern techniques than films "closed" between two solid substrates. Quite a few properties of adsorbed films are already well established, and it is advantageous to make use of this knowledge to get more insight into the phenomena that occur in friction contacts.

3.1. Structure of adsorbed layers

In what follows, we will consider the situation when the amplitude of attraction of the adsorbed particles (adparticles) to the substrate is stronger than the amplitude of mutual (lateral) interaction between the adparticles, i.e., when the adhesion is stronger than cohesion. In such a case the adsorbate wets the substrate and the first full monolayer, representing a quasi-two-dimensional (2D) system, forms before the building-up of the subsequent monolayers. Such a situation is most relevant in the context of phenomena in lubricant films.

A few recent decades have brought an immense amount of information on the rich variety of 2D phases that are formed on surfaces under various experimental conditions. They include 2D gases (and
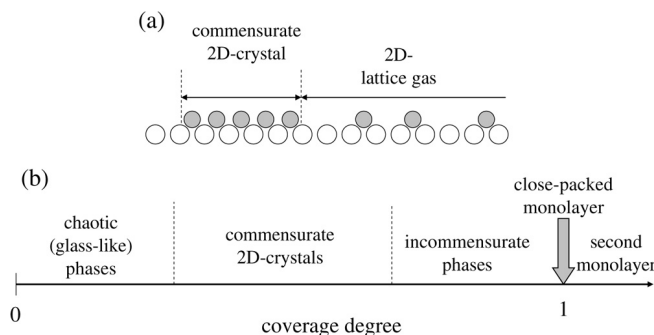
Fig. 6. Possible scenarios of formation of monolayers. (a) Two-dimensional condensation of attracting adparticles. (b) Structural states in the range $0 < \theta < 1$ in the case of lateral repulsion.

lattice gases), liquids, crystals, liquid crystals as well as phases with a peculiar order (so-called extended short-range order), which is specific of the 2D state only [82,83]. The diversity of 2D structures is caused by the superposition of interactions of adsorbed particles with the substrate (V_{as}) and with each other (V_{aa}).

When there is only a single adsorbed atom, it occupies a position corresponding to a minimum of the substrate potential. The coupling of the adatom with the substrate may be weak as in the case of physical adsorption (e.g., for adsorption of inert gases) or strong in the case of chemisorption, when the atomic and substrate electronic shells overlap [84]. Moreover, due to broken symmetry in the normal direction, adatoms often have a nonzero charge, and that leads to an additional coupling (the so-called image forces).

When there are two adsorbed atoms, they interact owing to different mechanisms [85,86]. As two atoms come close to one another and their electronic shells overlap, there emerges a "direct" interaction similar to the usual chemical coupling, but now perturbed by the surface. Due to nonzero charges of the adatoms, they interact according to the dipole–dipole mechanism which is long-ranged. This interaction is repulsive if their dipole moments are oriented parallel to each other (this is the case when the adatoms are chemically identical) and attractive if the dipole moments are antiparallel (e.g., in the case of interaction of an electropositive adatom with an electronegative one). The exchange by electrons through the substrate between the adatoms leads to their "indirect" interaction, which is oscillating, anisotropic and also long-ranged. Finally, there always exists a long-range elastic interaction between adparticles, because they always disturb the substrate [87].

To characterize the concentration of adparticles on the surface, let us introduce the value of degree of coverage, or simply coverage, which is defined as $\theta = n/n_m$, where n is the surface concentration of adparticles and n_m is their concentration in a close-packed monolayer. At $\theta > 0$, the interaction of adparticles is not pairwise, i.e., the energy of interaction of three adatoms is not equal to the sum of interaction energies of these three pairs.

Interplay of the interactions of adatoms with the substrate and between themselves gives rise to a great diversity of structures of adsorbed films and phase transitions between different phases, which generally have little in common with the bulk structure of the adsorbate [82,83]. It is necessary to emphasize the basic difference between the structures formed in the cases of attractive and repulsive lateral interactions.

Attracting adparticles tend to gather into clusters even at low coverages $\theta \ll 1$ (Fig. 6(a)). As a critical coverage is attained, a first-order phase transition (two-dimensional condensation) starts in the

adsorbed layer. It ends with formation of a dense phase, which covers the whole surface and usually has a structure commensurate with the substrate structure. This structure may correspond to a coverage $\theta < 1$ if the potential corrugation of the surface is high enough. However, if the attraction of the adatoms to the substrate is intense and if due to the difference of adsorbate and substrate atom radii the commensurate adlayer does not "screen" the substrate completely, the packing of the first monolayer may continue through transition to an incommensurate structure. This is a laterally stressed structure, and its densening continues until the adsorption energy, which is reducing as the first monolayer gets ever denser, becomes smaller than the adsorption energy in the second layer. As we shall see later, the incommensurate phases in adsorbed layers provide a high rate of the surface mass transport and are thus interesting objects in the context of elucidating the physics of the friction processes.

The phase diagrams of adlayers with repulsive lateral interactions are more diverse than those described above (Fig. 6(b)). First, rather many rarefied phases, i.e., phases with large interatomic distances in the elementary cell, are formed at low coverage degrees. Then, the first-order phase transitions are also observed in such layers [82]. This testifies that the lateral interaction changes from repulsion to effective attraction in some coverage intervals. However, the structure of 2D "condensates" that appear in this case may be far from being close-packed. The first-order phase transitions in repulsive adlayers are attributed to progressive reducing of the amplitude of the repulsive interaction as the adlayer density increases (and correspondingly the distance between the particles decreases). It is believed that this phenomenon may be due to strong mutual depolarization of adparticles [88] and, if one deals with adsorption of a metal, to the onset of a nonmetal–metal transition in the adlayer [89]. These interpretations, however, cannot explain why some systems may undergo a few first-order phase transitions within the coverage range $0 < \theta < 1$. An alternative (or perhaps supplementary) interpretation is based on taking into account the indirect interaction of adparticles, whose energy oscillates with distance [85]. This impose a discrete set of distances at which adparticles can arrange themselves on the surface. Typical systems of this kind are electropositive adlayers (alkali and alkaline-earth adatoms). The polarity of the adsorption bond in this case is very high, which entails a strong dipole–dipole repulsion of the adatoms. As a result, such adlayers usually show broad coverage regions where their structure is incommensurate with the substrate. The rich phase diagrams of these systems offer a convenient possibility for studying the interrelationship between the phase state of the adlayer and various surface characteristics such as adsorption energy, surface diffusion kinetics, catalytic activity, electron emission properties, etc. [90,91].

As the coverage increases to values $\theta > 1$, the adsorbed film may grow either via the layer-by-layer (Frank–van der Merwe) mechanism or via the Stranski–Krastanov mechanism. In the latter case, a few monolayers grow layer-by-layer, while afterwards three-dimensional (3D) islands start to grow and expand on the surface. In general, the growing film takes the structure corresponding to its bulk crystalline structure when its thickness exceeds a few layers.

By analogy with the data obtained for adsorbed films, the structure of a thin lubricant film should be determined by the interplay between the lubricant–substrate interaction V_{sl} and the lubricant–lubricant interaction V_{ll}, and for a film a few monolayers thick, the lubricant structure may substantially differ from the bulk one.

3.2. Energy exchange on surfaces

Surface science physicists are using several well developed experimental techniques to study dynamics of surface processes. First, vibrations in adsorbed layers can be measured with the help of IR
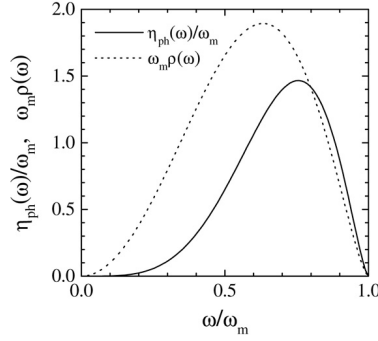
Fig. 7. Dependence of the local density of phonon states [Eq. (12), dotted curve] and the rate of one-phonon damping coefficient [Eq. (11), solid curve] on the frequency ω.

and LEELS spectroscopy. The frequencies of atomic oscillations give information on adsorption sites, while the width and shape of the vibrational line is directly connected with damping of the vibrations, i.e., the rate of energy exchange between the adparticle and the substrate. Experiments stimulated theoretical studies of these processes [92]. It was established that when the vibrational frequency ω is lower than the maximum (Debye) frequency ω_m of the phonon spectrum of the substrate, the adatom vibrations decay via the one-phonon mechanism with the rate [92,93]

$$\eta_{\text{ph}}(\omega) = \frac{\pi}{2} \frac{m_\alpha}{m_S} \omega^2 \rho(\omega), \tag{11}$$

where the surface local density of phonon states for the semi-infinite solid can be approximated by the function [93]

$$\rho(\omega) = \frac{32}{\pi} \frac{\omega^2(\omega_m^2 - \omega^2)^{3/2}}{\omega_m^6}. \tag{12}$$

The functions (11) and (12) are shown in Fig. 7.

Otherwise, when $\omega > \omega_m$ and the one-phonon channel is closed, the damping is due to multi-phonon mechanisms with a rate $\eta \sim 10^{-2}\omega$. The same is true when the elementary cell of the substrate is complex so that the phonon spectrum has a gap, and the vibration frequency lies inside the gap. In the case of chemisorption on a metal or semiconductor surface, additional damping emerges due to excitation of electron–hole pairs in the substrate; this mechanism also leads to the rate of order $\eta \sim 10^{-2}\omega$.

In the case of tribological systems, where the film is confined between two substrates, the same reasons could be applied for the processes between each of the two lubricant–substrate interfaces.

As the energy of an adsorbed atom becomes larger than the height E_d of the substrate potential, the adatom may migrate over the substrate. At low temperatures, $k_B T \ll E_d$, atomic motion is activated and corresponds to Arrhenius diffusion with the coefficient $D = Rl^2 \exp(-E_d/k_B T)$. The frequency factor R and the length of adatom jump l essentially depend on the damping η. For the one-dimensional diffusion, $R \propto \eta$ and $l \propto 1/\eta$ at low damping $\eta \ll \omega$, $R \sim \omega/2\pi$ and $l \approx a$ at intermediate damping $\eta \lesssim \omega$, and $R \sim a^2/2\pi\eta$ and $l = a$ in the overdamped case. For the two-dimensional substrate potential, these questions were studied, e.g., in the paper due to Braun and Ferrando [94].

When the concentration of adatoms is nonzero, their mutual interaction begins to play an important role, and the diffusion is determined by collective mechanisms as described in the next subsection.

3.3. Surface diffusion

Surface diffusion is involved as an important stage in many surface phenomena and technological processes based on them, such as crystal growth, catalysis, spreading, corrosion, sintering, etc. The equations describing diffusion in an initially inhomogeneous system, i.e., in the presence of a concentration gradient, were set up in 1855 by A. Fick by an analogy with the heat conduction equation derived in 1822 by J. Fourier.

The first Fick's law relates the diffusion flux J to the particle concentration gradient ∇n as

$$J = -D\nabla n, \tag{13}$$

where D is the diffusion coefficient (termed also the diffusivity). This simple expression, where D is independent of n, takes no account of interaction between the diffusing particles. In a real situation, however, the interaction between the particles does play an important role and the flux is described in a general form as

$$J = -L(\nabla\mu)_{p,T}, \tag{14}$$

where L is a transport coefficient and $(\nabla\mu)_{p,T}$ is the gradient of the chemical potential (e.g., see [95]). This expression can be rewritten to make it similar to Eq. (13):

$$J = -D(n)\nabla n. \tag{15}$$

Here the diffusion coefficient (termed chemical diffusion coefficient, or heterodiffusion coefficient) is concentration dependent since it incorporates the factor $\partial\mu/\partial\ln n$ and thus takes into account the interaction between the diffusing particles. The concentration dependence of D can also stem from variation of the frequency and length of the particle jumps with n. In the strict sense, diffusion always occurs in an ensemble of particles. The result of interaction within the ensemble is that diffusion in general, and surface diffusion in particular, is essentially a collective process. Intuition suggests that repulsion should enhance the diffusion while attraction should counteract it. This expectation is confirmed by experiments as well as simulations [96].

There exists a transparent analogy between the processes in the lubricant film and surface diffusion processes. The lubricant film within an operating tribocouple is subjected to a shear stress, which shifts the molecules with respect to the surfaces and to each other. The driving force in this case is an external mechanical force. As follows from Eq. (14), the mass transport in the case of surface diffusion is due to the gradient of the chemical potential $\nabla\mu$. This value (with the negative sign) is also termed a thermodynamic force:

$$F = -(\nabla\mu)_{p,T} \tag{16}$$

(e.g., see [97]). It should also be reminded that the particle mobility B and the diffusion coefficient D are related by the famous Einstein formula $B = \chi D/k_B T$, where $\chi = k_B T \left[n\left(\partial\mu/\partial n\right)_{V,T}\right]^{-1}$ is the static susceptibility (also known as the thermodynamic factor).

Let us consider some representative experimental data on surface diffusion (SD). There are two types of SD experiments which allow extraction of data on SD parameters and mechanisms. In the first of them one records the process of diffusional relaxation of the system from an initial nonequilibrium state to the final equilibrium state. This may be the process of evolution of an intentionally created concentration profile [98], or the process of nucleation and growth of islands in the initially homogeneous

but nonequilibrium system (the Ostwald ripening [99,100]), or the variation of the shape of an object (blunting of a tip, smoothening of an initially grooved surface, etc.). Another type of experiment is based on the observation of the mobility of particles (atoms, molecules, clusters) in equilibrium systems. For instance, one can record the random walks of individual particles using microscopies providing atomic resolution [101] or analyze the fluctuation of the number of particles in a small area [102].

There are a number of review papers on surface diffusion [98,102–105,107]. Here we will give a brief summary of the results which are essential for understanding some aspects of the friction processes.

Reliable evidence established about half a century ago is that the substrate atomic structure is a highly important factor which affects the kinetics of surface diffusion. Much later it was realized that another important factor in the diffusion process is the atomic structure of the diffusing layer itself [98]. In fact, systematic and detailed studies of the factors determining SD kinetics are few in number, because experimental investigations of surface diffusion are very laborious. Nevertheless, some general regularities relating diffusion kinetics to structure of adlayers and phase transitions in them are already reliably established. Let us now consider, in a summarized form, available experimental information on surface diffusion mechanisms and kinetics typical of adsorbed layers of various density.

3.3.1. Submonolayer coverages

The most salient feature of surface diffusion is actually its pronounced collective character originating from the interaction of diffusing particles. This effect reveals itself even at low coverages ($\theta \ll 1$) as the particles may unite into clusters. The clusters can differ from one another by the number of particles in them, by their shape, and by diffusion mechanisms, which are strikingly varied [105]. The clusters can jump as a whole; their displacement can also proceed by successive shifting of individual atoms or some groups of atoms, or by rolling if the clusters are ballshaped, etc. (see Fig. 8). It also appears that the mobility of the clusters may depend very critically on their size. A maximum diffusion rate is characteristic of the clusters having a so-called magic size. It typically corresponds to a special symmetry of the cluster shape which depends, in turn, on the structural fit between the substrate and the cluster.

The range of low coverages (typically $\theta \leq 0.1$) corresponds to a phase of the non-ideal 2D lattice gas. In this phase, the diffusion coefficient D gradually decreases with growing θ (see Fig. 9). The most probable reason for this is the progressing formation of the clusters, which generally have a lower mobility than individual atoms. Actually this is the stage of a subcritical nucleation. Let us note that the simultaneous existence of clusters which contain different number of atoms and have different mobilities means that the value D introduced to characterize the diffusion flux is here an averaged (effective) parameter.

This is even more so in the regions of the first-order phase transitions (PT-I) where the adlayer consists of two coexisting phases characterized by different structure and adatom mobility. The diffusion process has here a complex character. A particle is first detached from the dense phase (actually this is an act of two-dimensional evaporation), and the activation energy required for that is the sum of the binding energy in the dense phase and the activation energy of diffusion in the dilute phase [108]. Then the particle diffuses in the dilute phase and either adds to another island of the dense phase or creates a new nucleus of the dense phase with other particles. Anyhow, the diffusion coefficients determined experimentally in the PT-I regions are the smallest.

As described in Section 3.1, the PT-I region is usually followed by a commensurate–incommensurate (C–I) transition. The adlayer in this case is rather dense (approaching a close-packed monolayer). The C–I transition starts with local breaking of commensurability between the adlayer and the substrate
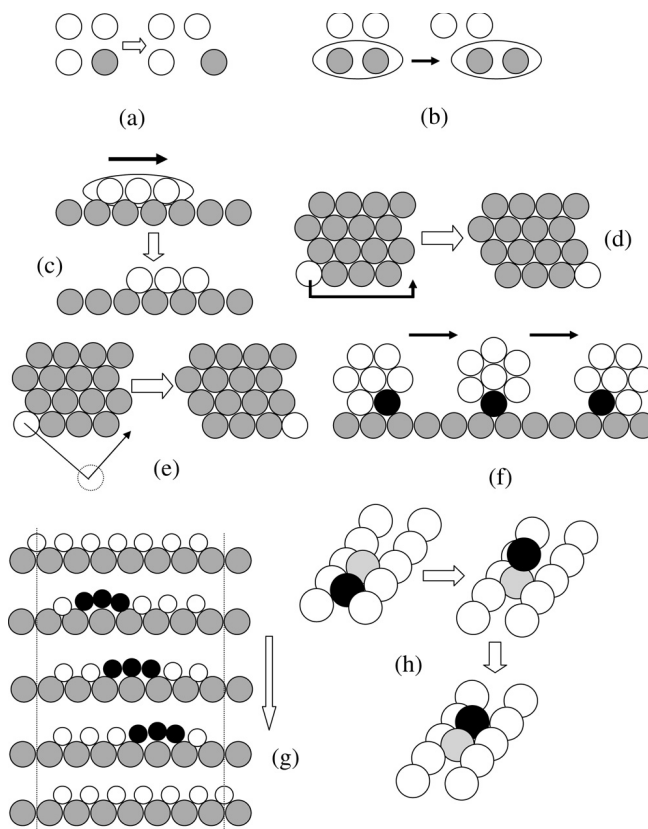
Fig. 8. Schematics of some diffusion mechanisms for clusters and atomic islands. (a) Sequential displacement of individual atoms. (b) The dimer shearing mechanism. (c) The gliding mechanism: the cluster glides as a whole from one position to the next. (d) The edge diffusion mechanism: the motion of an adatom along the island edge causes a shift of the center of mass of the island. (e) The evaporation–condensation mechanism. (f) Schematic of the rolling mechanism. (g) The dislocation (soliton) mechanism: adatoms in the dislocation (soliton) are shown as black balls. (h) Diffusion of a dimer in an atomic channel by the leapfrog mechanism. References to original works: see review [105].
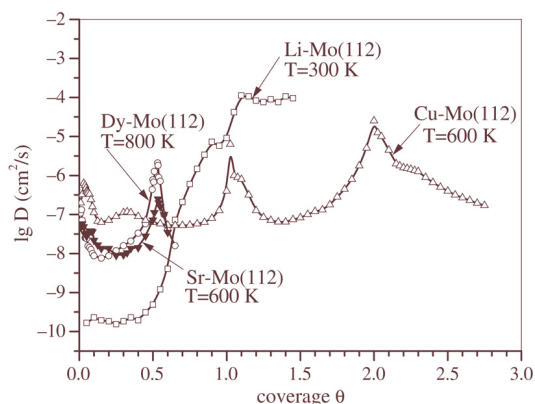

Fig. 9. Surface diffusion coefficients versus coverage for Li, Sr, Dy, and Cu on the Mo(112) surface [106].
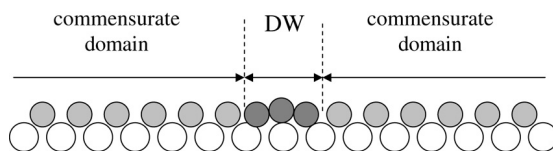
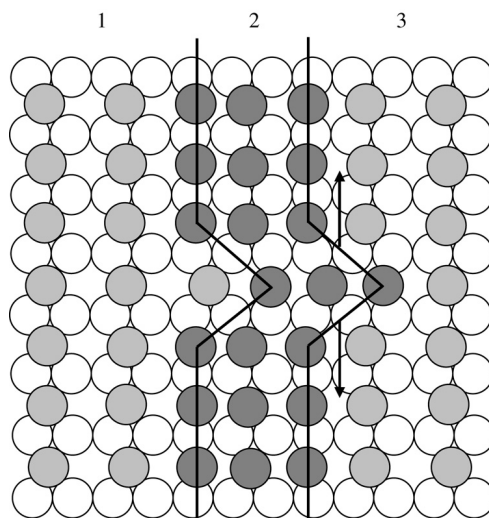Fig. 10. A domain wall (soliton) between two commensurate domains.

Fig. 11. Model of a domain wall with kinks in the $p(1 \times 2)$ commensurate structure. Regions 1 and 3 are the commensurate $p(1 \times 2)$ domains while region 2 is the soliton.

[109,110]. This occurs through formation of incommensurate regions (domain walls) between the commensurate domains (see Fig. 10). The domain wall (DW) incorporates extra ("superstoichiometric") adparticles. The width of the wall depends on the amplitude of the surface potential corrugation, the energy of lateral interaction, and temperature [82,111]. The DW width grows as the potential corrugation gets smoother, or as the lateral interaction or temperature increases. If the adatom concentration is below the stoichiometric value, the domain walls contain vacancies and also correspond to incommensurate regions. From a mathematical point of view, the domain walls can be treated as topological solitons [82,111,75].

The motion of the solitons provides the mass transport through the commensurate phase. The diffusion coefficient usually shows a more or less pronounced maximum at the early stages of the C–I transition (Fig. 9) which is attributed to the soliton diffusion mechanism. The activation energy of diffusion E_d in this coverage region passes through a minimum which is substantially lower than the activation energy corresponding to diffusion of single adatoms at $\theta \rightarrow 0$. This difference results from the collective character of the soliton diffusion. The elementary act in the soliton diffusion mechanism is a concerted displacement of a group of adatoms. While some of the adatoms in this group climb the potential barrier, others descend from it, and this ensures the low E_d value. The elementary configurational excitation of the domain wall is a pair of oppositely oriented kinks as illustrated in Fig. 11. This pair may disappear
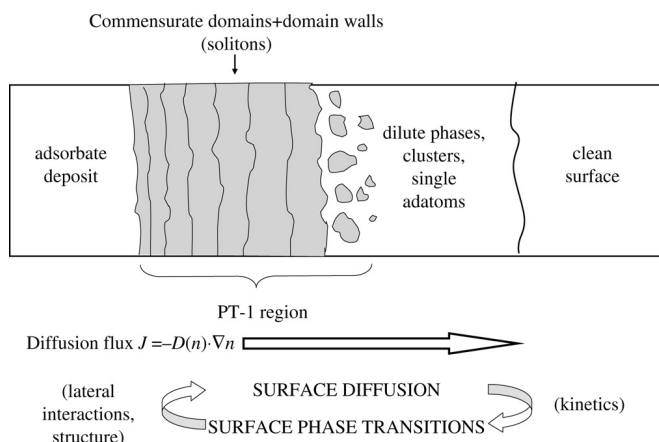
Fig. 12. A schematic of the adlayer phase states in the diffusion zone (top). The diagram at the bottom explains the origin of the interrelation between surface diffusion and surface phase transitions.

if the adatoms return to their initial positions, or the kinks may move in the opposite directions along the DW. In the latter case, the DW will be displaced by one period of the substrate lattice. All these movements occur fluctuatively, thus resulting in a meandering and random displacement of the soliton.

Suppose we have a commensurate surface phase which has a "free" edge at its one side and contacts a deposit of the adsorbate (in the form of a close-packed monolayer) at the other side (Fig. 12). Suppose also that the monolayer is compressed, which is a rather widespread situation in adsystems. The relaxation of the stress existing in the monolayer will occur through generation of the solitons in the commensurate phase. Due to their high mobility, the solitons can easily migrate through the C-phase. Each soliton coming to the free edge of the commensurate phase, expands it by one period of the substrate lattice. Thus, the C-phase containing even a small number of solitons, and under a low gradient of the soliton concentration, can expand over the surface with a high rate. Experiments carried out with a number of metal-on-metal systems showed that such a scenario is rather typical [112,105].

Due to strong variation of the diffusion coefficient with coverage (Fig. 9), which reflects the correlation of the diffusion kinetics with lateral interactions and phase transitions in the adlayer, there occurs a pronounced self-organization of the diffusion zone [113,112]. At each moment this zone represents a snapshot (a nonequilibrium phase portrait) of the adlayer whose different regions correspond to different adlayer structures determined by coverage and diffusion conditions (temperature, time, boundary conditions, etc.). The largest areas in the diffusion zone belong to phases characterized by the highest diffusion rate. An example of such a process recorded for Ba surface diffusion on Mo(011) [114] is presented in Fig. 13. Considering the diffusion zone as a nonequilibrium, nonlinear and open object, one may treat its self-organization in terms of Prigogine's dissipative structures.

3.3.2. Multilayer films

Since the lubricant film in a tribogap under the boundary friction regime is a few monolayers thick, it is understood that diffusion in and on multilayers (or, more precisely, oligolayers) is of particular interest in this context.

Let us consider what happens when the coverage in the initial deposit of the adsorbate exceeds one monolayer. A widespread situation is that the binding of the first monolayer with the substrate is stronger
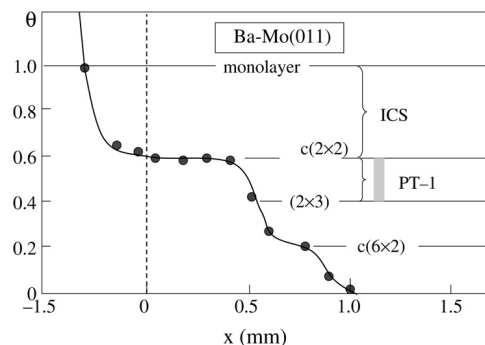
Fig. 13. A coverage profile recorded for Ba diffusing on Mo(011). The boundary of the initial supermonolayer step is shown by a dashed line. Ba structures corresponding to the peculiarities seen in the profile are also indicated. The region of the first-order phase transition (PT-I) is shaded. ICS are incommensurate structures [114].
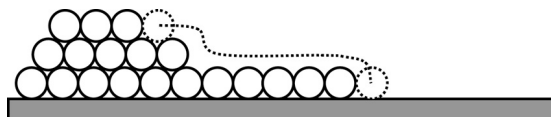

Fig. 14. The "unrolling carpet" mechanism of surface diffusion.

than between the first and second as well as between all subsequent monolayers. The most spectacular example is the multilayer adsorption of active gases (such as oxygen or hydrogen) on metals at low temperatures. The first monolayer is in this case bonded with the substrate by chemisorption energy of a few electron-volts per atom while the second and next monolayers are bonded with a physisorption energy of $\sim 10^{-1}$ eV. This leads to a diffusion mechanism which was discovered by Gomer [115] and received the name "unrolling carpet mechanism" (Fig. 14). Its characteristic feature is a lower mobility of adparticles within the first monolayer than in the second and next monolayers. The result is that the first monolayer expands over the surface by virtue of diffusion in the uppermost monolayer. Such a process seems to be typical for the films which grow on surfaces by the Stranski–Krastanov mechanism. Recall (see Section 3.1) that in this case the adparticles first form one (or maybe a few) full monolayers on the surface and only then gather themselves into three-dimensional islands.

However, the unrolling carpet diffusion mechanism is non-universal even in the case when the bonding between the first monolayer and substrate is stronger than between the next monolayers. For example, lithium adatoms on a tungsten (011) surface diffuse faster in the first monolayer than in the following ones despite the stronger bonding in the first monolayer [116,98]. This is ascribed to the intense lateral repulsion of Li adatoms within the close-packed first monolayer and to high mobility of the solitons in it. At the same time, the diffusion scenario proves to be very sensitive to the chemical nature and other properties of the adsorbate and substrate as well as to temperature and initial conditions of the diffusion. For example, simultaneous spreading of both the close-packed first monolayer and of the second monolayer of lithium was observed for a related system Li–Mo(011) [113] (Fig. 15).

The examples presented above illustrate that surface diffusion parameters essentially depend on the number of monolayer, i.e., on the distance of moving atoms from the substrate surface.
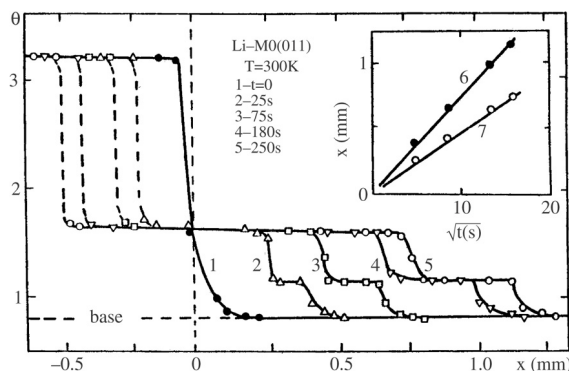
Fig. 15. Diffusion of Li out of an initial step ($\theta_{max} = 3.2$) on the Mo(011) surface precovered with a base ($\theta = 0.8$); curves 1–5 are coverage profiles. Inset: displacement of the leading edge versus $t^{1/2}$ (t is time) for $\theta = 1.07$ (curve 6) and $\theta = 1.6$ (curve 7). Data were obtained with V.V. Poplavsky.

3.3.3. Organic films

Since most present lubricants are of organic origin, the understanding of the mechanisms of surface diffusion of organic molecules is obviously of particular interest from the standpoint of friction. Up to now, however, these mechanisms have been explored to a much lesser extent than for inorganics [117–119]. The quite apparent reason for this is the much wider variety of organic compounds and the structural complexity of their molecules. Fortunately, the situation changes for the better with the advent of scanning tunnelling microscopy (STM). This technique allows observation of movements of individual molecules.

Considering that organic molecules may have a large size and a complex shape, one should expect in this case a frequent occurrence of various collective diffusion mechanisms. They may range from the situation when the molecule jumps as a whole to its displacement by successive movements of its fragments changing step-by-step the molecule configuration and position.

The dependence of the diffusion kinetics on the distance of the molecular layer from the substrate was revealed very graphically in the spreading of droplets of some substances. For instance, De Coninck et al. [120] observed that an initially rounded droplet of an oily liquid (polydimethylsiloxane) on a Si substrate evolves into a stepped pyramid after some time of spreading. The height of each step corresponds to one monomolecular layer. Thus, the spreading process results in a dynamical self-organization (structurization) of the droplet. This is a natural consequence of the fact that the local structure of a liquid depends on the distance from the liquid–solid interface.

Interesting results were obtained in a systematic STM investigation of the structure of monolayers formed on the reconstructed Au(111) surface by alkane molecules (C_nH_{2n+2}) with different n [121]. The lack of ordered structures in the interval $18 \leq n < 28$ was interpreted as the result of a high mobility of the molecules which causes melting of the monolayer. In turn, the enhanced mobility is explained in terms of a model which takes into account the misfit between the periods of the alkane chain (2.53 Å) and of the Au(111) surface lattice along the $\langle 110 \rangle$ direction (2.88 Å). Using a Lennard-Jones potential to describe the molecule–substrate interaction, it was found that the amplitude of substrate potential relief actually passes through a minimum at a "magic size" ($n = 16$) of the alkane molecule. The experiments [121], in which alkane molecules with $n = 10, 12, 14$ and 16 were used as lubricants, gave
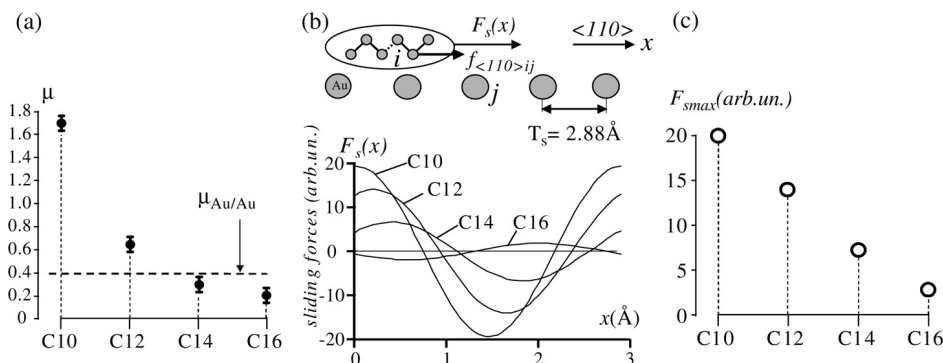
Fig. 16. (a) Variation of friction coefficient μ with the length of n-alkane molecule (experiment). (b) Top part: schematic model of an alkane molecule moving along the $\langle 110 \rangle$ direction on Au(111). Bottom part: variations of sliding forces $F_s(x)$ along the $\langle 110 \rangle$ direction on Au(111) for C_{10}, C_{12}, C_{14} and C_{16} molecules. (c) Theoretical dependence showing the variation of amplitude of sliding force $F_{s\,max}$ with molecule length [121].

qualitative support to the model [122]. The hexadecane ($n = 16$) lubricant was found to provide the lowest friction coefficient (Fig. 16).

3.3.4. Surface electromigration

Consider now briefly some data on surface electromigration. Recall that electromigration is the mass transport on the surface and within the volume of conductors induced by passing a direct electric current. Here we are more interested in surface electromigration, since there exists some analogy between this process and processes in a friction contact. Actually, in both cases one has a force directed parallel to the surface that acts on surface atoms and molecules and causes their drift. In a friction contact, this is an external force that causes the surfaces to move relative to each other. As a constant voltage is applied to a conductor, its surface atoms and atoms adsorbed on it experience forces of two origins. One of them is the Coulomb force, which is significant if the surface particles possess a considerable electric charge. Another is due to momentum transferred from the charge carriers (electrons or holes) which scatter on the surface. The latter force is often termed the electron (hole) wind.

The Coulomb and "wind" forces can act either in the same direction or in opposite directions, depending on the particular situation (the electronic structure of the conductor and the polarity of the adsorption bond). Thus, the mass transport can be directed towards either the anode or the cathode. Detailed information on surface electromigration processes can be found in recent reviews and original papers [123–125].

The results which appear most interesting from the standpoint of friction relate to the structural transformations of surfaces subjected to electromigration. For example, the atomic steps which initially were more or less uniformly distributed over the surface can gather into rather dense bunches in the course of electromigration. The step bunches are separated by wide flat terraces. This process is sensitive to the presence of adsorbed layers and atomic islands on the surface. The step bunching on surfaces due to electromigration can be treated as the emergence of dissipative structures [126]. Of course, the transformations that occur with surfaces in the friction contacts need not be the same as in the case of surface electromigration. However, the existence of basic parallels between electromigration and friction processes suggests that it may be productive to consider the effects observed in both the cases in a general

approach. Namely, they may be treated as results of self-organization of matter under nonequilibrium conditions.

Finally, let us summarize the information presented in this section. What benefit can the tribologists derive from data on surface processes? The answer is that without a deep insight into the physics of these processes, the friction problems cannot be properly understood. The most important evidence relevant to problems of friction is as follows.

- Atoms and molecules at surfaces interact with the substrate and with each other through a number of mechanisms. Some of the interactions may be far-ranging, anisotropic, oscillating with distance and substantially dependent on the chemical nature of the substrate and adsorbate.
- Superposition of these interactions gives rise to a rich diversity of surface structures formed by adsorbed particles and of the phase diagrams of adsorbed films.
- The energy exchange between the adparticles and the substrate is mainly due to excitation of phonons in the substrate through the one-phonon mechanism. The rate of this damping decreases fast with the distance of the adatom from the substrate.
- The interactions between the adsorbed particles result in pronounced collective effects within the adlayers. They find particularly strong manifestations in surface diffusion. Its kinetics depends dramatically on the adparticle concentration in submonolayers and on the distance from the substrate surface in multilayers.
- The collective diffusion mechanisms enhance the sensitivity of the diffusion rate to the presence of surface defects and various impurities within the diffusing adlayers [127]. This effect may be essential for understanding the changes in the lubricant characteristics that occur due to wear of the rubbing surfaces.
- Diffusion in the adlayers is accompanied by their dynamical self-organization, which exerts a substantial effect on the general scenario and the outcome of the diffusion process.

4. Static friction

As was emphasized in the Introduction, the static friction is determined by the structure of the interface, where the sliding will occur. A simple analysis shows [128,129] that for the contact of two *commensurate and perfectly aligned* surfaces one has $f_s \neq 0$, although the magnitude of f_s decreases exponentially with the length of the common period. For non-rigid substrates, the value of f_s is typically lower than that for the rigid substrates because of the decrease of the activation energy for the moving atoms when they can push the substrate atoms apart to make a wider pathway between them [128,129] (the same effect was also observed for the kinetic friction [130,131]).

In the case of a contact of two *incommensurate rigid infinite* surfaces, it must be $\mu_s \equiv f_s/f_{\text{load}} = 0$ [132,133,128,129]. When there are two bare surfaces which are *not rigid* (as, e.g., in the case of "dry" friction, when there is no lubricant between the substrates), an analog of the Aubry transition (see above Section 2.4) should occur with the change of stiffness of the substrates (or the change of the load [134]). This effect was observed in simulation [133]: the surfaces are locked together for a weak stiffness, and freely slide one over another in the case of high stiffness. The simulations show a large variation of the friction with relative orientation of the two bare substrates [135,136]. Similarly to the 1D FK system, where the amplitude of the Peierls–Nabarro barrier is a nonanalytic function of the atomic concentration, in the 2D system the static frictional force should be the nonanalytic function of the misfit angle between

the two substrates and the pulling direction. This was pointed out by Gyalog and Thomas [137], where the 2D FK–Tomlinson model was considered. However, surface irregularities as well as fluctuations of atomic positions at nonzero temperatures makes this dependence smooth and less pronounced. For example, MD simulation due to Qi et al. [140] of the Ni(100)/Ni(100) interface at $T = 300$ K showed that for the case of perfectly smooth surfaces, the $\pi/4$ rotation leads to a factor of 34–330 decrease of static friction. However, if one of the surfaces is roughed with the amplitude 0.8 Å, this factor reduces to 4 only, which is close to values observed experimentally. Müser and Robbins [133] noted that for a contact of atomically smooth and chemically passivated surfaces, realistic values of the stiffness are above the Aubry transition point, so it should be $f_s = 0$ for such a contact. An approximately zero static frictional force was actually observed experimentally in the contact of tungsten and silicon crystals [138]. More recently the FFM experiment made by Dienwiebel et al. [139] demonstrated a strong dependence of the friction force on the rotation angle for a tungsten tip sliding over a graphite surface. This result was explained in the following way: a thin flat flake of graphite, parallel to the natural lattice planes of graphite, is transferred to the tip, so that the sliding occurs in fact between the incommensurate relatively rotated graphite layers.

For two *disordered* but smooth rigid surfaces (e.g., a contact of two amorphous substrates) one has $F_{\text{load}} \equiv N_s f_{\text{load}} \propto A$ and $F_s \propto N_s^{1/2}$, so that $\mu_s \propto A^{-1/2}$. This prediction was checked with simulation by Müser et al. [128,129]. Thus, we again come to the $f_s \to 0$ result for the $A \to \infty$ limit.

For a *finite-size contact*, Sørensen et al. [141] in MD simulations of "dry" friction of a Cu tip over the Cu(111) crystal surface, have found that for nonmatching surfaces (obtained by rotation of the tip relative to the substrate) a local pinning can occur at the corners of the interface (i.e., similar to the pinning of free ends of the finite 1D FK chain). Therefore, in this case one should expect $F_s \propto N_s^{1/2}$, so that $f_s \equiv F_s/N_s \propto A^{-1/2}$ and $\mu_s \propto A^{-1/2} \to 0$ in the $A \to \infty$ limit.

If one takes into account the *elasticity* of the substrates, then the $f_s \to 0$ prediction should not change — the two flat smooth solid surfaces should exhibit no static friction. Moreover, the same remains true even if there are point defects (impurity atoms or vacancies) at the interface, at least when the defect potentials are relatively weak. This was shown by Sokoloff [142,143] with the help of scaling arguments. Indeed, let E_1 be a gain in energy due to sinking of the defect to a nearest interfacial potential minimum at the interface, and E_2 be the increase in the elastic potential energy of the substrate due to atomic displacements of the substrate atoms around the defects (i.e., the elastic energy of the so-called Larkin–Ovchinikov domain [144], which is the region over which the solid distorts to accommodate the defect). Estimations [145,146,143] show that these domains are as large as the interface, so that $E_2 \gg E_1$, i.e., the elastic energy is much larger than any atomic-scale energy due to point defects. This prevents the two solids to be pinned together, because the forces at randomly distributed pinning sites tend to cancel each other. Since all that remains are fluctuations, this implies that again $F_s \propto A^{1/2}$ and $\mu_s \to 0$ in the $A \to \infty$ limit. A scaling analysis due to Sokoloff [143] shows that even fluctuations in the concentration of atomic-level defects at the interface do not lead to nonzero f_s.

According to Sokoloff [143], the sliding of a 3D solid over another 3D substrate just belongs to a marginal case in the scaling theory, i.e., the dimension 3 is just the critical one. When the length scales are increased, neither the elasticity nor the substrate force becomes irrelevant. Whichever one dominates at one length scale will dominate at all scales. Thus, there exist only two regimes: a weak pinning regime, when the elastic forces dominate over the interfacial forces (and the Larkin length is effectively infinite), and a strong pinning regime in which the interfacial forces dominate and the Larkin length is effectively very small. The case of atomically flat surfaces and weak defect potentials corresponds to the

former regime and exhibits no static friction ($F_s \propto A^{1/2}$ so that $\mu_s \propto A^{-1/2}$). Thus, zero or very small static friction should be expected in most cases. This prediction, however, strongly contradicts numerous experiments.

However, Sokoloff [142,143] has pointed out that the situation is just the opposite for the case of contact of *micrometer-length-scale asperities.* In this case $E_2 \ll E_1$, because a pair of asperities from the two surfaces in contact can be *atomically matched* by moving the asperity parallel to the interface a distance of the order of an atomic spacing, which leads to a negligible cost in elastic potential energy. Thus, the case of micron-scale asperities belongs to the regime of strong pinning, and there is static friction ($F_s \propto A$ so that $f_s > 0$).

Recently Sokoloff [147] used the scaling arguments to explain the mechanism of boundary lubrication as well. The idea is that lubricant molecules make the surfaces more smooth, e.g., due to filling the holes between the two rough surfaces in contact. This results in the force pushing the surfaces together being supported over a larger area of real contact, which may switch the interface from the strong pinning (i.e., high static friction) to weak pinning (i.e., low friction) regimes.

A further subtle question is about the value of f_s at $T > 0$, because in this case for any *finite* size of the contact the mobility is nonzero. It is exponentially small if the activation energy $\Delta \varepsilon_s$ is smaller than $k_B T$, and relatively high otherwise. To distinguish the $f_s = 0$ and $f_s \neq 0$ cases, one has to study the scaling of f_s with the system size. In the "thermodynamic" limit $A \to \infty$ the value of μ should tend to zero in the sliding state and remain finite in the locked state. This question was studied by Müser and Robbins [133]. The authors pointed out that for the contact of two *commensurate* surfaces $\Delta \varepsilon_s \propto A$ (and, thus, $\mu_s \neq 0$ in the $A \to \infty$ limit) even when the substrates are separated by a "fluid" lubricant. Indeed, the interaction of the substrates is screened due to the lubricant and, therefore, it may strongly decrease with increasing of the lubricant width (typically according to an exponential law), but the proportionality $\Delta \varepsilon_s \propto A$ still remains valid. In more detail, the periodic potential of one surface induces a commensurate density modulation parallel to the surface in the lubricant. The magnitude of the density modulation decreases exponentially with the distance from the first surface, but remains finite. The second surface, whose periodicity is commensurate with this modulation, should always feel a periodic force that pins the substrates together. The simulations by Curry et al. [149] and Müser and Robbins [133] confirm this result. The exponential decrease of f_s with the width of the ideal crystalline lubricant film was also observed in the hard-lubricant simulations (see Fig. 45 of Section 5.6).

Thus, analytical approaches based on elastic theory predict that in most cases the static frictional force is zero or very small. This is so for the contact of atomically flat surfaces, except in an unrealistic case of the commensurate perfectly aligned surfaces. Moreover, the contact of rough surfaces is also characterized by zero f_s, except for Sokoloff's statement about micrometer-length-scale asperities. The conclusion about zero static friction, however, does not agree with numerous experiments. To explain the experimentally observed nonzero values of f_s, let us recall that there always exists a lubricant or other "third bodies" between the surfaces in contact. Then, because the local pressure at asperities is huge, it results in *plastic* deformation of the lubricant (and, maybe, the asperities as well [148]), making a contact locally "commensurate". Simulation results (see Section 5.6 below) indicate that typically there are $\lesssim 50\%$ "commensurate" atoms at the sliding interface which pin the substrates together. Moreover, Müser et al. [128,129,133] pointed out that already introducing *mobile* atoms at a concentration $\theta \sim 0.2$ into the interface between incommensurate (even completely rigid) or disordered surfaces leads to nonzero f_s and makes the Amontons' law to operate (i.e., μ_s becomes independent on A and load). Of course, other possible "third bodies" may play the same role. The lubricant atoms can accommodate
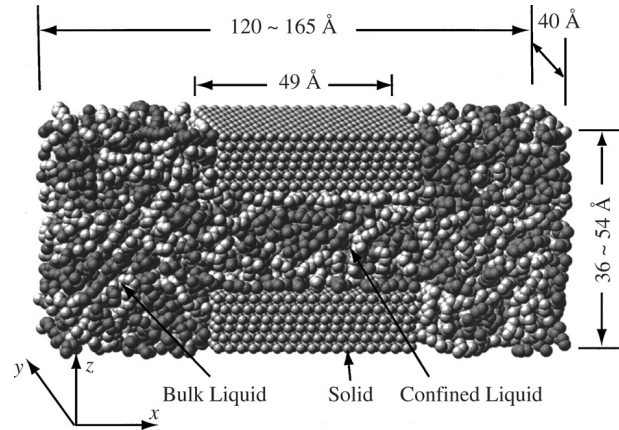
Fig. 17. The computational cell used in the Grant Canonical Ensemble Molecular Dynamics method (from [40]).

the surface corrugation of both walls simultaneously, i.e., they occupy the "++" positions, where the lubricant atoms lie at the minima of potentials from both surfaces; this locks the two surfaces together. The simulation [133] showed that now the motion of the top substrate is diffusional (no pinning) at large T, but the substrates become locked together when the temperature decreases, or the load increases, or the size of the system increases; the latter indicates that $\Delta\varepsilon_s \propto A$ (in fact, the authors of [133] observed in simulation not the complete locking of two substrates but a crossover from the free diffusion to a subdiffusional motion of the top substrate, $\langle \delta x_{\text{top}}^2(t) \rangle \propto t^{\alpha}$ with the exponent $\alpha \approx 0.2$). An interesting observation is that the lubricant itself need not be in a crystalline or glassy state to produce the pinning of the substrates. However, the question whether the locking exists for all T in the thermodynamic limit (as it is for the commensurate surfaces), or there is the locked-to-sliding transition with increase of temperature, still remains open. Sokoloff [143] also noted that if the lubricant is inserted into the interface between two asperities in contact according to the picture described above, then the value of μ_s could be very small ($\mu_s \sim 10^{-5}$) compared with what is typically observed experimentally. Moreover, as was pointed out in [150], the Müser–Robbins mechanism of static friction will operate only when the lubricant atoms are inserted between two identical substrates and interact approximately with the same strength with both of them. Otherwise, if the lubricant atom interacts stronger with one of the substrates, it will stick to that substrate, and in this case we come back to the situation described above — the contact of two substrates with static defects, which should exhibit no static friction.

5. Kinetic friction

As usual in computer simulation, one can use two simulation techniques to study tribological systems, the Monte Carlo (MC) method or the MD technique. The MC technique provides the equilibrium configuration of the system [37–39] and, therefore, it can be used to find the static frictional force. The MD technique is rigorous for nonequilibrium systems, but it is much more time consuming. It was developed in two versions, the Grand Canonical Ensemble Molecular Dynamics (GCMD) method and the Molecular Dynamics method based on Langevin equations.

The GCMD method was developed by Gao et al. [40–42]. The three-dimensional computational cell for the GCMD simulation of the confined lubricant is shown in Fig. 17. The cell is repeated using 3D
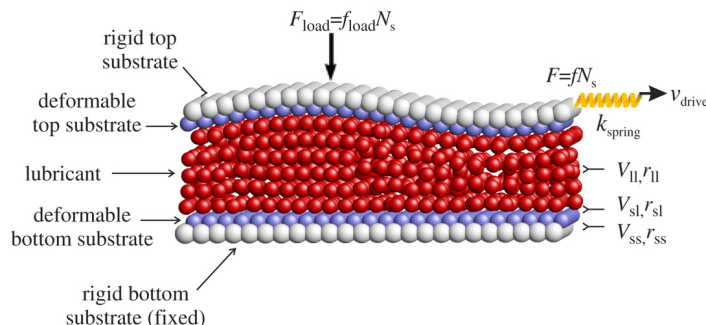
Fig. 18. The model used in MD simulation of friction. Each substrate consists of two layers, the rigid layer and the deformable substrate layer which is in contact with the lubricant. The lubricant atoms fill the space between the substrates. The atoms of the rigid layer of the bottom substrate are fixed, while the rigid layer of the top substrate can move due to applied forces.

periodic boundary conditions. It contains rigid substrates (shown by small spheres in Fig. 17) of finite extent in the x direction and extending through the cell in the y direction. The dimension of the cell in the x direction (L_x) varies dynamically in response to the applied external pressure in that direction, taking different values depending on the gap width d between the opposing solid surfaces. The width d is kept fixed in a given simulation run. The cell is filled with a liquid lubricant. A part of its molecules is in the confinement and the rest outside it. L_x is taken to be large enough such that bulk liquid behavior can be established in the regions outside the confinement. The motion equations are Newtonian; the temperature can be controlled via scaling of atomic velocities at the initial part of the run. This technique is best adjusted to study lubricant structure as a function of the gap width d. The structure (liquid or solid) can be determined by calculation of the structure factor, the diffusion coefficients, and from the response to shear stress applied to the substrates.

The MD technique based on Langevin equations was developed by Robbins et al. and used in a series of studies [151,152,43,153,44,154–156,128,133,129–131]. In the present review we describe only this variant of the MD technique (with an improvement proposed by Braun and Peyrard 2001 [157]). Moreover, we will concentrate on simple models of the lubricant and substrates in order to pick up the main physical aspects of the problem. A rather detailed list of MD simulation results with applications to experimentally studied systems can be found in the review papers [8,10].

A serious restriction of the MD technique is that it typically uses periodic boundary conditions with a fixed number of particles. However, a trick with finite-size substrates in the GCMD as described above, or the one with a curved substrate (see below) helps to overcome this problem, at least partially.

5.1. Molecular dynamics model

A typical three-dimensional system for tribology simulation comprises a few atomic-layers lubricant film between two (top and bottom) substrates as shown in Fig. 18. For example, in the approach proposed in Ref. [157], each substrate consists of two layers. The rigid layers form the boundaries of the system, while deformable substrate layers are in contact with the lubricant. Each rigid substrate part has N_s atoms henceforth called s-atoms organized into, e.g., a square lattice with the lattice constant a_s. The atoms of the bottom rigid substrate part are fixed while the top substrate part moves rigidly. Between the rigid substrate parts we insert atoms of two different kinds: $2N_s$ s-atoms model the surfaces of the substrates

and $N = N_{al}N_l$ l-atoms ("lubricant" atoms) form the lubricant film. Periodic boundary conditions are used in the x and y directions.

In such a model with periodic boundary conditions, unfortunately, the results could be sensitive to the number of lubricant atoms N: if N does not match exactly the number of atoms in closely-packed layers, then extra atoms or vacancies will produce structural defects, especially in small systems accessible in the simulation. To reduce uncertainties due to this difficulty, one may use a geometry with curved substrates [158]. For instance, in the system shown in Fig. 18 the z-coordinate of the rigid layer of the top substrate varies as

$$z = Z_2 + \frac{1}{2}h_x r_{sl}\left[1 - \cos\frac{2\pi(x - X_2)}{L_x}\right] + \frac{1}{2}h_y r_{sl}\left[1 - \cos\frac{2\pi(y - Y_2)}{L_y}\right]. \tag{17}$$

Here $L_{x,y}$ is the size of the system in the x or y direction, $h_{x,y}$ are the corresponding curvature parameters, and X_2, Y_2, Z_2 are the center of mass coordinates of the rigid layer of the top substrate. A similar expression can be used for the z coordinate of the bottom substrate. Such a geometry is also more close to a real situation, where the surfaces are often rough.

To each atom of the rigid layer of the top substrate we apply a force consisting of a driving force f along the x axis and a loading force f_{load} along the z direction. The driving force f may either correspond to the dc force applied directly to the atoms (in the constant-force algorithm), or it may correspond to a spring force, when a spring of elastic constant k_{spring} is connected to the top rigid layer, and its end moves with a constant velocity v_s (the algorithm with the attached spring).

Equations of motion. First of all let us explain why we have to use the Langevin motion equations in the study of the far-from-equilibrium state of the driven system. In order to achieve the thermal equilibrium state in a 3D model using Newtonian equations, one has to consider $\gg 10^3$ atoms (at the present stage computer simulation allows one to model $\sim 10^6$ atoms maximum). Therefore, realistic simulation times would be of the order $\lesssim 10\,\tau_0 \sim 10^{-12}$ s. These times are too short even for reaching the steady state, and of course they are very far from typical experimental times. Also, anyway the approach with solely Newtonian equations cannot incorporate electron–hole damping as well as other lost degrees of freedom.

The kinetic friction is due to energy losses. They are produced at the sliding interface, and then the energy must go away from the interface to the substrates, where it will be absorbed being transformed into the internal degrees of freedom of the substrates (phonons, e–h pairs). Finally the heat has to be removed from the system. Thus, we cannot use solely Newtonian equations, because the external driving will increase the system energy up to infinity. A standard approach in such situations is to model the substrates as made of many atomic layers, and then to use the Langevin equations for a few layers far away from the interface (below in Section 6.1 we describe such an approach). However, in simulation there always exists the competition "large system $\longleftrightarrow$ long times". Because the most important task is a detailed modelling of the interface itself, there are no reasons to include too many substrate layers. Therefore, it is reasonable to use the Langevin equations for the lubricant atoms and for the atoms of one or only a few substrate layers, while all other missed degrees of freedom can be treated implicitly through an external damping coefficient in the Langevin equations.

However, a critical question is how the external damping coefficient η_{ext} in the Langevin equations is defined, because it is just its value that determines the rate of energy flow out of the friction zone and, finally, governs the kinetic friction. If thermal equilibrium is of interest, an actual value of η_{ext} is irrelevant (although the rate of approach to equilibrium depends on damping and achieves a maximum at

$\eta_{\text{ext}} \sim \omega_0$). In their numerous simulations [151,152,43,153,44,154–156,128,133,129–131], Robbins and coauthors used the following trick: the Langevin damping is applied only to the degrees of freedom that are perpendicular to the sliding direction, and the authors claim that the actual value of the coefficient does not affect the results. It could be so at high temperatures, e.g., close to or above the bulk melting temperature of the lubricant, as was simulated in those studies, because the atomic interaction is highly anharmonic under such circumstances. In a general case, however, more reliable results should be expected, when one uses a realistic damping that depends both on the coordinate z of a given atom (i.e., on its distance from the substrates) and on its velocity v with respect to the substrates, since the probability of excitation of phonons in the substrates depends on the relative velocity of the lubricant atom as compared with the phononic (sound) speed in the substrate (see Section 3).

Now let us describe the standard set of equations used in tribological simulations [157]. The Langevin motion equations for all "mobile" atoms have the form

$$m_\alpha \ddot{r}_{i\alpha} = f_{i\alpha}^{(\text{int})} + \sum_{S=1}^{2} f_{i\alpha,S}, \tag{18}$$

where $\alpha = s$ or $\alpha = l$ for "substrate" or "lubricant" atoms respectively. The force $f^{(\text{int})}$ is due to interaction between the mobile atoms in the system,

$$f_{i\alpha}^{(\text{int})} = -\frac{\partial}{\partial r_{i\alpha}} \sum_{i'\alpha'}^{\text{all}} V_{\alpha'\alpha}(r_{i'\alpha'} - r_{i\alpha}). \tag{19}$$

The last term in Eq. (18) describes the interaction of a "mobile" s- or l-atom with the bottom ($S = 1$) and top ($S = 2$) substrates. The force $f_{i\alpha,S}$ itself consists of three contributions as usual in Langevin equations,

$$f_{i\alpha,S} = f_{i\alpha,S}^{(\text{int})} + f_{i\alpha,S}^{(\text{fric})} + f_{i\alpha,S}^{(\text{ran})}. \tag{20}$$

The first contribution $f_{i\alpha,S}^{(\text{int})}$ comes from the potential interaction of a given (ith) atom with all "immobile" atoms of the Sth (bottom or top) rigid substrate,

$$f_{i\alpha,S}^{(\text{int})} = -\frac{\partial}{\partial r_{i\alpha}} \sum_{i'=1}^{N_S} V_{s\alpha}(R_{i'S} - r_{i\alpha}), \tag{21}$$

where the sum now includes all "immobile" s-atoms of the corresponding substrate and $R_{i'S}$ is the coordinate of the i'th atom of the Sth rigid substrate. The second and third terms in Eq. (20) describe the energy exchange between mobile atoms and the rigid substrates, which approximately takes into account the missing degrees of freedom of the substrates. The term $f_{i\alpha,S}^{(\text{fric})}$ describes a viscous damping when an atom moves relative to the corresponding substrate,

$$f_{i\alpha,S}^{(\text{fric})} = -m_\alpha \eta \left(z_{\text{rel}}, v_{\text{rel}} \right) \left(\dot{r}_{i\alpha} - \dot{R}_S \right), \tag{22}$$

where $\eta \left(z_{\text{rel}}, v_{\text{rel}} \right)$ is the external damping coefficient, $z_{\text{rel}} = (-1)^{(S-1)}(z_{i\alpha} - Z_S)$, $v_{\text{rel}} = \dot{r}_{i\alpha} - \dot{R}_S$, and $R_S \equiv \{X_S, Y_S, Z_S\}$ is the center of mass coordinate of the Sth substrate (for the bottom substrate $R_1 \equiv 0$). Finally, the third contribution $f_{i\alpha,S}^{(\text{ran})}$ in Eq. (20) describes the random (Gaussian) force acting

on the ith atom from the Sth substrate. Its amplitude is determined by the substrate temperature T, i.e., the corresponding correlation function is

$$\langle f_{i\alpha,S}^{(\mathrm{ran})}(t)\, f_{i'\alpha',S'}^{(\mathrm{ran})}(t')\rangle = 2\eta_R(\dots)\, m_\alpha k_B T \delta_{ii'}\delta_{\alpha\alpha'}\delta_{SS'}\delta(t-t'). \tag{23}$$

Here the function $\eta_R(\dots)$ is coupled with the external damping coefficient $\eta(\dots)$ by the relationship [159,94]

$$\eta_R(z,v,T) = \int_0^\infty d\epsilon\, e^{-\epsilon} \eta(z,\widetilde{v}(\epsilon)), \qquad \widetilde{v}^2(\epsilon) = v^2 + \frac{2k_B T}{m_\alpha}\epsilon. \tag{24}$$

Finally, motion of the rigid layer of the top substrate is described by the Newtonian equation

$$M_s \ddot{R}_2 = N_s f_{\mathrm{ext}} + F_S, \tag{25}$$

where $M_s = N_s m_s$ is the mass of the rigid layer of the top substrate, $f_{\mathrm{ext}} = \{f, 0, f_{\mathrm{load}}\}$ is the external force applied to it, and $F_S = -\sum_{i\alpha}^{\mathrm{all}} f_{i\alpha,S=2}$ according to the third Newton law (conservation of the total momentum of the system).

Parameters of the model. Most of the simulation results presented below are given in "natural units" (n.u.) which correspond to atomic-scale values, i.e., the numerical values of the model parameters have been chosen such that, if energy were measured in electron-volts and distances in Angströms, we would have realistic values for a typical tribological system. The results described below were obtained, following Ref. [157], for all atoms interacting via a 6-12 Lennard-Jones pairwise potential

$$V(r) = V_{\alpha\alpha'}\left[\left(\frac{r_{\alpha\alpha'}}{r}\right)^{12} - 2\left(\frac{r_{\alpha\alpha'}}{r}\right)^6\right] \tag{26}$$

where, however, the parameters of the potential (26) are different for different kinds of atoms. Between two substrate atoms we use V_{ss} and the equilibrium distance is $r_{ss} = a_s$, between two lubricant atoms, V_{ll} and r_{ll}, and the interaction of the lubricant atom with the substrate atom is described by the parameters V_{sl} and r_{sl}.

It is useful to couple the natural units with the Système International (SI). The basic parameters that are unchanged in the simulations, are the amplitude of interaction within the substrates ($V_{ss} = 3$), which sets the energy parameter, the substrate lattice constant ($a_s = 3$) that sets the length scale, and the mass of lubricant atoms ($m_l = 1$) as the mass parameter. Then, we have for the unit of length $1\,\mathrm{m} = 10^{10} v_r^{-1}$ n.u., for the unit of mass $1\,\mathrm{kg} = 6\times 10^{24} v_m^{-1}$ n.u., for the unit of energy $1\,\mathrm{J} = 6.25\times 10^{18} v_e^{-1}$ n.u., for the unit of force $1\,\mathrm{N} = 6.25\times 10^8 (v_r/v_e)$ n.u., for the unit of pressure $1\,\mathrm{Pa} = 6.25\times 10^{-12}(v_r^3/v_e)$ n.u., for the unit of time $1\,\mathrm{s} = 0.98\times 10^{13}\left(v_e/v_m v_r^2\right)^{1/2}$ n.u., and for the unit of velocity $1\,\mathrm{m/s} = 1.02\times 10^{-3}(v_m/v_e)^{1/2}$ n.u. (the coefficients $v_e \sim v_r \sim v_m \sim 1$ were defined in Ref. [157]). In particular, the load force $f_{\mathrm{load}} = -0.1$ n.u. corresponds to the pressure $P = -f_{\mathrm{load}}/a_s^2 = 1.11\times 10^{-2}$ n.u. $= 1.78\times 10^9$ Pa. To compare with experimentally used values, note that a realistic pressure is $P \sim 10^7$ Pa, and the maximum pressure above which the plastic deformation begins, is $P \approx 2\times 10^8$ Pa for gold (a minimal value for metals), $P \approx 10^9$ Pa for steel, and $P \approx 10^{11}$ Pa for diamond (the largest possible value). As for velocities, a typical value when the transition from stick–slip to smooth sliding is observed experimentally, is $v_c \sim 1\,\mu\mathrm{m/s} = 10^{-9}$ n.u.

The relation between the two parameters, $V_{sl} \leftrightarrow V_{ll}$, is the most important issue of the tribological system, because it determines the behavior of the lubricant at sliding. In the case of a "soft" lubricant,

$V_{ll} \ll V_{sl}$, two lubricant layers are strongly coupled to the substrate surfaces, and the sliding should occur somewhere at the middle of the film's width. As a result, the lubricant is melted at sliding, and the stick–slip motion corresponds to the melting–freezing mechanism. Qualitatively different behavior is exhibited by the "hard" lubricant, when $V_{ll} > V_{sl}$. In this case the lubricant remains in the solid state during sliding, the sliding takes place at the lubricant–substrate interface, and the stick–slip is due to the inertia mechanism. In the simulation results presented below, other model parameters are typically the following. The interaction between the substrate and the lubricant is always much weaker, $V_{sl} = 1/3$, than the interaction within the substrate; that prevents the substrates from wearing. For the lubricant itself, we consider two cases: the soft lubricant with $V_{ll} = 1/9$ and the hard lubricant with $V_{ll} = 1$ although, in both cases, the lubricant is less rigid than the substrates. The equilibrium distance between lubricant atoms is $r_{ll} = 4.14$, i.e., it is "incommensurate" with the equilibrium atomic distance in the substrate. The parameter r_{sl} characterizing the interaction between the substrate and the lubricant is $r_{sl} = \frac{1}{2}(r_{ss} + r_{ll}) = 3.57$. For the atomic masses is used $m_l = m_s = 1$, which gives a characteristic frequency of $\omega_s = \left[V_{ss}''(r_{ss})/m_s \right]^{1/2} = 4.9$ and a typical period of $\tau_s = 2\pi/\omega_s = 1.28$.

For the external damping in the Langevin equations, Braun and Peyrard [157] proposed to use the expression

$$\eta_{ext}(z, v) = \eta_1(z)[\eta_{ph}(v) + \eta_{eh}], \tag{27}$$

where $\eta_1(z)$ describes the exponential decrease of the damping when an atom moves away from the substrate, $\eta_1(z) = 1 - \tanh[(z - z^*)/z^*]$, and the characteristic distance z^* was chosen as the distance between the layers in the substrate ($z^* = 2.12$ in the simulation). Thus, for the atoms in the s-layer, where $z \approx z^*$, we have $\eta_1 \sim 1$, while for the atoms in the utmost (closest to the substrate) lubricant layer we obtain $\eta_1 \sim 0.1$. For the velocity dependence of the one-phonon damping it was proposed to use $\eta_{ph}(v) = \eta(2\pi v/a)$ with $a = a_s$ for the motion along the substrate (i.e., the atom vibrates with the washboard frequency $\omega_{wash} = 2\pi v/a_s$ when it slides over the substrate periodic potential) and $a = z^*$ for the motion in the z direction, where the function $\eta_{ph}(\omega)$ is given by Eqs. (11) and (12) of Section 3 [the cutoff (Debye) frequency was taken as $\omega_m = 15$]. Of course, such an approach is not rigorous. First, the dependence (11) was derived for vibrations of a single adatom. Thus, it can be applied for the case of amorphous structure of the lubricant, while for the case of crystalline structure one has to take into account the conservation of momentum in phonon scattering. Second, the substitution of the washboard frequency is also approximate. In a rigorous approach we have to use a nonlocal retarded response function instead of the local damping coefficient. However, although the described approach is not rigorous, it is much more realistic than the use of some artificial constant damping coefficient. Finally, the damping due to the creation of electron–hole pairs in the metal or semiconductor substrate was taken as $\eta_{eh} = 10^{-2}\omega_s$.

In the model described above as well as in most models used in tribology simulations, the utmost substrate layers are rigid. Although their phonon degrees of freedom are included implicitly through the damping coefficient, we nevertheless totally lose their elasticity. Of course, this is typical for MD simulations: the elastic interaction is long-ranged, thus it is almost impossible to include it rigorously in a MD model. An elastic interaction between the lubricant atoms may in principle be included artificially, e.g., by adding a corresponding term to the interaction (26). Besides, for the tribology system under a high load the elastic deformation of the substrates at the contact may be of great importance. Persson and Ballone [158] proposed to connect the rigid and mobile substrate layers by artificial springs, which have both longitudinal and transverse stiffness and thus model the elastic properties of a semi-infinite

substrate. This approach works well in modelling of static properties of the system, such as the lubricant structure, the static frictional force, and even a slow process of squeezing of the lubricant. As for modelling fast processes that occur during sliding, such an approach may lead to artificial results, because a continuum acoustic phonon spectrum of the substrate is substituted by the spring with a single frequency, which may come in resonance with the washboard frequency of the sliding system.

Finally, comparing the GCMD method with that described above, we should note that they are quite close to one another. The GCMD uses the (P, E, N) ensemble (i.e., with the constant pressure, energy and the number of atoms), while Robbins' approach operates with the (P, T, N) ensemble (i.e., with constant temperature). A problem with the constant-energy ensemble is that it cannot be used for kinetics, because the pumped energy will destroy the system if it is not removed by some artificial method. Another essential difference between these two methods is the following. In the GCMD method the external "load" is applied in fact to the x sides of the simulation cell (the size L_x is varied dynamically to keep a given pressure), while the width d of the lubricant film is fixed. In the Robbins' model the x and y sizes are kept fixed, and the load is applied to the substrates, so that the pressure is again kept constant, but now the lubricant width is changed dynamically to adjust to a given pressure, the number of atoms and the available space in the xy box.

5.2. Melting of a confined film

As was mentioned in Section 2, a thin film of a few molecular diameters width is often solidified, because the confinement decreases the entropy of the film and shifts the bulk melting transition to higher temperatures ([18,43,44,40–42], see also [4,7] and references therein). The SFA high precision experiments [160–162] confirm such a behavior. Theoretically, a continuum approach based on a Ginzburg–Landau expression for the free energy and a mean-field theory [163] provides a qualitative explanation of this effect. Another analytical approach based on the Lindemann criterion and the confinement of the fluctuations by the walls also provides a qualitative [164] and even quantitative [165] description of the melting of a thin confined film. However, recent experimental studies [166] have shown that the confinement-induced "solid" does not have a well defined structure. In this section we describe, following Ref. [165], the melting process of the lubricant as follows from MD simulation.

An important parameter of the lubricant, available in experiment and connected to its thermodynamic state, is its specific volume. For the confined lubricant, only the thickness of the film can change and, therefore, the variation of the specific volume shows up in the variation of the coordinate z_{top} of the top substrate. Fig. 19 shows the variation of z_{top} when the initial GS configuration is adiabatically heated and then cooled down. For the lubricant thicknesses of $N_l = 1$ to 5 layers, the general behavior of the system is the same. While heating, a sharp increase of z_{top} is observed at a temperature T_m that depends on N_l as shown in Fig. 20. While cooling the soft lubricant, its behavior depends on the number of lubricant layers: for $N_l = 1$ or 2 a sharp transition that brings the system back to lower values is found, while for larger N_l, z_{top} decreases smoothly. The fits of the $T_m(N_l)$ dependences shown in Fig. 20 lead in the $N_l \to \infty$ limit to values in good agreement with the bulk values of the melting temperature obtained by the Monte Carlo calculations of the LJ solid. Therefore, the transition observed during heating appears to be consistent with the melting transition.

The analyzing of atomic trajectories at the transition shows that the increase of film thickness is due to the *formation of an additional layer in the film* (see Fig. 21, left panel) that agrees with experimental observation [161]. Moreover, looking at Fig. 21 one can notice that even in the high temperature
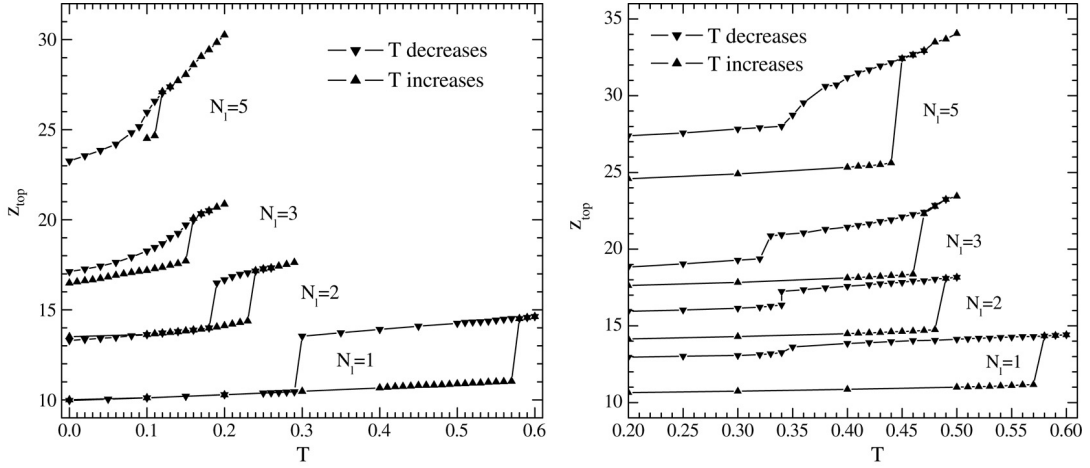
Fig. 19. Vertical coordinate z_{top} of the top substrate as a function of temperature for different lubricant film thicknesses, in the case of the soft lubricant ($V_{ll} = 1/9$, left panel) and the hard lubricant ($V_{ll} = 1$, right panel).
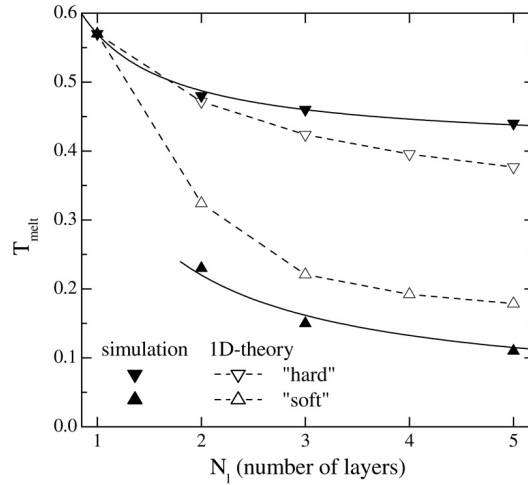

Fig. 20. The melting temperature T_m as a function of the number of lubricant layers for $f_{load} = -0.1$. The filled markers correspond to MD simulation results while the open markers are the theoretical values from [165]. The solid curves describe the fits $T_{melt} = 0.405 + 0.165/N_l$ for the hard lubricant and $T_{melt} = 0.045 + 0.350/N_l$ for the soft lubricant.

"liquid" phase the lubricant is still organized into layers, again in agreement with experiments and other simulations.

In order to distinguish the solid and liquid phases, experiments with a small shear force are most often used. Fig. 22 shows that below T_m the lubricant behaves like a rigid body, with only a negligible displacement under the shear stress, while for $T > T_m$ the top substrate takes a nonzero equilibrium velocity, indicating a fluid lubricant. However, Fig. 21 also indicates that the properties of the "solid" lubricant phase are not trivial. Following trajectories of the particles in the MD simulation, one can notice many jumps from one lubricant layer to another, even at temperatures $T \ll T_m$. The high mobility of the lubricant atoms is also attested by the calculation of their diffusion coefficient versus T. The average
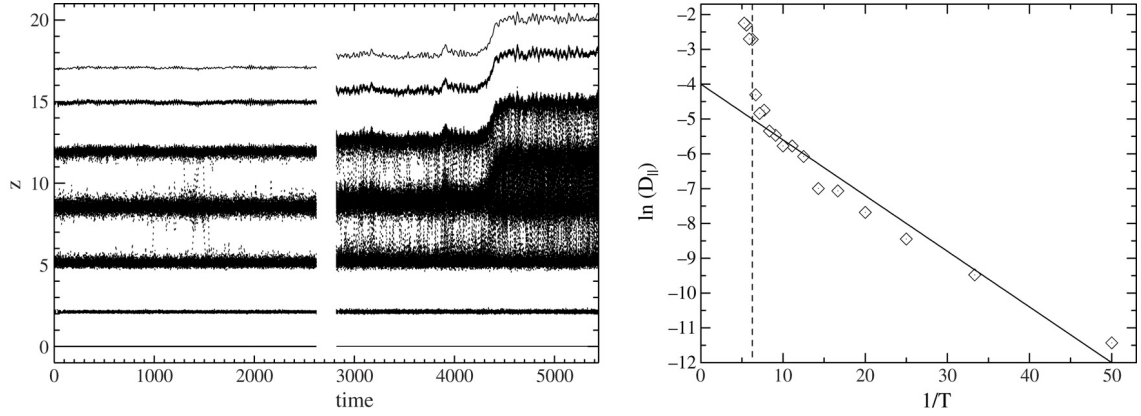
Fig. 21. Left panel: Time evolution of the z coordinates of all atoms at temperatures $T = 0.08$ (left part of the figure) and 0.16 (right part of the figure) for the soft lubricant. The vertical lines which connect the layers show that particles are changing layers. At $T = 0.16$, the time snapshot has been centered on the moment where the system melts by creating a new layer. The figure shows that the transitions of the particles between layers become more frequent while melting, but the change is not abrupt. Right panel: Diffusion coefficient of the particles along the layers $D_\parallel$ versus inverse temperature in semi-logarithmic scale.
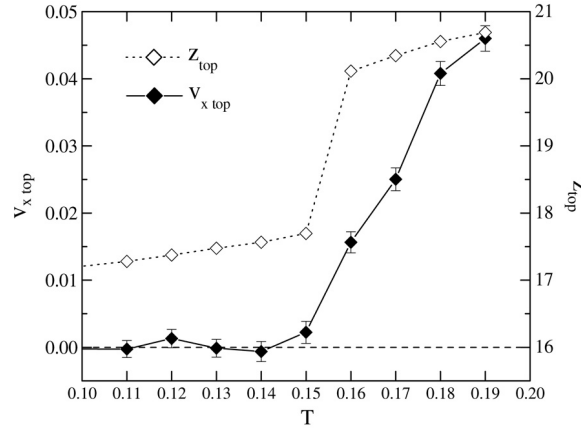

Fig. 22. Comparison between the temperature variation of z_{top} and of the equilibrium velocity of the top substrate when a small shear stress, $f = 0.001$ per one substrate atom of the rigid layer of the top substrate, is applied to the system (soft lubricant, $N_l = 3$).

diffusion coefficient parallel to the layers $D_\parallel$ and the diffusion coefficient orthogonal to the layers D_z, which is one order of magnitude smaller than $D_\parallel$ but nonzero, both show a similar temperature variation. The diffusion coefficient increases sharply when T reaches the melting temperature, but it is already rather large for $T < T_m$. In this domain its temperature dependence may be approximated by an Arrhenius law $D \propto \exp(-E_a/T)$ with $E_a \approx 0.16$, indicating an activated process (it is interesting that, according to simulation, $E_a \approx k_B T_m$). A high diffusion in the solid confined film was observed experimentally [166]. Thus, MD simulations as well as the experiments point out that the mobility of the atoms in a highly confined solid is much greater than in a bulk solid phase. This can be understood qualitatively by the influence of the substrate which distorts the perfect solid configuration
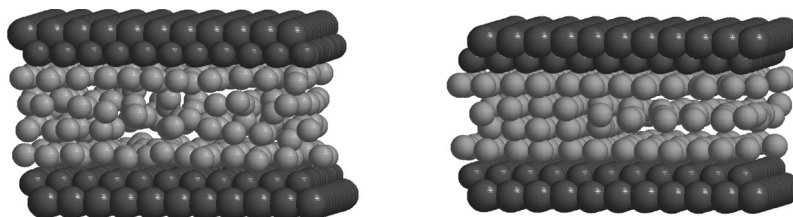
Fig. 23. Configurations of the soft lubricant with $N_l = 3$ upon freezing at $T = 0.13$ (left panel) and after freezing in a metastable configuration at $T = 0$ (right panel). Figures were produced with RasTop software [167].

because it is generally incommensurate with the solidified film. Therefore, the solid phase of the film is formed of ordered domains separated by grain boundaries, or discommensurations. Within these discommensurations the atomic density is generally lower than in the ordered domains, leaving vacant space for diffusion.

When one cools down the melted film, Fig. 19 shows that it does not retrace the path observed during heating, but demonstrates a large hysteresis between melting and freezing, as could be expected for the first-order melting transition. For very thin films ($N_l = 1$ or 2), a sharp freezing transition is observed at a temperature significantly lower than T_m. For the soft lubricant, the freezing restores the structure that the film had at the same temperature before the melting transition. Hard lubricant films as well as thicker soft lubricant films freeze in a metastable state. Fig. 23 shows sample configurations for a film having initially three layers ($N_l = 3$). In Fig. 23, one notices that a defected 4-layer configuration persists below T_m, and when the film is cooled down to $T = 0$, a configuration having three layers in one region and four layers in another is found. Annealing of such a configuration in the presence of a small shear may bring the film back to its equilibrium state (see also Section 5.5). The qualitative difference between the behaviors of narrow films ($N_l = 1$ and 2) and thicker ones ($N_l \geq 3$) is due to the influence of the substrate. For $N_l = 1$ or 2, all lubricant layers interact with the substrates which tend to impose a given configuration. This is not the case for thicker films. The specificity of $N_l = 2$ with respect to higher values was also observed in experiments attempting to decrease the thickness of a lubricant film by applying a strong pressure [160–162]. Pressure alone is not sufficient to decrease the width below $N_l = 3$ but, by applying additionally a shear stress, the lubricant width can be decreased down to two layers.

In an actual tribological system, the surfaces are not perfectly flat. In order to study an influence of the quality of the confining surfaces, simulations with curved surfaces were also performed [165]. In these cases the sharp jump in z_{top} is no longer observed and is replaced by a smooth evolution. This effect has a simple explanation. The spatial variation of the thickness of the film leads to the coexistence of domains that do not have the same number of layers. The melting of these domains should occur at different temperatures, the thicker regions start to melt first and then drive the melting of the thinner regions. Moreover, as the boundary between domains with different thicknesses is full of defects in the atomic packing, they also contribute to preventing a well defined transition, and the melting is blurred. However, the effect of substrate curvature is exaggerated by the small size of the simulated system. In an actual experiment one can expect that flat surfaces will extend over hundreds of lattice spacings, allowing melting to occur rather sharply.

The dependence $T_m(N_l)$ can be calculated analytically with the help of a theory based on the empirical Lindemann criterion. Recall that it states that melting starts when the amplitude of mutual displacement
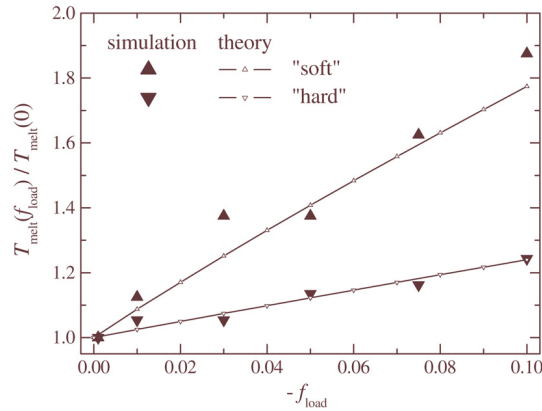
Fig. 24. Dependence of the melting temperature on the load for the $N_l = 3$ system: comparison of the phenomenological theory with simulation data.

of nearest neighboring atoms reaches some threshold value of order 10% of the lattice constant. At higher amplitude of vibrations the anharmonicity effects become too strong and destroy the crystalline order. In the case of a thin film, mutual displacements are expected to decrease for the confined film, where the oscillations of the boundary atoms are suppressed. Therefore, one expects the increase of the melting temperature as compared with the bulk value. Such a theory was developed by Braun and Peyrard [165]. The calculations show that, as expected, the mutual displacements are maximal at the lubricant–substrate interface for the hard-lubricant case, and at the middle of the soft-lubricant film where the internal interactions are weaker than the interactions with the substrates. Then, using the Lindemann criterion, one may assume that in the hard-lubricant system the melting starts at the interface, while in the soft-lubricant case the melting starts in the middle of the lubricant. As one can see from Fig. 20, the agreement between the theory and simulation is fairly good. Moreover, the described approach can also be used to study the effect of the external pressure. When $f_{load} \neq 0$, the interatomic distances should correspond to the minimum of the potential $V_f(r) = V_{LJ}(r) - z f_{load}$. When the load grows, the equilibrium distance corresponding to the minimum of $V_f(r)$ decreases and, due to the anharmonicity of the LJ potential, the strength of the interaction increases. This results in the increase of the melting temperature with load as shown in Fig. 24.

Thus, the dynamics of the confined film is significantly affected by the substrates, both in the solid and in the molten phases. The solid phase, able to sustain shear stress, shows intense diffusional motion of the atoms. The melting temperature depends strongly on the confinement, and this dependence may be explained by a phenomenological microscopic theory based on the Lindemann criterion.

5.3. A soft lubricant: The melting–freezing mechanism

The first systematic MD study of sliding for two substrates separated by a thin lubricant film, based on Langevin motion equations, has been done by Thompson and Robbins [151,152]. The authors considered the case of the soft lubricant, when the amplitude of molecular interactions in the lubricant, V_{ll}, is weaker than the lubricant–substrate interaction, V_{sl}. It was shown that for the film of width $\gtrsim 10$ molecular diameters at the temperature $k_B T = 1.1 V_{ll}$ (which is about 30% above the bulk melting temperature), for the case of $V_{sl} \geq 2 V_{ll}$ one lubricant layer is locked to the corresponding substrate (i.e., one layer

is glued to the bottom, and one to the top substrate), while slip occurs within the lubricant, between the first and second layers. If the lubricant–substrate interaction increases, e.g. for $V_{sl} \geq 15 V_{ll}$, then two (instead of a single) lubricant layers are glued to each (top and bottom) substrates. When the top substrate is driven with a low velocity through an attached spring, the system dynamics demonstrates stick–slip motion due to the melting–freezing mechanism.

In this section we describe the results of MD simulation of the soft-lubricant system based on the model of Section 5.1. The simulations show that the behavior of a thick lubricant (of three or more layers wide) and a thin lubricant (less than two layers wide) is qualitatively different.

5.3.1. A thick lubricant film ($N_l \geq 3$)

In the case of the soft lubricant film ($V_{ll} = 1/9$) of thickness larger than two atomic layers, the stick–slip motion corresponds to the melting–freezing mechanism. At low driving the lubricant undergoes periodic shear-melting transitions and recrystallization, while at high velocities uniform sliding occurs where the film no longer has time to order [4,151]). However, a detailed MD study with the help of the constant-force algorithm shows that there are two different steady-state sliding regimes, the "layer-over-layer" sliding (LoLS) regime, when the lubricant layers keep an ordered structure at sliding, and the "liquid-sliding" (LS) regime, when the lubricant is melted due to sliding. These two regimes exist for different intervals of the driving force.

When the top substrate is driven with a constant velocity through a spring, we observe the transition from the stick–slip motion to the smooth sliding which takes place at $v_c \lesssim 0.1$ as shown in Fig. 25 for the $N_l = 5$ system. The maximal frictional force f_s during the stick–slip, $f_s \sim 0.02$, is lower than the static frictional force. This shows that f_s should grow with the time of stationary contact. During stick in the stick–slip regime, the lubricant is ordered in a crystalline five-layer configuration, while the slip corresponds to the LoLS regime, and the sliding occurs typically at the interfaces between the utmost and adjacent lubricant layers. At the onset of the smooth sliding regime, i.e., at $v_s = 0.1$ for the parameters used in Fig. 25, the system dynamics also corresponds to the LoLS regime. When the spring velocity increases, e.g., to the value $v_s = 0.3$, the middle three layers 3D melt (although the lubricant keeps the layered structure) while the utmost layers remain ordered. The distribution $v_x(z)$ exhibits a linear dependence across the lubricant. With further growth of the spring velocity, the temperature (and "disorder") of the lubricant increases. The smooth sliding motion at $v_s \gg 0.1$ corresponds to the liquid-sliding regime. The dependence of the kinetic frictional force, the lubricant temperature and its width on the spring velocity are presented in Fig. 26 by stars. Note that the kinetic frictional force very weakly changes with the spring velocity (and may even slightly decrease when the velocity increases).

Layer-over-layer sliding. The LoLS regime is observed in the constant-force algorithm, if one starts from the $v_s = 0.1$ smooth-sliding state of the spring algorithm (Fig. 25, rightmost column). The simulation results are presented in Fig. 26 by open circles. The LoLS regime is stable for velocities of the top substrate of the order of $v_{top} \sim 0.1$, namely for dc forces $0.03 < f < 0.11$ (for $f_{load} = -0.1$). The velocity remains within the interval $0.05 < v_{top} < 0.3$; the system locks at lower forces/velocities and becomes unstable at larger ones (in the latter case the lubricant structure is destroyed and either the system locks in a defective configuration, or the lubricant film melts and the system goes to the liquid-sliding state). The lubricant effective temperature grows with the velocity but remains lower than the melting one. Therefore, the lubricant is in a "solid" state; however, similarly to what was observed during melting (Section 5.2), there is an exchange of atoms between different lubricant layers in this "solid" state. In the LoLS state the lubricant takes the well-defined configuration as, e.g., shown in
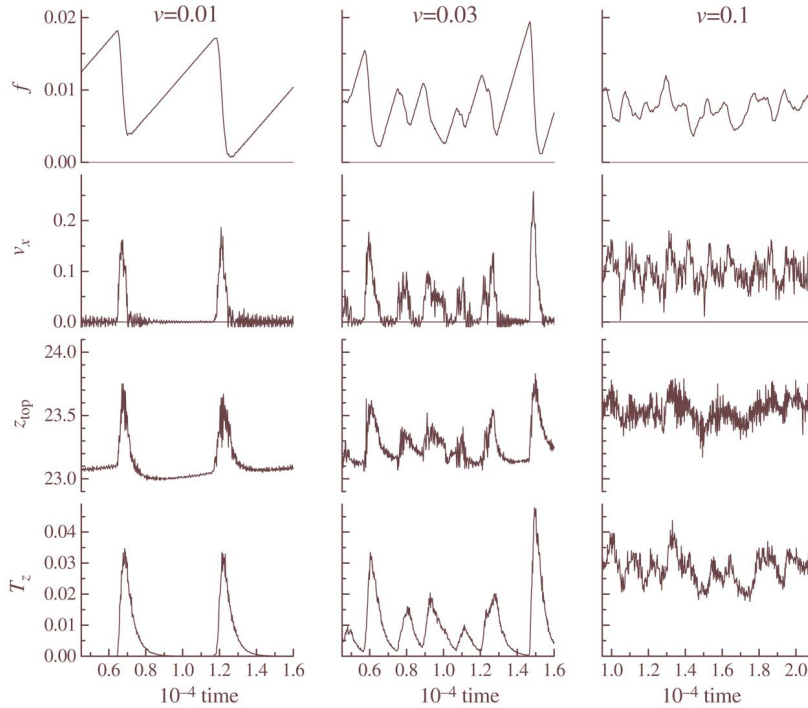
Fig. 25. Dynamics of the $N_l = 5$ soft flat system with the attached spring of the elastic constant $k_{spring} = 3 \times 10^{-4}$ for three values of the spring velocity: $v = 0.01$ (left column), $v = 0.03$ (middle column), and $v = 0.1$ (right column). The top row shows the spring force, the second row shows the velocity of the top substrate, the third row shows the lubricant width, and the bottom row shows the lubricant temperature.

Fig. 27 (left panel); the utmost lubricant layers are glued to the corresponding substrates and move together with them, while the other three layers slide (creep) one over another. This steady-state sliding is, however, not too stable. Due to atomic exchange, the 2D atomic concentrations in the layers may vary during sliding, and when two adjacent layers happen to have close concentrations, they become commensurate, lock together and move with the same velocity, while the main sliding occurs at the most "incommensurate" interface.

Liquid sliding. The LS regime exists for dc forces $f > 0.01$; at lower forces the system locks in a metastable defective configuration such as that shown in Fig. 27 (right panel). The dependences of the system parameters on the driving velocity are shown in Fig. 26 by solid circles. For a lower force $f = 0.011$, the system exhibits smooth sliding with $v_{top} \sim 1$. In this regime the two utmost layers are approximately ordered and glued to the corresponding substrates, while the middle layers are 3D molten (see Fig. 27, middle panel). When the force increases to $f = 0.012$, the whole lubricant becomes 3D molten, and $v_{top} \gg 1$. The sliding heats the lubricant to a temperature larger than the melting one, so that the driving itself maintains the lubricant in the melted state.

Energy losses. Fig. 28 shows the distribution of energy losses across the lubricant calculated by the method described in Ref. [157]. The results are presented for two sliding regimes of the $N_l = 5$ system, the LoLS regime and the LS regime. In both cases the largest losses are in the rigid substrate layers. In the LS regime, when the velocity linearly changes with z, the losses are approximately uniformly
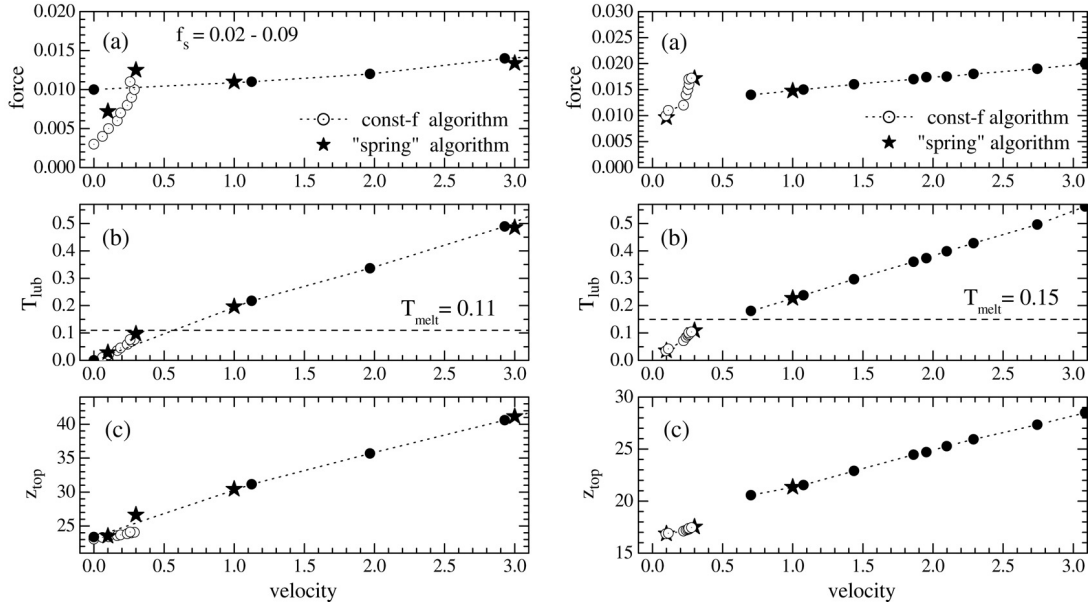
Fig. 26. Kinetic frictional force (a), the lubricant "temperature" (b), and the width of the lubricant film (c) as functions of the driving velocity for the soft $N_l = 5$ (left panel) and $N_l = 3$ (right panel) systems with flat geometry. Stars show the data obtained with the help of the spring algorithm, while circles and dashed curves show the results obtained with the constant-force algorithm (open circles are for the layer-over-layer sliding regime, and solid circles are for the liquid-sliding regime).
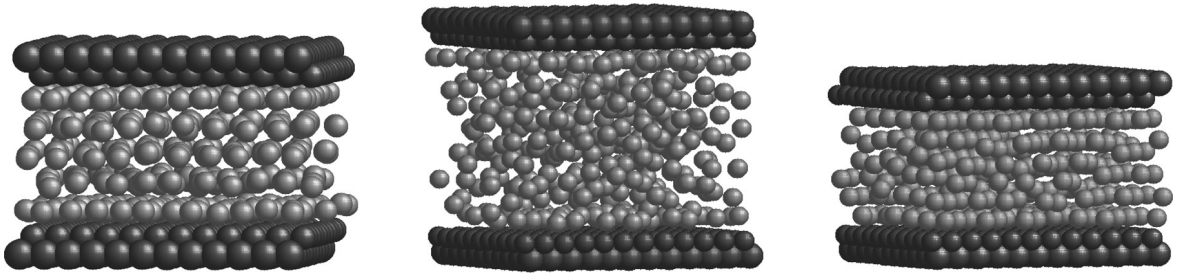

Fig. 27. Configurations of the $N_l = 5$ soft lubricant with flat geometry. Left panel: the configuration during layer-over-layer sliding at $f = 0.008$. Middle panel: the configuration in the liquid sliding at $f = 0.011$. Right panel: the configuration when the system locks at $f = 0.01$ after the LS state.

distributed across the lubricant. However, in the LoLS regime, where the sliding takes place mainly between the layers 1–2, 2–3 and 4–5 (while the third and fourth layers move together), the losses are large just where the sliding takes place as one could expect.

Transitions between different steady states. The sliding regimes described above, typically cannot be obtained with the help of the constant-force algorithm by adiabatic increase of the driving if one starts from the annealed static configuration. For example, for the $N_l = 5$ system the static frictional force, $f_s \sim 0.02$–0.09, is much larger than driving forces in the steady-state regimes. Therefore, the lubricant film melts just when it begins to move at $f = f_s$, the two substrates split one from another, and the velocity v_{top} of the top substrate goes to infinity. Moreover, the LoLS regime cannot be obtained
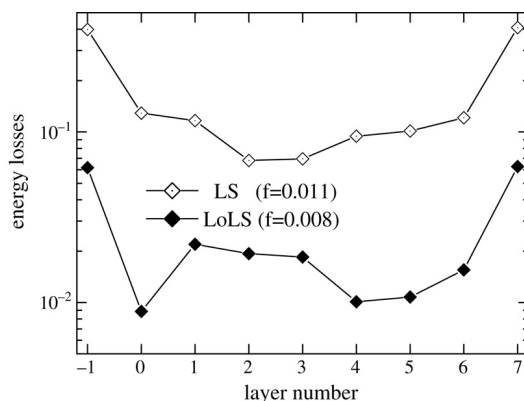
Fig. 28. Distribution of the energy losses across the soft lubricant for the $N_l = 5$ system with flat geometry. The lower curve is for the LoLS regime ($f = 0.008$), and the upper curve, for the LS regime ($f = 0.011$). The numbers -1 and 7 correspond to the rigid substrate layers, the numbers 0 and 6 correspond to the mobile substrate layers, and the numbers 1–5 correspond to the lubricant layers.
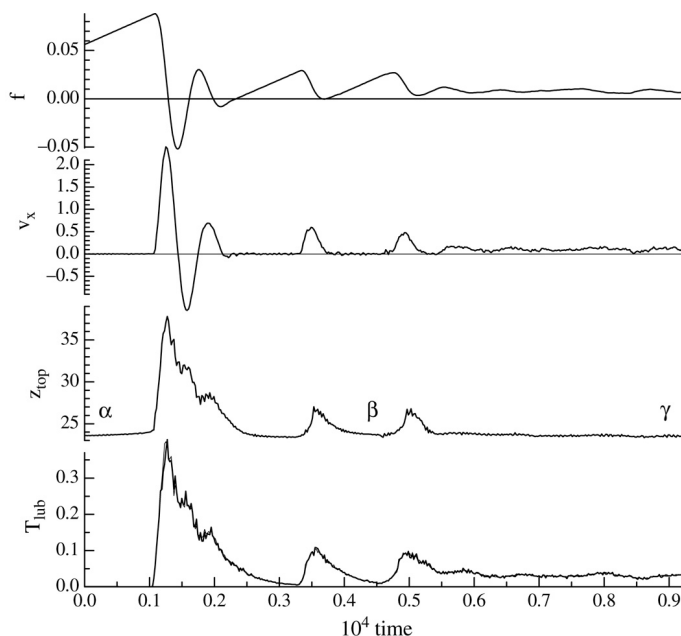

Fig. 29. Sliding-induced self-ordering of the soft lubricant: evolution of the flat $N_l = 5$ system at $v_s = 0.1$.

from the LS regime too; the liquid-sliding state locks when the driving decreases adiabatically. The only transition observed with the adiabatic change of the force, is the one from the LoLS state to the LS state with the increase of the driving force. However, both sliding regimes are observed in the simulation with the spring algorithm, when the spring force decreases after the slip onset. Note also that for the thinner $N_l = 3$ lubricant, the LoLS regime is more stable than for a thicker ($N_l = 5$) one.

Sliding-stimulated ordering of the lubricant. When the lubricant slides due to driving through the attached spring at a low velocity, it can self-order as, e.g., is demonstrated in Fig. 29. For example, if one
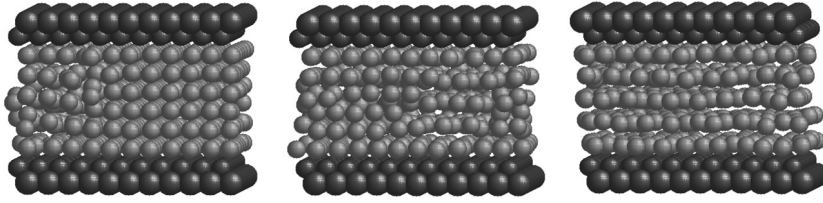
Fig. 30. Self-ordering of the flat $N_l = 5$ system during its sliding with the velocity $v_s = 0.1$ as shown in Fig. 29: the configurations "α" (left panel), "β" (middle panel), and "γ" (right panel).

starts from an annealed configuration like that shown in Fig. 30 (left panel), which corresponds to the starting point "α" of Fig. 29, then the sliding begins when the spring force achieves the value $f \sim 0.09$, while the typical driving force is about $f \sim 0.01$ for smooth sliding. In the result, the lubricant melts during slip and then freezes again during stick, but now in a more ordered configuration, e.g., like that shown in Fig. 30 (middle panel), which corresponds to the point "β" of Fig. 29 and is characterized by $f_s \sim 0.02$–0.03. After several such cycles, the lubricant finally takes an ordered five-layer configuration as shown in Fig. 30 (right panel), which corresponds to the final point "γ" of Fig. 29. After that, the system exhibits the LoLS smooth-sliding regime, and freezes in an ordered five-layer configuration if the driving decreases.

Onset of sliding. Fig. 29 also demonstrates possible mechanisms of the beginning of sliding. It is evident that the threshold force f_s and the system dynamics at the onset of sliding first of all depend on the starting configuration. Namely, if the starting configuration contains a small concentration of defects that pin the substrates (such as shown in Fig. 30, middle panel) so that f_s only slightly exceeds the kinetic frictional force, then the interstitial defective atoms are pulled back into the lubricant layers, the lubricant film is ordered, and the sliding begins with the layer-over-layer regime. On the other hand, when the starting configuration is far from the ordered sliding configuration (e.g., as the annealed configuration like that shown in Fig. 30, left panel), then at the onset of sliding the lubricant has to be reordered by plastic deformation/flow, its effective temperature grows above the melting one, and the lubricant film melts almost immediately with the beginning of sliding.

Role of the load. The sliding mechanisms described above remain qualitatively the same for other values of the loading force. A change of f_{load} only shifts the threshold force f_s, the force intervals for the LoLS and LS regimes and the critical velocity v_c. The dependences of these parameters on f_{load} are approximately linear. For example, for the $N_l = 5$ system with the help of the spring algorithm we obtained for the kinetic frictional force the dependence $f_k \approx f_{k0} + \alpha_k f_{\text{load}}$ with $f_{k0} \approx 0.0022$ and $\alpha_k \approx 0.05$ for the LoLS regime at $v_s = 0.1$. For the LS regime at $v_s = 0.3$ we again found a linear dependence, but now with the parameters $f_{k0} \approx 0.0029$ and $\alpha_k \approx 0.097$. Emphasize that in both sliding regimes the coefficients α_k are much smaller than that for the static frictional force, where $\alpha_s \sim 0.5$. It is interesting also that the parameter f_{k0} is positive. For example, for the LoLS regime one should apply a negative load ($f_{\text{load}} \approx 0.044$; recall that positive f_z moves the top substrate upward) to break the interatomic forces within the lubricant and to pull the surfaces away one from another to obtain the zero friction.

Role of the substrate temperature. For the soft lubricant, the mobility increases with T, i.e., the kinetic friction decreases when the substrate temperature increases. However, in the LS regime, when the lubricant is melted due to driving, the substrate temperature has almost no effect provided T is not too close to T_m. If $T < T_m$, then the system is still locked at low forces, i.e., the system exhibits the
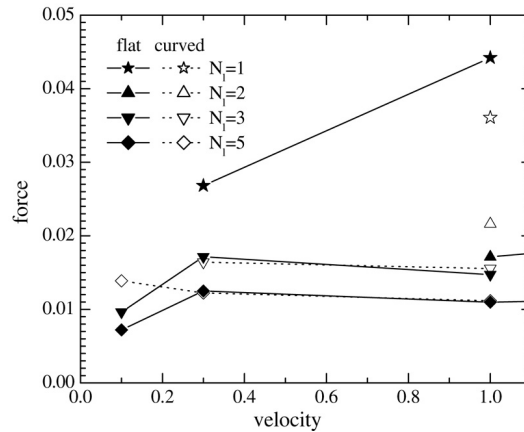
Fig. 31. The kinetic frictional force versus the driving velocity for the flat (solid symbols and curves) and curved (open symbols and dashed curves) geometry for different widths of the lubricant: $N_l = 1$ (stars), 2 (triangles), 3 (down triangles) and 5 (diamonds).

stick–slip behavior at low spring velocities, although the threshold values of the force f_s and the velocity v_c decrease when T increases. At temperatures close to or higher than T_m, on the other hand, there are no sharp transitions between the stick–slip and smooth sliding regimes: instead of the stick–slip behavior one observes a creep motion at low driving velocities in this case. When T is larger than T_m, then the velocity is nonzero at any $f > 0$.

Finally, note that a thinner lubricant is characterized by a higher kinetic friction as summarized in Fig. 31.

5.3.2. A thin lubricant film ($N_l \leq 2$)

The system behavior changes qualitatively for very thin lubricant films, $N_l \leq 2$, when *all* lubricant atoms directly interact with the substrates.

In the case of a *two-layer* lubricant film, $N_l = 2$, both its layers are glued to the corresponding substrates in the immobile state, and the film structure is crystalline. As a result, the static frictional force is high, $f_s \sim 0.06$, and does not change essentially with the time of stationary contact. Because of so large a value of the static frictional force, the lubricant always melts at the beginning of sliding, so that the LS regime exists only. The hysteresis of the $v_{top}(f)$ dependence, as well as the mechanism of the stick–slip motion, always corresponds to the melting–freezing one. Due to the large value of f_s, the threshold velocity of the transition to the smooth sliding regime, $v_c \sim 0.6$, is also much higher than for a thicker lubricant film.

The kinetic frictional force again only slowly depends on the driving velocity, e.g., f_k changes from 0.016 to 0.03 for the velocities $v_{top} = 0.6$–5, and again it is much lower than the static frictional force. All this is reasonable, because the lubricant is melted during sliding. As an example, Fig. 32 demonstrates the configurations of the system with the curved top substrate. The annealed configuration in this case corresponds to two lubricant layers in the narrow region and three layers in the wide region; the same configuration is observed during stick at velocities $v_s < v_c$ (Fig. 32, left panel). The static frictional force, $f_s \sim 0.06$–0.08, is determined by the atoms which are confined in the narrow region. At the onset of sliding, first the LoLS regime is observed: the bottom layer remains immobile (glued to the bottom
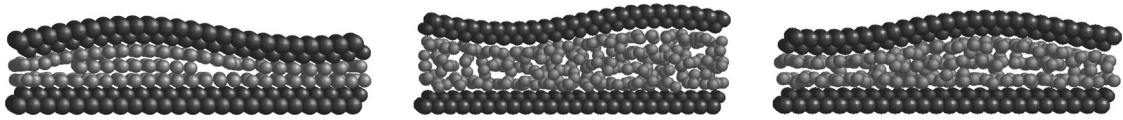
Fig. 32. Configurations of the curved $N_l = 2$ lubricant during stick–slip with $v_s = 0.1$ in the stick (left panel) and slip (middle panel) states. Right panel: the configuration in the smooth sliding regime with $v_{\text{spring}} = 1$.

substrate), the top layer is glued to and moves together with the top substrate, and the middle layer which is present in the wide region only, also moves with the top substrate. Then, due to growth of the velocity during the slip, first the middle layer and soon the whole lubricant 3D melts (Fig. 32, middle panel), and the LS regime is achieved. In the smooth sliding regime, $v_s > v_c$, the lubricant is always melted, but the steady-state configuration now depends on the sliding velocity: at lower values of the velocity, $v_s \gtrsim v_c$, the lubricant still has two layers in the narrow region and three layers in the wide region (Fig. 32, right panel), while at higher velocities it is completely 3D melted (Fig. 32, middle panel).

For the *one-layer* lubricant film, $N_l = 1$, the static frictional force is the largest, $f_s \gtrsim 0.1$. Contrary to the scenarios described above for thicker films, the one-layer film does not melt during sliding (in the case of flat geometry). At the onset of sliding in this case we first observe the motion of two domain walls which soon transform into a channel of moving lubricant atoms, and then the transition to the "running" state of all lubricant atoms is observed. This scenario is similar to that observed for a driven adsorbed layer [168]. The stick–slip motion is now due to an inertia mechanism similar to the hard-lubricant system (see Section 5.4 below). The reason is that the melting temperature of the very thin film is very high. Moreover, the kinetic frictional force essentially depends on the velocity, approximately as $f_k \approx 0.05\, v_{\text{top}}$ (see Fig. 33, solid symbols). The threshold velocity for the transition to smooth sliding is now $v_c \lesssim 0.3$, i.e. it is lower than that for the melting–freezing mechanism of the two-layer film (but still much higher than for thick films).

In the case of curved geometry, however, the $N_l = 1$ lubricant film does melt at the beginning of sliding. For the constant-force algorithm, the kinetic friction slowly changes with the velocity, $f_k \approx 0.02\, v_{\text{top}}$ (Fig. 33, open symbols), which is closer to what was observed for thicker lubricant films. Recall that the annealed $T = 0$ configuration corresponds in this case to a crystalline structure with one layer in the narrow region and two layers in the wide region as shown in Fig. 34 (left panel). The static friction is determined by pinning the substrates in the narrow region, where the structure of the lubricant film is commensurate with both substrates. When the system begins to move at $f = f_s$, the lubricant 3D melts (see Fig. 34, middle panel), and its temperature increases up to $T \sim 1$ which is much higher than the melting temperature. If the applied force varies in this LS regime, the velocity, the lubricant temperature and its width change linearly with the force. If the force decreases, at $f \approx 0.067$ the velocity v_{top}, the lubricant temperature and its width jump-like decrease, and the lubricant structure changes to a well-layered configuration where, however, the layers are 2D disordered (see Fig. 34, right panel). In this case the LoLS regime operates. With the further decrease of the force, the velocity decreases approximately linearly with f until it reaches a value $v_{\text{top}} = v_b \approx 0.17$ at $f = f_b \approx 0.023$. After that, the sliding stops, and the lubricant again takes almost ideal configuration. Thus, the lubricant freezes in a more ordered state, and in the next stick–slip events the film remains ordered during sliding (the stick–slip is due to inertia mechanism).
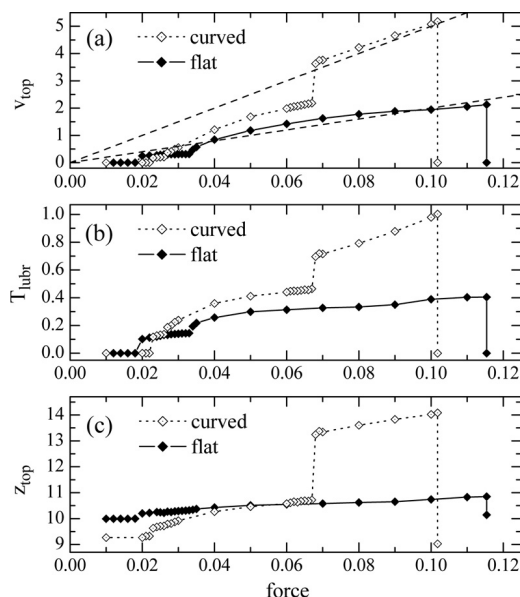
Fig. 33. Velocity of the top substrate (a), lubricant temperature (b) and its width (c) as functions of the applied dc force for the one-layer soft lubricant film. Solid symbols are for flat surfaces, and open symbols, for the curved geometry. Dashed lines in (a) correspond to linear fits described in the text.
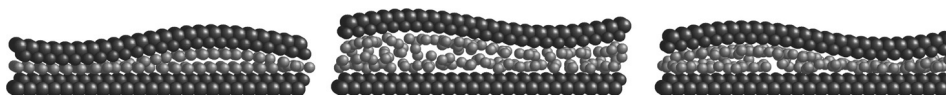

Fig. 34. Configurations of the $N_l = 1$ soft lubricant with the curved geometry. Left panel: configuration just prior the sliding at $f = f_s - 0 \approx 0.102$. Middle panel: configuration during sliding at $f = 0.07$ when $v_{top} \approx 3.7$. Right panel: configuration during sliding at $f = 0.06$ when $v_{top} \approx 2$.

Finally, a rather detailed MD simulation of kinetic friction for *submonolayer* lubricant films has been done by He and Robbins [130,131]. In these simulations the substrates were also rotated relatively each other to some angle in order to study incommensurability effects. The main result of simulation is that the tribological kinetic friction μ_k satisfies Amontons' law (friction is proportional to load), it only weakly depends on the temperature and on the strength of the substrate–lubricant interaction, and μ_k takes values of order 75%–85% of the static friction coefficient. He and Robbins [130,131] have observed that at low driving velocities (e.g., $v < 1$ m/s) the motion corresponds to a creep motion, i.e., to the "atomic-scale stick–slip" which, clearly, may only weakly depend (due to "memory effects") on the driving velocity. Only some (few) atoms overcome the barriers of the substrate potential at the same time moment, and these atoms move ("pop") with high (atomic-scale) peak velocities. These observations may explain why the kinetic frictional force is approximately equal to the static frictional force for submonolayer lubricants, as well as why the experimentally measured kinetic friction often does not depend on the velocity.

The friction strongly depends on the commensurability between the substrate lattice constant and the mean distance of the interaction in the lubricant. However, the friction coefficient is insensitive to the concentration of lubricant atoms (for $\theta < 1$), because increasing the number of atoms spreads the load and the driving force over more atoms. Also, it was found that μ_k logarithmically depends on the sliding velocity: the coefficient α in the Amontons' law depends on the driving velocity as $\alpha \approx C \ln v$ with $C \approx 1.1 \times 10^{-3}$. Such a dependence may be explained as emerging due to thermally activated atomic jumps.

5.4. A hard lubricant: The perfect sliding

The soft lubricant considered in the previous section belongs to conventional lubricants. Its main advantage is that due to strong coupling with the surfaces, the lubricant is hardly to be squeezed out from the contact area. Besides, due to sliding-induced melting of the lubricant film, it provides a relatively low kinetic friction.

The use of hard lubricants, which remain in a solid state at sliding, is also very promising, especially in nano- and microdevices. Well known examples include layered materials such as graphite, MoS_2 and Ti_3SiC_2. The reason of low frictional forces for solid lubricants is in incommensurability between two crystalline surfaces. In an ideal case, when two 2D surfaces are incommensurate or at least not perfectly aligned, the static friction is zero, and the kinetic friction is very low too. However, if the ideal crystalline structure of the lubricant is destroyed, i.e., due to sliding, it may take an amorphous structure characterized by a quite high friction.

The hard-lubricant system with $V_{sl} \leq 0.4 V_{ll}$ was firstly studied by Thompson and Robbins [151]. It was shown that for the film of width $\gtrsim 10$ molecular diameters at $k_B T = 1.1 V_{ll}$ (i.e., 30% above the bulk melting temperature), the lubricant slides over the substrates at slip, so that there is a jump Δv_x of velocity between the substrate and the first lubricant layer; the jump Δv_x decreases when the ratio V_{sl}/V_{ll} increases. The case of an amorphous lubricant has also been studied by Thompson et al. [44]. The authors observed that when the lubricant (made of chain molecules) is frozen in a glassy state, all the shear occurs at the interface. Below in this section we describe, following Ref. [157], the simulation results obtained with the help of the model of Section 5.1 for the hard-lubricant system.

Rigid lubricant: the "universal" dependence. In the solid-sliding regime, when the top rigid substrate with one attached s-layer moves as a whole with the velocity $\langle v_{\text{top}} \rangle$, the bottom rigid substrate with one attached s-layer does not move at all, and the lubricant film moves as a whole with the velocity $v_l = \frac{1}{2} \langle v_{\text{top}} \rangle$, the *washboard frequency* is equal to

$$\omega_{\text{wash}} = 2\pi v_l/a_s = \pi \langle v_{\text{top}} \rangle/a_s. \tag{28}$$

The balance of forces for the top substrate takes the form $F \equiv N_s f = N_{al} m_l \eta^* v_l$, where we introduced the total viscous damping coefficient η^* for an atom in the utmost lubricant layer. In the "perfect-sliding" approximation the atoms in the utmost lubricant layers feel only the external damping $\eta_{\text{ext}}(v_{\text{top}}) \approx \eta_1(z_l) [\eta_{\text{ph}}(\omega_{\text{wash}}) + \eta_{\text{eh}}]$ due to energy exchange with the substrates. Assuming that $\eta^* = \eta_{\text{ext}}$, we obtain a *"universal" ("perfect-sliding") dependence*

$$v_{\text{top}}^{(\text{uni})}(f) = \frac{2N_s}{N_{al}} \frac{f}{m_l \eta_{\text{ext}}}. \tag{29}$$

The dependence (29) depends neither on the number of lubricant layers nor on the substrate mass, because it describes the steady state. It is shown in Fig. 35 together with simulation results for the
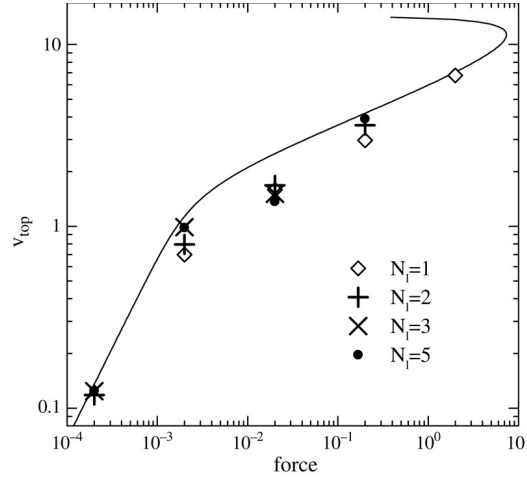
Fig. 35. The "perfect-sliding" dependence (29) and the $T = 0$ simulation results for the hard lubricant with the ideal structure.

hard lubricant. One can see that they agree rather well at small ($f < 10^{-3}$) as well as at high ($f > 1$) forces, when the washboard frequency lies outside the lubricant phonon spectrum and, thus, the internal motions of the lubricant are not excited. The following two conclusions follow from the dependence (29): (i) at small forces, $f_b \lesssim f \ll f_f$, the effective friction is very small, $\eta_{\text{eff}} \propto \omega_{\text{wash}}^4 \propto v_{\text{top}}^4$, and (ii) the maximal driving force and velocity are $f_{\max} < 7$ and $v_{\max} < 11$ (these values are determined by the model parameter ω_m). A further increase of f leads to unstable motion, because the pumped energy cannot be taken out from the system.

   The simulation results for the lubricant with the ideal crystalline structure. The results of simulation for the hard lubricant with the ideal crystalline structure are presented in Figs. 35 and 36. These results can be summarized as follows:

- At $v_{\text{top}} \sim 1$, when the washboard frequency is within the phonon zone of the lubricant, the $v_{\text{top}}(f)$ dependence exhibits a plateau due to excitation of phonons within the lubricant. These resonances can in principle be described analytically [157]. Unfortunately, this approach is not too useful, because it uses a number of poorly defined fitting parameters.
- The dependence $v_{\text{top}}(f)$ exhibits *hysteresis* as shown in Fig. 36. The sliding starts when the driving force exceeds the static friction f_s. Then, if the force f decreases down below the backward threshold $f = f_b \ll f_s$, the velocity drops from a finite value $v = v_b \sim 0.03$–0.1 to zero, and the system comes back to the crystalline configuration. The minimal values f_b and v_b are discussed below in Section 6.1.
- *The lubricant is heated due to driving.* The distributions of velocities for all forces can be approximated by Gaussian curves if we use *different* "temperatures" for the lubricant and the s-atomic substrate layers as well as for different degrees of freedom. Therefore, the effective lubricant temperature can be introduced as $T_\alpha = m \langle (v_\alpha - \langle v_\alpha \rangle)^2 \rangle$, where $\langle \ldots \rangle$ designates the averaging over time and, e.g., over all atoms in a given layer. The simulations [157] show that (i) the lubricant temperature increases with f until it finally melts at some $f = f_f$, and (ii) $T_z \gg T_x \gtrsim T_y$ so that the driven system is strongly *out of equilibrium.* At low forces or velocities the temperature is not uniformly distributed over the lubricant film; the boundary layers which are in moving contact
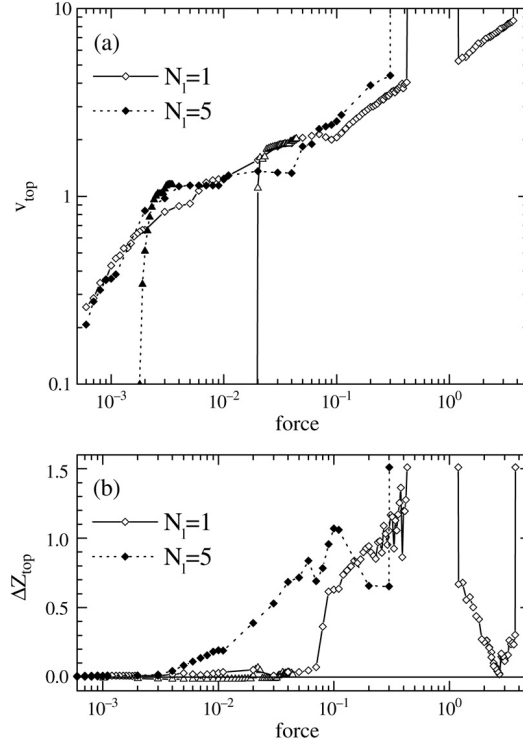
Fig. 36. The dependences of the velocity of the top substrate v_{top} and the change of the lubricant width Δz_{top} as functions of the driving force f for the hard lubricant with the ideal crystalline structure. Open symbols are for one-layer film, and solid symbols, for $N_l = 5$.

with the substrates have a higher temperature than those in the middle of the lubricant. But at large forces, $f \sim 0.02$–0.2 when $v_{top} \sim 1$–4, the lubricant temperature is approximately uniform across the lubricant. This indicates that anharmonicity effects, which are responsible for energy exchange between different layers within the lubricant, become large enough at high driving.

- *The energy losses are mainly at the sliding interfaces.* The simulations [157] show that the energy is lost mainly due to the motion of atoms along the direction x of the driving. The energy is lost mainly within the rigid substrates and in the utmost lubricant layers (i.e., in the layers which are in moving contact with the substrates) as has to be expected.

The simulation results obtained with the help of the algorithm with the attached spring are presented in Fig. 37 for the $N_l = 3$ system, which demonstrates a typical behavior. The sequence of the transitions with the increase of the driving velocity is the following: stick–slip at low velocities $\rightarrow$ irregular (chaotic) motion at an intermediate velocity $\rightarrow$ smooth sliding corresponded to perfect-sliding regime at high velocities. In the stick–slip regime, the lubricant "temperature" increases during slips but remains much lower than the melting temperature, $T_{lub} \ll 0.1$. The lubricant width also increases just at the onset of sliding, but the variation is very small, less than 1%. The critical velocity of the transition from stick–slip to smooth sliding is $v_c \sim v_b$, e.g., $v_c \gtrsim 0.03$ for the $N_l = 3$ system; it is larger for $N_l = 1$ ($v_c \sim 0.1$) and smaller for $N_l = 5$ ($v_c \sim 0.03$). During smooth sliding the kinetic frictional force is extremely small, $f \sim 10^{-4}$–10^{-3}, and strongly increases with the driving velocity (so that the second Amontons' law
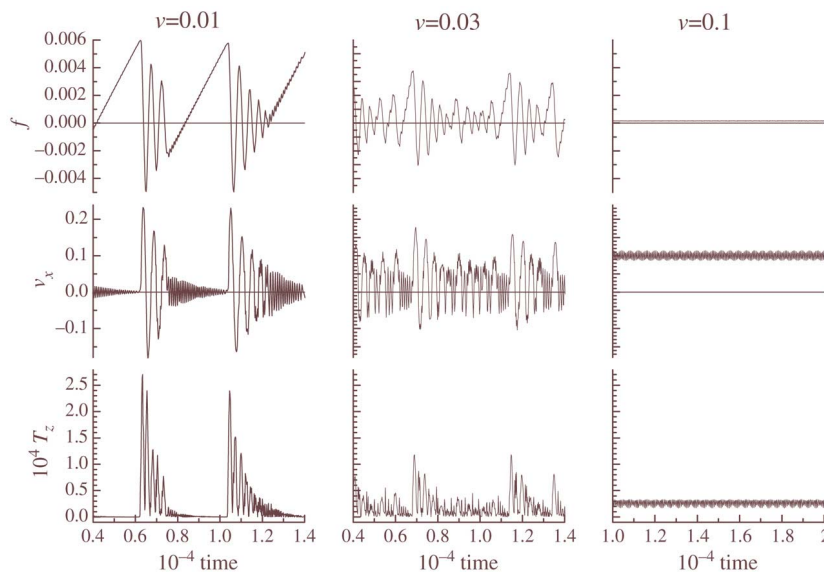
Fig. 37. System dynamics of the $N_l = 3$ crystalline lubricant between flat substrates obtained with the attached spring algorithm (the elastic constant of the spring is $k_{spring} = 3 \times 10^{-4}$) for three values of the driving velocity: $v = 0.01$ (left column), $v = 0.03$ (middle column) and $v = 0.1$ (right column). The top row shows the spring force, the middle row, the velocity of the top substrate, and the bottom row, the lubricant temperature.

does not operate for the perfect sliding). Also, the static frictional force in the stick–slip regime does not depend on the driving velocity, i.e., we do not observe any "aging" of the lubricant film.

Amorphous lubricant. As was described in Section 5.2, if the temperature increases above T_m and then decreases back to zero for the hard-lubricant system, the lubricant film freezes in a metastable state and takes a configuration with defects and/or dislocations, which we will call "amorphous". The static frictional force is not uniquely defined in the case of "amorphous" lubricant, because f_s depends on a given metastable configuration. The same is true for the dependence $v_{top}(f)$. A typical example is shown in Fig. 38 for the $N_l = 5$ system. In the solid-sliding regime the lubricant film slides as a whole. The sliding may be asymmetric, especially at low driving — the lubricant film may stick to either the bottom or the top substrate, so that the sliding takes place at a single lubricant/substrate interface. The lubricant is heated due to sliding (now $T_x \approx T_y \approx T_z$), but its temperature remains below T_m, so that the lubricant keeps the configuration with defects. The mobility of the frozen lubricant is much smaller than that of the ideal hard lubricant film for the same interval of the forces. However, during sliding the lubricant may reorder as will be described in Section 5.5; that results in the increase of v_{top}.

Using the algorithm with the attached spring for the "amorphous" lubricant, we again see the typical scenario of the transition from stick–slip to smooth sliding. But because f_s is much larger in this case than for the lubricant with the ideal structure, v_c is also larger, e.g., for the flat geometry we obtained $v_c \gtrsim 0.5$ for $N_l = 2$ and $v_c \lesssim 0.3$ for $N_l = 3$ and 5. The typical dependences are shown in Fig. 39 for $N_l = 2$ (top row) and $N_l = 5$ (bottom row).

Role of temperature. The $v_{top}(f)$ dependences at different temperatures of the substrate are shown in Fig. 38. When the driving force is below the static frictional one, $f < f_s$, so that the velocity is zero in the $T = 0$ case, in the $T > 0$ case the velocity increases with T due to thermally activated (creep) motion.
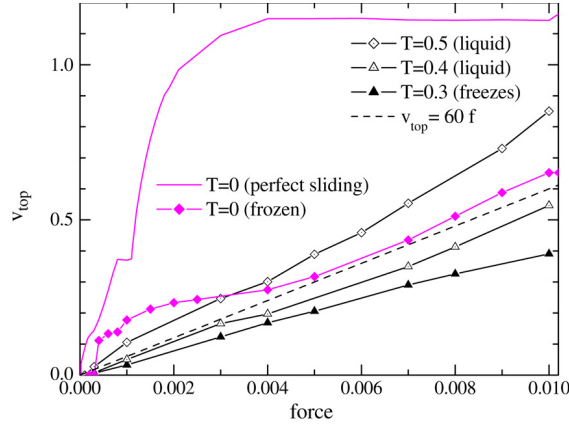
Fig. 38. v_{top} versus f for the $N_l = 5$ flat "amorphous" system at different temperatures as shown in the legend.
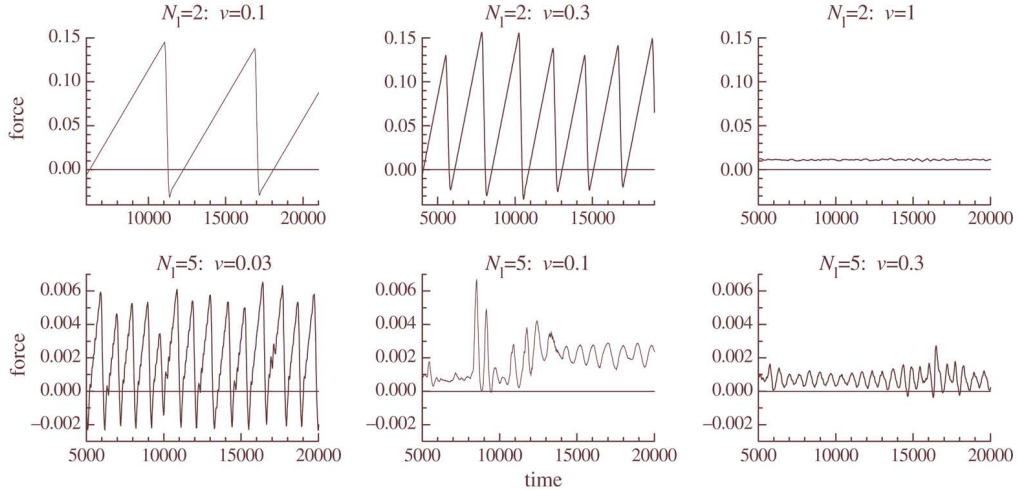

Fig. 39. The frictional force versus time obtained with the spring algorithm for three values of the driving velocity (as indicated in the legend) for the $N_l = 2$ (top row) and $N_l = 5$ (bottom row) flat "amorphous" system.

However, if the system is in the perfect solid-sliding regime, then v_{top} decreases with T increasing up to the temperature when the film melts. With further increase of T, when the lubricant is in the molten state, v_{top} increases, but it remains lower than that for the $T = 0$ perfect-sliding steady state. If then the temperature decreases to zero, the lubricant freezes in a metastable configuration. From Fig. 38 one can see that the mobility of the frozen lubricant is much lower than that of the perfect solid lubricant. Again, however, the velocity decreases when T increases until the lubricant melts; after that v_{top} grows with T. However, if, after the melting, T decreases back to smaller values but the dc force keeps a nonzero value ($f > 0$) so that the system remains in the steady sliding state, then the lubricant film freezes in the layered "amorphous" state being sliding as a whole. In this case v_{top} decreases to smaller values than it had before the melting, and v_{top} decreases with T decreasing, i.e., now the behavior is just opposite to that observed for the perfect-sliding regime. The combined dependences $v_{\text{top}}(T)$ at different dc forces
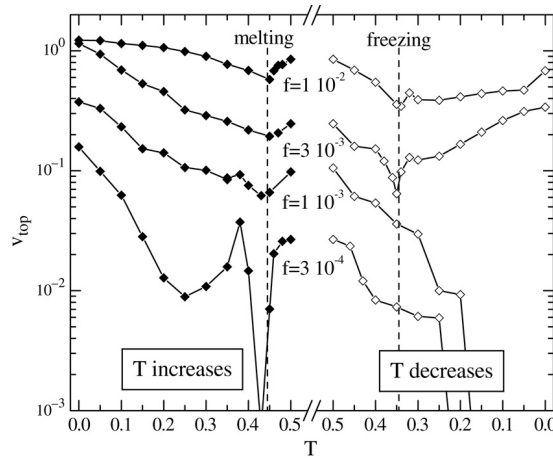
Fig. 40. The velocity of the top substrate v_{top} as a function of the substrate temperature T for the flat $N_l = 5$ system for four different values of the dc force. Left part (solid symbols) shows the dependences when T increases starting from the perfect-sliding regime until the lubricant melts, while the right part (open symbols) corresponds to T decreasing from the molten steady state to the frozen state. Dashed vertical lines show the melting and freezing temperatures from Section 5.2.

for the $N_l = 5$ system are presented in Fig. 40. Note that the kinetic frictional force demonstrates a peculiarity (which is very strong at low driving) at melting and freezing points, as is typical for phase transitions — close to and at the transition point all kinetic processes slow down.

5.5. Self-ordering of the lubricant film

The use of solid lubricants may be a very promising way, especially in micro-devices. As was shown above, if the lubricant film has a crystalline structure and is confined between two substrates which are atomically flat, the friction coefficient in such a perfect-sliding system may be as low as $\mu \sim 10^{-3}$–10^{-2} or even lower. The critical velocity of the transition from stick–slip to smooth sliding is also quite small, $v_c \sim 10^{-2}c$. Unfortunately, such an ideal system can hardly be realized experimentally. Even specially prepared surfaces are not perfectly smooth on a mesoscopic scale, and a lubricant has typically numerous structural defects. As a result, the static frictional force f_s is large enough, and the solid lubricant will melt at the onset of sliding. Then, at stick, the film solidifies back, but again into a state with many defects, because the cooling of the confined film is very rapid due to a good thermal contact with the substrates. In such a system one finds $\mu > 0.1$ and $v_c \sim 0.1c$, i.e., the tribological characteristics are of the same order as (or even more worse than) those of liquid lubricants.

In Ref. [170] it was discussed whether the system itself can approach the desired perfect-sliding regime for a suitable choice of the solid lubricant. Indeed, the effective lubricant temperature T_l increases during sliding. It is this increase of the temperature that leads to melting of the lubricant in the melting–freezing mechanism of stick–slip. However, if T_l remains lower than the melting temperature T_m, the lubricant film could remain solid and, at the same time, its structure can become more ordered due to annealing of structural defects, especially if T_l is close to T_m. As was shown in Section 5.2, the melting temperature of the lubricant film is proportional to the interaction amplitude V_{ll}. Therefore, for an appropriate choice of V_{ll} one can find a situation where $T_l \lesssim T_m$, i.e., where the sliding-induced heating brings the system close to but lower than the melting temperature. In this case the lubricant will
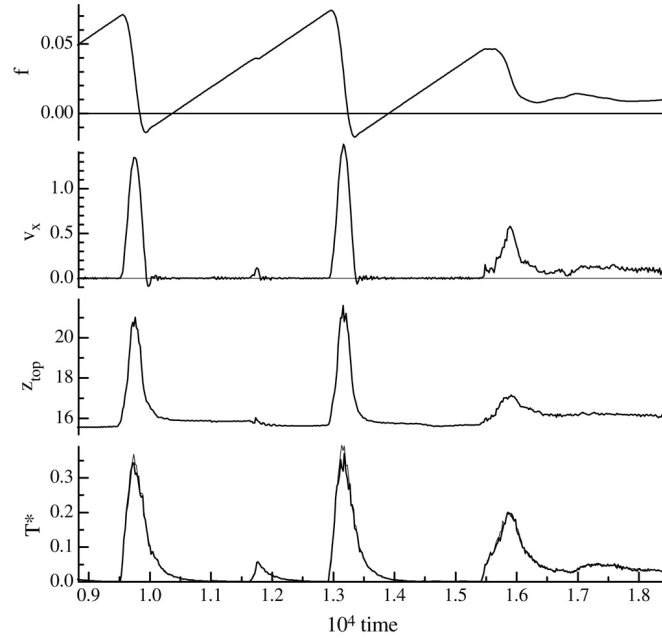
Fig. 41. Reordering of the lubricant: spring force, velocity of the top substrate, lubricant width, and effective lubricant temperature as functions of time at $v_s = 0.1$ for the $V_{ll} = 0.5$ system. Configurations before reordering (at stick in the stick–slip regime) and after it (at smooth sliding) are shown in Fig. 42.

remain solid during sliding, but its structure may reorder due to the annealing of the defects, and the system can approach the ideal case of perfect sliding.

Simulations [170] show that this indeed is the case. We have given already an example of self-ordering of the soft lubricant (Section 5.3, Fig. 29). Another example is shown in Fig. 41 for the case of $V_{ll} = 0.5$ with the driving velocity $v_s = 0.1$: the system is in the stick–slip regime at the beginning, but the solid lubricant is heated and reordered during slips, the structural defects (such as vacancies, interstitials, grain boundaries, etc.) are annealed, and the regime changes to the smooth sliding one. The configurations before reordering and after it are shown in Fig. 42(a) and Fig. 42(b) respectively. In the former configuration, the lowest lubricant layer is highly commensurate with the substrate, so that the sliding begins at the middle of the lubricant by removing the structural defects. On the contrary, in the latter configuration, the lubricant is more ordered and its lowest layer is incommensurate with the substrate, thus the sliding easily occurs at this interface.

The friction force for different values of the interaction amplitude V_{ll} is presented in Fig. 43. Note that the system itself chooses a configuration during annealing and sliding, therefore the values f_s and f_k are not unique but may change from run to run. This is indicated by "error bars" in Fig. 43, which just show a scatter of the corresponding values in different simulation runs. One can observe two clear-cut features of the behavior of the frictional force. First, the mechanism of the stick–slip motion changes from the melting–freezing to the inertia mechanism at $V_{ll} \gtrsim 0.5$, i.e., for $V_{ll}/V_{sl} \gtrsim 1.5$. Most importantly, one can observe that for $V_{ll} \approx 0.8$ the kinetic frictional force f_k achieves a minimum as low as $f_k \approx 10^{-4}$–10^{-3}. The friction coefficient in this case takes values of order $\mu \lesssim 10^{-2}$ which are more than one order of magnitude lower than those attainable with conventional liquid lubricants.
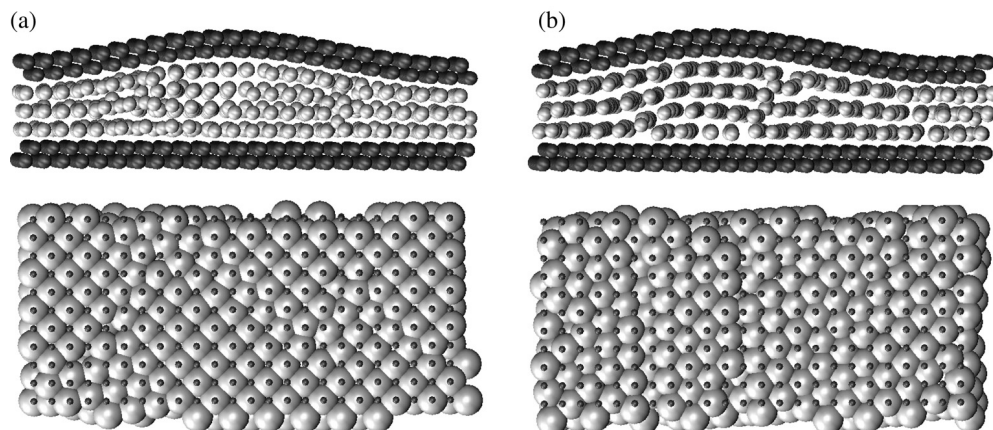
Fig. 42. The panels (a) and (b) show the configuration before and after reordering, correspondingly (at the beginning and at the end of the dependence shown in Fig. 41) for the system with $V_{ll} = 0.5$ driven with the velocity $v_s = 0.1$. Each panel has side and bottom views; in the latter there is only one layer of substrate shown, and the atomic radii are adjusted in order to visualize clearly the commensurability between the lubricant and the substrate (figures produced with Visual Molecular Dynamics software [169])
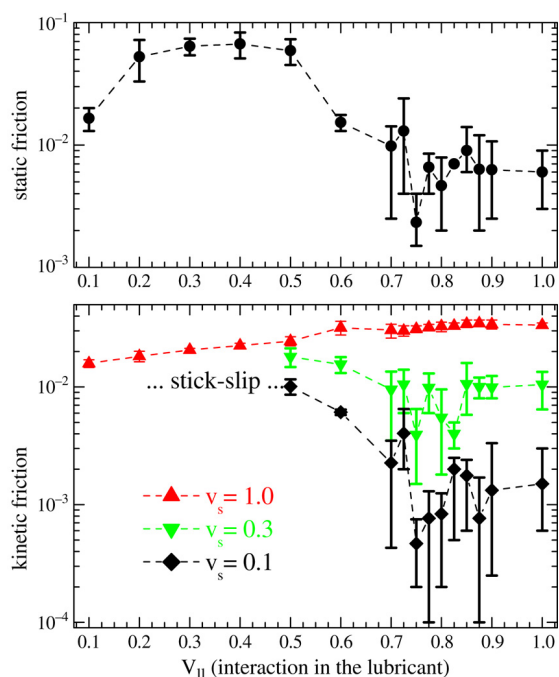
Fig. 43. Static f_s and kinetic f_k frictional forces for three values of the driving velocity ($v_s = 0.1$, 0.3 and 1 as indicated in the legend) as functions of the interaction amplitude V_{ll} in semi-logarithmic scale. The "error bars" show deviation of the simulation results in different runs.

Thus, there exists *an optimal choice of the strength of interatomic interaction V_{ll} within the lubricant that leads to the minimization of the kinetic friction* as well as to the low critical velocity of the stick–slip

to smooth sliding transition. The optimal value of V_{ll} should be high enough (relatively to the amplitude V_{sl} of the interaction of lubricant atoms with the substrates) so that the lubricant remains in a solid state during sliding. At the same time, the value of V_{ll} should not be too high, in order to allow annealing of the structural defects in the lubricant. For the parameters used in Fig. 43, the optimum is achieved at $V_{ll} \approx 2.5 \, V_{sl}$.

From a thermodynamic point of view, self-ordering of the lubricant system should be a general phenomenon. Indeed, a "free energy" of the driven system is $\propto E + f_k v_s t$. The ordering of the lubricant film lowers both the potential energy E and the frictional force f_k, thus decreasing the free energy.

The ordering of the lubricant film may be even more important for lubricants made of complex molecules such as, e.g., linear alkanes (*n*-hexadecane and *n*-dodecane) or branched alkanes (e.g., squalene). For example, the ordering of a six-layer *n*-dodecane lubricant film between mica walls was recently observed in large-scale MD simulation [171]. In the ordered state, the effective viscosity was even lower (by 2–8 times) than the dodecane bulk viscosity. In this system, however, the lubricant film was not solidified, but a "layer-over-layer" sliding was observed instead. These simulation results are in agreement with the experimental data [172,173].

5.6. A phenomenological approach

A general analytical theory of friction can hardly be developed because of the too complicated character of the processes involved. However, in what follows we present some attempts to explain qualitatively the values of the static and kinetic frictional forces observed in the simulations.

Static frictional force. For a *submonolayer* lubricant film, $\theta < 1$, an explanation of the Amontons' law for the static friction

$$f_s = f_{s0} + \alpha_s f_{\text{load}} \tag{30}$$

on the microscopic scale was proposed by Müser et al. [128,129]. In this case the lubricant atoms can accommodate the surface corrugation of both walls simultaneously, if they occupy the "++" positions, where the lubricant atoms lie at the minima of potentials from both surfaces. This locks the two surfaces together. Thus, these atoms work like one-atomic "asperities"; then the Amontons' law simply follows from the relation $(f_{\text{load}} \sim -\partial V_{sl}/\partial z) \sim (f_s \sim -\partial V_{sl}/\partial x)$.

Similar arguments can be used to explain the simulation results for a closely packed lubricant film obtained with the help of the model of Section 5.1. Fig. 44 shows that the Amontons' law operates for the *soft* lubricant. The static frictional force is relatively large, $f_{s0} \approx 0.09$ for $N_l = 1$ and $f_{s0} \sim 0.025$–0.035 for $N_l \geq 2$. For a thicker lubricant the two utmost lubricant layers are glued to the corresponding substrates, and sliding should occur somewhere in between the pinned layers. This explains why f_{s0} is approximately independent of the number of layers for $N_l > 2$. The simulation results can be approximated by the Amontons' law (30) with $f_{s0} \approx 0.035$ and $\alpha_s \approx 0.6$. Using the simplest model of the rigid square lattice constructed of lubricant atoms with the lattice constant $r_{ll} = 4.14$ and one lubricant atom on the top of this lattice interacting with the latter by the LJ potential of the amplitude $V_{ll} = 1/9$, we obtain that the threshold force (the driving force that allows the atom to overcome the activation barrier) depends on the loading force as $f_x \approx f_{x0} + \alpha_0 f_z$ with $f_{x0} \approx 0.13$ and $\alpha_0 \approx 0.5$ (a crude estimation may be obtained as follows: the energy at the hollow site is $E_0 \sim -4/9$, the energy at the bridge site is $E_b \sim -2/9$, so the barrier is $\Delta E = E_b - E_0 \sim 2/9$ and the distance is $\Delta a = 4.14/2$, this gives $f_{x0} \approx \Delta E/\Delta a \approx 0.1$). If we suppose that there are n_d "pinning centers" which accumulate
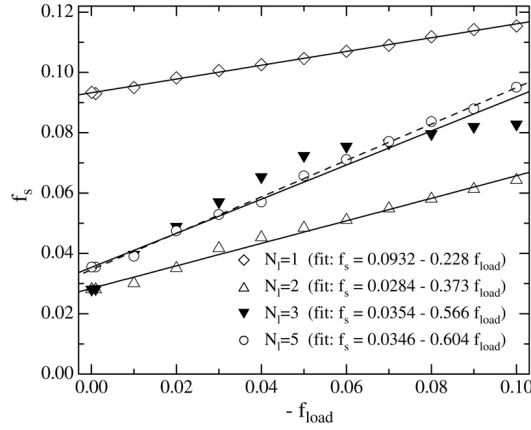
Fig. 44. The static frictional force f_s versus the loading force f_{load} for different widths of the soft lubricant film: $N_l = 1$ (open diamonds), 2 (open triangles), 3 (solid down triangles), and 5 (open circles) in the case of flat geometry. Solid lines correspond to fits by the Amontons' law (30) with the parameters given in the legend.
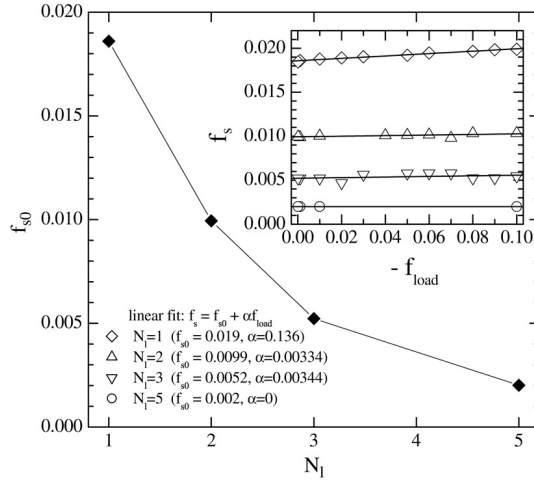

Fig. 45. f_{s0} as a function of the number of layers N_l for the flat geometry of the hard lubricant with the ideal crystalline structure. Inset: The static frictional force f_s versus f_{load} and the corresponding linear fits (the fitting parameters are given in the legend).

all the stress in a given metastable configuration and prevent the system from sliding, the couplings due to these defects have to be broken at the beginning of sliding. Therefore, we have $f_z n_d = f_{load} N_s$ and $f_x n_d = f_s N_s$, that leads to the Amontons' law with $f_{s0} = f_{x0} n_d / N_s$ and $\alpha_s = \alpha_0$. Comparing with the simulation results of Fig. 44, we obtain a reasonable agreement for the $N_l \geq 3$ film, if we put $n_d/N_s \sim 0.26$, i.e. if there are about 40% "pinning" (commensurate) atoms at an interface between the lubricant layers.

In the case of the *hard "amorphous"* lubricant, the simulation with the model of Section 5.1 leads to the static frictional force $f_s \sim 0.1$–0.15, and it again follows the Amontons' law (30) with $\alpha_s \gtrsim 0.3$ (for $N_l = 1$–3). These values can also be explained with the help of the simple one-atom model as described

above, which gives $f_{s0} = 0.39$ and $\alpha_0 = 0.32$. Therefore, the value of the static frictional force indicates that there 40%–60% pinning atoms at the lubricant/substrate interface. Thus, we see that in all these cases the static frictional force is determined by the number of "pinning" atoms in a particular stick configuration.

However, for the ideal crystalline structure of the lubricant, the simulation results are different as shown Fig. 45. The dependence of f_s on the load f_{load} can be fitted by the Amontons' law (30), but the values of α_s are much smaller: $\alpha_s \approx 0.14$ for $N_l = 1$, and it is very small for $N_l = 2$ and 3, where we get $\alpha_s \sim 3 \times 10^{-3}$. The exponential decrease of the static force f_s with N_l can be explained by the arguments described above in Section 4.

Kinetic frictional force. The kinetic friction emerges due to energy losses during motion of lubricant atoms with respect to the substrates. The kinetic energy associated with this motion is transferred into the substrates (through excitation of substrate phonons) and finally is dissipated in the substrates, being transformed into heat. Therefore, the most natural way of calculation of the kinetic friction is through energy balance arguments. Namely, the energy $dE_{in}/dt = Fv_{top} = N_s f v_{top}$ pumped into the system per one time unit due to the external driving must be equal to the energy dE_{diss}/dt dissipated in the substrates. The only way of energy dissipation in the model of Section 5.1 is through the viscous damping term $m_l v \eta(z, v)$ in the motion equations. This damping depends on the distance z from the corresponding substrate and on the relative velocity v according to the expression $\eta(z, v) = \eta_1(z) \eta_2(v)$, where the first factor $\eta_1(z)$ describes the exponential decrease of the damping when an atom moves away from the substrate, and the second factor $\eta_2(v)$ describes the velocity-dependent excitation of phonons in the substrate given by Eqs. (11) and (12) of Section 3.

When the lubricant has an effective temperature T_l, then its atoms move with a thermal velocity $\langle v_{th} \rangle = (k_B T_l / m_l)^{1/2} \sim 0.3\text{–}0.7$ at temperatures $T_l \sim 0.1\text{–}0.5$. Thus, if a lubricant atom is near a substrate at a distance z_l from the nearest surface and moves with an average velocity v_l with respect to it, then it loses per unit of time the energy

$$\epsilon(v_l; T_l) = m_l \eta_1(z_l) \int dv \, \eta_2(v) \, v^2 \, P(v - v_l; T_l), \tag{31}$$

where $P(v; T) = (m_l / 2\pi k_B T)^{1/2} \exp(-m_l v^2 / 2k_B T)$ is the Maxwell distribution.

Let N'_{al} be the number of atoms in the lubricant layer just adjusted to the surface of the substrate, and v_{lx} be the average x-velocity of atoms in this layer relative the substrate, while $v_{ly} = v_{lz} = 0$ for the motion along y and z. Now we can estimate the total energy losses as $dE_{diss}/dt \approx s N'_{al} [\epsilon(v_{lx}; T_l) + 2\epsilon(0; T_l) - 3\epsilon(0; T_{sub})]$,, where we subtracted the energy dissipated due to thermostat (the factor $s = 2$ for the case of symmetric sliding describes the fact that there are two sliding interfaces). From the equality $dE_{in}/dt = dE_{diss}/dt$ we finally obtain

$$f_k \approx m_l G \eta_1(z_l) \, \mathcal{F}(v_{top}), \tag{32}$$

where $G \equiv s N'_{al} / N_s$ and $\eta_1(z_l)$ are "geometrical" factors which weakly depend on the velocity and temperature through a change of the lubricant structure during sliding, while the last factor is the main one that determines the dependence of the kinetic friction on the driving velocity and the temperature,

$$\mathcal{F}(v_{top}) = v_{top}^{-1} \int_{-\infty}^{\infty} dv \, \eta_2(v) \, v^2 \left[P(v - v_{lx}; T_l) + 2P(v; T_l) - 3P(v; T_{sub}) \right]. \tag{33}$$

The factor $\mathcal{F}$ grows with the driving velocity as well as with the temperature. For example, if we take into account only the minimal contribution η_{eh} in Eq. (27), then the factor $\mathcal{F}$ becomes equal to

$$\mathcal{F}_{\min}(v_{\mathrm{top}}) = \eta_{\mathrm{eh}} \left[v_{lx}^2 + (3 k_B / m_l)(T_l - T_{\mathrm{sub}}) \right] / v_{\mathrm{top}}, \tag{34}$$

which grows linearly with the velocity (at $T_l = T_{\mathrm{sub}}$) as well as with the lubricant temperature (for fixed v_{top} and T_{sub}).

Next, we must take into account that the lubricant temperature grows with the driving velocity, e.g., $T_l = T_{\mathrm{sub}} + T_v(v)$, where $T_v(v)$ is the heating due to driving. Simulations suggest that $T_v(v)$ changes approximately linearly with the velocity. However, in the limit $v_{\mathrm{top}} \to 0$ it should be $T_v \propto v^2$ (note that the same dependence operates for a body embedded into a flowing liquid in classical hydrodynamics). In a general case the lubricant temperature can again be found with the help of energy balance arguments. The energy pumped into the lubricant, R_+, emerges due to "shaking" of the lubricant during sliding by an oscillating force of an amplitude $f_0 \sim f_s$ and the washboard frequency. The pumped energy should be equal to the dissipated energy $R_- \propto \int \mathrm{d}v\, \eta(z, v)\, v^2 \left[P(v, T_l) - P(v, T_{\mathrm{sub}}) \right]$. Such an approach allows us to find T_v analytically.

Then, we must take also into account the dependence of the geometrical factors G and η_1 in Eq. (32) on temperature. First, the lubricant width grows with the lubricant temperature due to thermal expansion, $d \approx d_0 + \beta_{z0} T_l$. As a result, the distance of lubricant atoms from the nearest surface will grow with temperature, $z_l \approx z_{l0} + \beta_{zl} T_l$, which leads to exponential decrease of η_1. In the case of the *liquid lubricant*, when the lubricant structure is changed with driving velocity and temperature, we have to take into account additionally that the number of atoms that interact with the substrates, N'_{al}, decreases when the film width grows. This effect may compensate or even overcome the increase of the kinetic friction with T due to the factor $\mathcal{F}$. One can show that the decrease of the geometrical factor G in Eq. (32) can be described by the dependence $N'_{al} \propto \left[1 + \beta_N (T_l - T_m) \right]^{-2/3}$.

Finally, we have to know the velocity v_{lx} of the lubricant atoms in the utmost lubricant layer relative to the substrate. It can easily be determined for the solid lubricant system: $v_{lx} = \frac{1}{2} v_{\mathrm{top}}$ for the symmetric sliding, $v_{lx} = v_{\mathrm{top}}$ for the asymmetric sliding, and $v_{lx} = 0$ for the LoLS regime of the soft lubricant. In the liquid-lubricant case, when the distribution $v_x(z)$ is approximately linear across the lubricant, we have $v_{lx} \approx \alpha_l v_{\mathrm{top}} z_l / d$, where $\alpha_l \lesssim 1$ for the soft lubricant and $\alpha_l \gtrsim 1$ for the hard lubricant.

The described approach easily leads to the universal dependence (29) for the ideal crystalline structure of the lubricant. For the temperature dependence of friction in this case we can take from the simulation data for the five-layer system $z_{l0} \approx 5.21$, $\beta_{zl} \approx 0.3$ and $f_0 \approx 0.2$. The phenomenological dependences obtained with these parameters are presented in Fig. 46. One can see that they are in good agreement with the simulation data. In a general case the phenomenological parameters introduced above can be extracted from the simulation data or even estimated from first principles.

Connection with the hydrodynamic viscosity. For the planar geometry used in the simulations presented above, the frictional force per unit area is $F_\alpha / A = p\, \delta_{\alpha z} - \sum_\beta \sigma'_{\alpha\beta} \delta_{\beta z}$, where Greek letters are for Cartesian coordinates, $(\alpha, \beta, \ldots) = (x, y, z)$, A is the total area of the surfaces in contact, p is the pressure, and the shear tensor in the linear approximation for uncompressed liquid is determined by the *viscosity coefficient* $\widetilde{\eta}$ through the relation

$$\sigma'_{\alpha\beta} = \widetilde{\eta} \left(\frac{\partial v_\alpha}{\partial x_\beta} + \frac{\partial v_\beta}{\partial x_\alpha} \right).$$
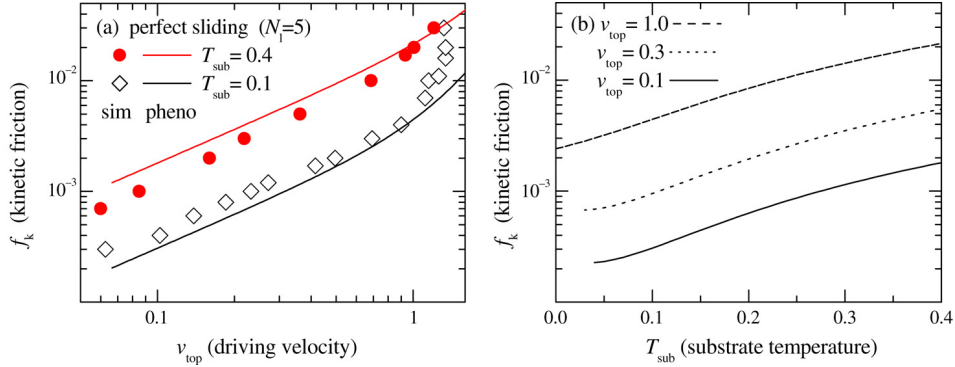
Fig. 46. The phenomenological dependences for the perfect sliding of the $N_l = 5$ hard lubricant for $f_0 = 0.2$. (a) The dependence of the kinetic frictional force on the sliding velocity at $T_{sub} = 0.1$ (open diamonds) and $T_{sub} = 0.4$ (solid circles). The symbols correspond to simulation data. (b) The dependence of the kinetic friction on the substrate temperature for three sliding velocities $v_{top} = 1, 0.3$ and 0.1.

The total kinetic frictional force in the hydrodynamic approach is $F = -A\sigma'_{xz} = -A\widetilde{\eta}\partial v_x/\partial z \approx -A\widetilde{\eta}v_{top}/d$, where d is the width of the lubricant film. In the model of Section 5.1 we have $F = -fN_s$ and $A = a_s^2 N_s$ which leads to

$$\widetilde{\eta} = fd/v_{top}a_s^2.$$

In the simulation we typically observed the values $f \sim 0.01$ and $v_{top} \sim 1$ for the soft-lubricant system. Taking $a_s = 3$ for the lattice constant and $d \sim 30$ for the five-layer lubricant film, we see that the simulations lead to the "hydrodynamic" viscosity coefficient with values of the order of $\widetilde{\eta} \sim 0.03$. Even for the one-layer lubricant film, where typical simulation values are $f \sim 0.05$ and $d \sim 10$, we obtain $\widetilde{\eta} \sim 0.05$. To compare, recall that typical bulk values for the viscosity coefficient lie within the range $\widetilde{\eta} \sim 10^{-5}$–$1$ kg m^{-1} s^{-1} (e.g., $\widetilde{\eta} = 10^{-5}$ for air, 10^{-3} for water, and 1 kg m^{-1} s^{-1} for glycerine, respectively). In the dimensionless ("natural") unit used in the simulation, these values correspond to $\widetilde{\eta} \sim 6 \times 10^{-4}$–$60$ n.u. Thus, the simulations lead to quite small values of the hydrodynamic viscosity coefficients. This result seems to contradict the conventional opinion, but in fact it is in agreement with experiments. For instance, the viscosity of water confined between two mica plates to films of thickness down to 1–2 molecular layers is within a factor of 3 or so of the viscosity of bulk water [174,175]. The experimental [173] and MD simulation [171] study of a thin dodecane lubricant film between mica walls also showed that the effective viscosity of the confined film is of the order of or even lower than the bulk viscosity. Also, we should mention the results of Becker and Mugele [176], where the dynamics of squeezing of a thin OMCTS film was studied, and the authors came to the conclusion that mutual friction between adjacent lubricant layers is close to the bulk viscosity. On the other hand, in experiments the "smooth" sliding is typically observed at velocities $v_{top} \sim 1$ μm/s, or $v_{top} \sim 10^{-9}$ n.u. in the dimensionless units. Such values lead to the "hydrodynamic" viscosity coefficient $\widetilde{\eta} \sim 10^7$, i.e. to the typical (but wrong) conclusion that the viscosity of the confined film is extremely high.

It is instructive to estimate also the dimensionless Reynolds number R for the lubricant film. The latter is defined as $R = \rho v d/\widetilde{\eta}$, where ρ is the lubricant density. As is known, the values $R \gg 1$ indicate a turbulent motion (which should correspond to the LS regime of the lubricant), while lower values of R correspond to the laminar flow (which would correspond to the LoLS regime of the MD model). Taking

$\rho = N_l N_{al}/(N_s a_s^2 d)$, we obtain $R = (N_{al}/N_s a_s^2)(N_l v_{\text{top}}/\widetilde{\eta})$, that gives the values $R \sim 1\text{--}10$ (smaller values are for thinner films), so that the lubricant is somewhere in between the laminar and turbulent regime, as indeed is observed in the simulation.

Finally, note that typical simulation values for the "tribological" friction coefficient $\mu \equiv f/f_{\text{load}}$ are $\mu \sim 0.1\text{--}0.5$ which are close to experimentally observed ones.

6. Stick–slip and smooth sliding

Both experiments and simulations show that in all cases when the static frictional force is nonzero, $f_s > 0$, the system exhibits a transition from stick–slip at low driving velocities to smooth sliding at high velocities. In most cases, smooth sliding is a more desired regime (one exception is bowing a violin); thus the problem emerges of how to avoid or reduce the stick–slip regime. However, to do this, first of all one has to understand the mechanisms of stick–slip motion and the transition to smooth sliding. The phenomenological theory described in Section 2.3, unfortunately, remains purely phenomenological in that the corresponding equations cannot be derived from a microscopic-scale simulation. On the other hand, the stick–slip motion predicted in the simulations strongly disagrees with experiments in the values of the critical velocity v_c. In what follows we discuss this question.

6.1. Microscopic smooth sliding: A minimal velocity

As follows from simulation, hysteresis of the $v(f)$ dependence and, therefore, the stick–slip motion may appear due to two different mechanisms: the melting–freezing of the lubricant for the soft lubricant (Section 5.3), or inertial effects for the hard (solid) lubricant as described in Section 5.4 (the latter mechanism is similar to the bistability of an underdamped driven atom in the inclined periodic potential). In both cases, however, the velocity on decreasing of the force, $v_b = v(f_b)$, is of *atomic-scale order*, $v_b \sim 1\text{--}10$ m/s. If the top block is driven with a velocity v through an attached spring, we obtain smooth sliding for $v > v_c$ and stick–slip for $v < v_c$. Always, however, $v_c \sim v_b$ is on the atomic scale, e.g. $v_c \sim 10^{-2} c$ (c is the sound speed), which is more than six orders of magnitude higher than the experimentally observed values.

In Section 2.4 we mentioned that the characteristic velocity of the transition depends on the mass of the moving substrate, $v_m \propto M^{-1/2}$. When the sliding block is considered as a *rigid* one, then $M = N_s N_\perp m$, where m is the atomic mass, N_s is the number of atoms at the interface, and $N_\perp$ is the number of atomic layers in the block. Therefore, one may speculate that for a macroscopically large block, $N_\perp \to \infty$, the velocity at the transition may be made as small as desired, e.g., such as that observed experimentally. This picture, however, is wrong for a *nonrigid* substrate, where only the first (closest to the interface) atomic layer stops at the transition, so that $M = m N_s$, and v_m is of atomic-scale value. In what follows we show that for the case of a planar geometry of the sliding contact this is always true, even if the sliding block has an infinite mass. Moreover, when the moving object has its own internal degrees of freedom which can be excited due to sliding, then the transition is discontinuous, contrary to the continuous transition for a single particle.

Of course, it is not possible to simulate a three-dimensional semi-infinite substrate. But a one-dimensional model can be simulated with sufficient accuracy. Namely, let us consider the model shown in Fig. 47, where the top substrate consists of N atoms ("layers"), the first layer moves in the external
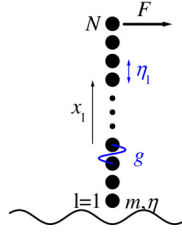
Fig. 47. The 1D tribological model: the top substrate consists of N atoms ("layers"), the first layer moves in the external sinusoidal potential due to the bottom substrate, and the dc force F is applied to the last layer of the top substrate.

sinusoidal potential due to the bottom substrate, and the dc force F is applied to the last layer of the top substrate, so that the equations of motion are

$$\ddot{x}_1 + \eta \dot{x}_1 + \eta_1 (\dot{x}_1 - \dot{x}_2) + g(x_1 - x_2) + \sin x_1 = 0, \tag{35}$$

$$\ddot{x}_l + \eta_l (2\dot{x}_l - \dot{x}_{l-1} - \dot{x}_{l+1}) + g(2x_l - x_{l-1} - x_{l+1}) = 0, \qquad l = 2, \dots, N-1, \tag{36}$$

$$\ddot{x}_N + \eta_N (\dot{x}_N - \dot{x}_{N-1}) + g(x_N - x_{N-1}) - F = 0. \tag{37}$$

To simulate the semi-infinite substrate, the damping η_l inside the moving block can be chosen to be zero at the interface and to increase smoothly far away from the interface, e.g.,

$$\eta_l = \eta_m \frac{h_l - h_1}{h_N - h_1}, \qquad h_l = \tanh\left(\frac{l - L_d}{\Delta L}\right), \quad l = 1, \dots, N. \tag{38}$$

In numerical results presented below it was chosen $L_d = 0.6 N$, $\Delta L = N/7$ and $\eta_m = 10\,\omega_s$ (here $\omega_s = 1$). Thus, a wave emerged at the interface due to sliding, will propagate inside the substrate and will be damped there.

The simulation results for this model are presented in Fig. 48. One can see that, when the force decreases down to the value f_b, the average velocity of the top substrate decreases reaching the value v_b and then abruptly drops to zero. The transition itself is shown in Fig. 49. The inset of Fig. 49 clearly demonstrates the wave emerged at the interface at the stop moment which then propagates into the top substrate.

It is interesting that if one chooses η_l in Eqs. (35)–(37) to be a constant, then the wave emerged at the sliding interface and propagated through the substrate, will be reflected from the top surface of the slab and go back, so that a standing wave is excited, especially at small enough values of η_l. This standing wave prevents from the transition to the locked state, so the sliding state will persist for much smaller values of the dc force. This resonance effect evidently depends on the width of the top block — the narrower is the slab, the larger is v_{top} and the smooth sliding persists for smaller forces. Such a model describes the situation when the top block corresponds to a thin slab; the slab can be glued to another large block so that a reflecting interface exists.

Besides the 1D model allowing the accurate simulation of a pseudo-infinite substrate, it also allows the *exact* analytical solution. An idea is to use the linear response theory [177] and the Green function technique [178]. Namely, when the top block moves with an average velocity $\langle v \rangle$, the atoms in the lowest layer of the top block oscillate with the washboard frequency $\omega_0 = (2\pi/a)\langle v \rangle$ (plus higher harmonics). The rate of energy losses (i.e., the energy absorbed by the top block per one time unit) can be calculated as $R = \frac{1}{2} f_0^2 \omega_0 \, \text{Im}\,\alpha(\omega_0)$, where f_0 is the amplitude of the force oscillations which is determined
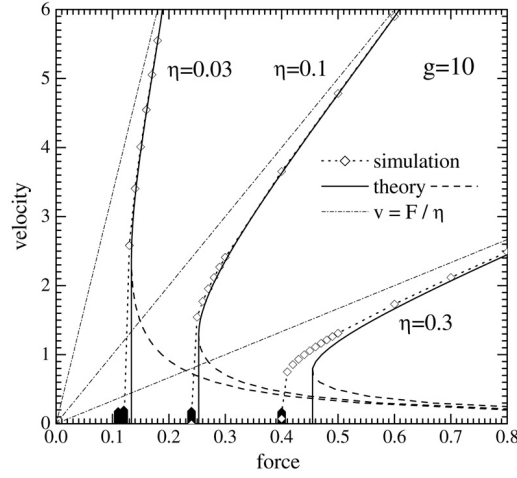
Fig. 48. The dependences $v(F)$ for the 1D top substrate with $g = 10$ for three values of the external damping coefficient $\eta = 0.03$, 0.1 and 0.3. The approximate analytical results are shown by solid curves (the unstable branches by dashed curves), the dash–dotted lines describe the trivial contribution $v = F/m\eta$, and the simulation results, by open diamonds and dotted curves.
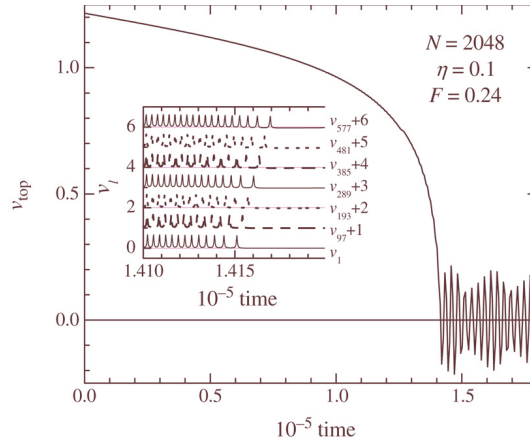

Fig. 49. The transition from the smooth sliding to the locked state: the average velocity of the top substrate versus time at the force $F = 0.24$ for the 1D top substrate of $N = 2048$ atoms for $g = 10$ and $\eta = 0.1$. Inset: the velocities of some selected layers of the top substrate.

by the periodic potential of the bottom substrate, and $\alpha(\omega)$ is the generalized susceptibility [177]. The susceptibility $\alpha(\omega)$ can be expressed through the causal phonon Green function $G(\omega)$ [178] as $\alpha(\omega) = -G(\omega)/m$. Thus, the rate of energy losses can be presented as $R = (\pi f_0^2/4m)\,\rho(\omega_0)$, where $\rho(\omega)$ is the density of phonon modes in the top substrate, $\rho(\omega) = -(2/\pi)\,\omega\,\mathrm{Im}\,G(\omega)$. The energy absorbed by the top substrate during its motion for one period of the external potential is equal to $E_{\mathrm{loss}}^{(1)} = 2\pi R/\omega_0 = Ra/\langle v \rangle$. This leads to the contribution $F_{\mathrm{rad}} = E_{\mathrm{loss}}^{(1)}/a$ to the frictional force. The total frictional force is then equal to $F = F_{\mathrm{rad}} + F_\eta$, where $F_\eta = m\eta a^{-1} \int_0^a \mathrm{d}x\, v(x)$ emerges due to the damping η. Thus, if one knows the phonon Green function for the semi-infinite substrate, one can calculate the frictional force (other details can be found in Ref. [179]).
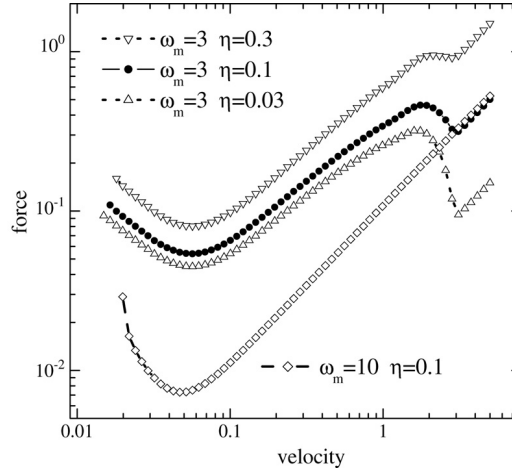
Fig. 50. The dependence $F(v)$ for the 3D model of the semi-infinite top substrate for different model parameters as shown in the legend.

Applying this technique to the 1D model of Fig. 47, where the exact expression for the Green function is known [178], we obtain the results shown by solid curves in Fig. 48 which are in good agreement with the simulation ones. Moreover, we can apply the described analytical approach to a 3D model of the semi-infinite substrate, i.e., to the problem which cannot be studied by MD methods. Using an approximate phonon spectrum of the semi-infinite crystal [93], we obtain the dependences shown in Fig. 50 (note that in the 3D model we must take into account not only the main harmonic of the washboard frequency, but the higher harmonics as well). The function $F(v)$ has a minimum at $v = v_b \sim 0.01$–0.1 where $F(v_b) = F_b$. The part of the $F(v)$ dependence to the right of the minimum, $v \geq v_b$, corresponds to the stable motion, while the solution in the $v < v_b$ interval is unstable. Therefore, when the velocity decreases below v_b, the system must jumplike be transformed to the locked state. Thus, if the dc force applied to the upper layer of the top substrate decreases, then the transition from the sliding regime to the locked state takes place at $F = F_b$ when the average velocity of the top block is nonzero, $v_b > 0$. The threshold values F_b and v_b do not depend on the total mass of the top block, although they depend on the elasticity of the block — the stiffer is the substrate, the lower are both threshold values.

The results described above correspond to a tribological system with a planar geometry, when the area A of the contact scales with a characteristic linear size R of the sliding block as $A \propto R^2$. But these conclusions cannot be applied to STM-like devices, where a tip of a macroscopic size moves over a surface, while the real contact area consists of only one or a few atoms. In the latter case the total mass of the tip is important, and v_c would depend on M as MD simulation due to Luan and Robbins [180] predicts.

6.2. Macroscopic smooth sliding: An earthquakelike model

The MD simulation, as described above, always leads to the critical velocity of the transition from stick–slip to smooth sliding which is on the atomic scale, e.g., $v_c \sim 10^{-2} c$, or $v_c \sim 1$–10 m/s. This strongly contradicts experimentally observed values of order $v_c \sim 1$ μm/s, which is more than six orders of magnitude lower. As a typical example, we mention the SFA study of the one-layer hexadecane
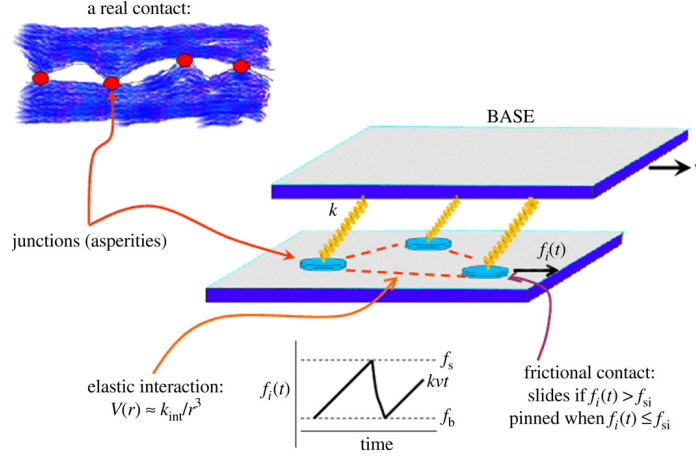
Fig. 51. The earthquakelike model.

($C_{16}H_{34}$) film of the width $d = 0.4$ nm (determined by the diameter of chain molecules) between two mica surfaces [181]. At the load $P = 2.6 \times 10^6$ Pa this system shows the friction coefficients $\mu_s = 0.5$ and $\mu_k = 0.25$, and the critical velocity of $v_c \approx 0.4$ μm/s.

Thus, the microscopic mechanism of the stick–slip to smooth sliding transition observed in MD simulations has little in common with the experimentally observed macroscopic one. In what follows we describe, following Ref. [182], an earthquakelike model, which demonstrates stick–slip behavior at low velocities and changes to "smooth" sliding at high v. The "transition" takes place at $v_c \sim a/\tau$, where a is the average distance between junctions and τ is an "aging" time of a single junction. Reasonable values for these parameters (e.g., $a \sim 10^{-6}$–10^{-3} m and $\tau \sim 1$–10^3 s) lead to experimentally observed values of v_c. The model predicts that experimentally observed smooth sliding actually corresponds to atomic-scale stick–slip motion of individual junctions, and that the "transition" itself is a smooth one if one increases the resolution of the velocity increments.

The model is a 2D variant of the Burridge–Knopoff (BK) spring-block model of earthquakes [183] similar to that studied by Olami, Feder, and Christensen (OFC) [184]. Let the two blocks touch one another at (point) junctions which pin the relative position of the blocks (see Fig. 51). The junctions form an array $\{r_i\}$ randomly distributed in 2D space, $r_i = r_{i0} + (\xi_i - 0.5)\Delta r$, where $i = 1, \ldots, N$ numbers the junctions, r_{i0} corresponds to a uniform distribution (the triangular lattice), ξ_i is a standard random number, and the parameter Δr describes the amplitude of randomness. The junctions interact elastically via springs of strength k_{ij}. All junctions are connected through springs of strength k with the fixed bottom block and coupled frictionally with the top block moving with a constant velocity v. The elastic constants are $k \sim \langle k_{ij} \rangle \sim \rho c^2 a$, where ρ is the mass density of the block, c is the transverse sound velocity, and $a = \langle r_{ij} \rangle$ [31]. The potential energy $V(r)$ of the elastic interaction between two defects separated by a distance r in a solid [185] as well as on a crystal surface [186] follows the law $V(r) \approx k_{int}/r^3$, where k_{int} is a parameter describing the elastic properties of the block. Thus, k_{ij} are determined by the expressions $k_{ij} = 3 k_{int}/|r_j - r_i|^5 \left[5 (x_j - x_i)^2/(r_j - r_i)^2 - 1 \right]$.

In a scalar variant of the model, only the x component of the force is considered. Let $u_i(t)$ represent the shift of the ith junction from its nonstressed position. The local force $f_i(t)$ associated with each junction is the sum of the force from the bottom block, $f_i^{(b)}(t) = ku_i(t)$, where $u_i(t) = u_i(t_0) + v(t - t_0)$

is due to frictional coupling with the top block, and the elastic forces from other junctions, $f_i^{(int)}(t) = -\sum_j k_{ij}[u_j(t) - u_i(t)]$. As the top stage moves, the surface stress at any junction increases continuously. A single junction is pinned whilst $f_i(t) < f_s(t)$. When the force on a given junction, i, reaches the critical value $f_i(t) = f_s(t)$, this junction starts to slide. At this point, a rapid local slip takes place, during which the local stress in the block drops to the value f_b. The sliding takes a time $t < 10^{-10}$ s [8, 10,157] and thus can be considered as an instantaneous one. The coordinate u_i of the relaxing junction (instantly) changes to the new position $u_i = \left(f_b + \sum_{j \neq i} k_{ij} u_j \right) / \left(k + \sum_{j \neq i} k_{ij} \right)$. The slip of one junction redefines the forces on its neighbors; this can result in further slips (an avalanche); the triggered "earthquake" will stop when there are no junctions left with a force above the threshold. Then the junctions are pinned again, and the whole process repeats itself. As the initial configuration we use random shifts of all junctions, $u_i(0) = \xi_i \Delta x_{ini}$.

Following the discovery of self-organized critical (SOC) behavior in a BK-type model [187], many studies of this type were performed [188–190]. If we set $\Delta r = 0$, the model reduces to the OFC model [184]. For periodic boundary conditions (PBC) the steady state of the OFC model is always periodic [191,192]. However, for open boundary conditions (OBC), the model exhibits SOC behavior and the probability distribution $P(s)$ of the number of relaxations s in a single avalanche follows the power law $P(s) \propto s^{-\chi}$ with the exponent χ continuously varying with k_{int} (or v). In both cases the OFC model does not demonstrate a transition from stick–slip to smooth sliding.

The main new feature that must be incorporated into the model is the "age-function" idea of the phenomenological models (see Section 2.3), i.e., we have to assume that the static frictional force depends continuously on the time of stationary contact of a given junction. In Ref. [182] we used a simple exponential dependence (let $t = 0$ correspond to the moment when the junction is pinned),

$$f_{si}(t) = f_s + (f_{sm} - f_s) \left[1 - \exp(-t/\tau) \right]. \tag{39}$$

Notice that $f_{si}(t)$ re-initializes every time the junction relaxes and, thus, it is different for different junctions.

A rather comprehensive study of the *one-dimensional* variant of the BK-type model for the parameters suitable for the tribological system and with incorporation of the $f_s(t)$ dependence (39) has been done by Persson [31]. The important result of his study is that this type of model can explain the logarithmic time dependence of relaxation processes at nonzero temperatures: it emerges due to thermally-activated processes which occur near the sharp cutoff at $f = f_s$ in the distribution of surface stresses. However, the resulting $f(t)$ dependences do not reproduce the experimental ones too well, and the reason lies in the one-dimensionality of the model.

Without loss of generality we can put $k = 1$, $a = 1$, $\tau = 1$, and $f_s = 1$. In the simulation results presented below it was used $f_{sm} = 2 f_s$ which corresponds, e.g., to the squeezing of a two-layer lubricant film into a one-layer configuration (see Section 5.4), $f_b = 0.1$, $\Delta r = 0.3$, $\Delta x_{ini} = 1$, $k_{int} = 0.1$ (recall $12 k_{int} \sim k$), and $N \gtrsim 10^3$ (for real systems $N/A \sim 10^2$–10^5 cm^{-2} as was mentioned in Section 2), although the results remain qualitatively unchanged when all these parameters are varied over a wide range [182].

The study of different versions of the model leads to the conclusion that in order to reproduce typical experimentally observed $f(t)$ dependences, the "minimal" model must (i) be two-dimensional, (ii) incorporate the $f_s(t)$ dependence (39), and (iii) have a random spacial distribution of contacts, $\Delta r \neq 0$. A typical dependence of the total frictional force $f(t)$ for different velocities v is shown in Fig. 52(a).
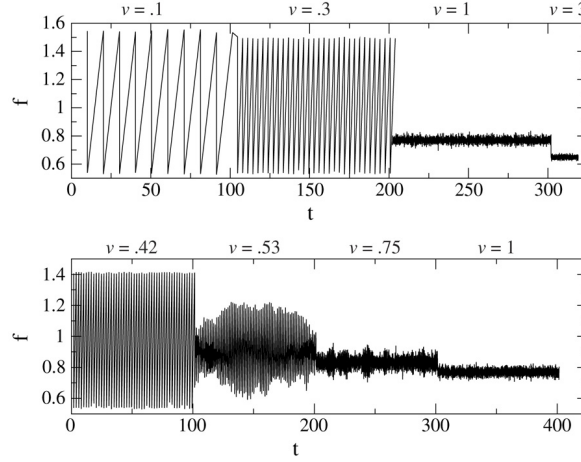
Fig. 52. (a) Total frictional force $f(t)$ versus time for driving velocities $v = 0.1, 0.3, 1$, and 3. (b) Details of the transition for velocities around v_c: $v = 0.42, 0.53, 0.75$, and 1 (the parameters of the earthquakes model are the following: $N = 30 \times 34$, $f_b = 0.1$, $f_s = 1$, $f_{sm} = 2$, $k_{int} = 0.1$, $\Delta r = 0.3$, $\Delta x_{ini} = 1$).
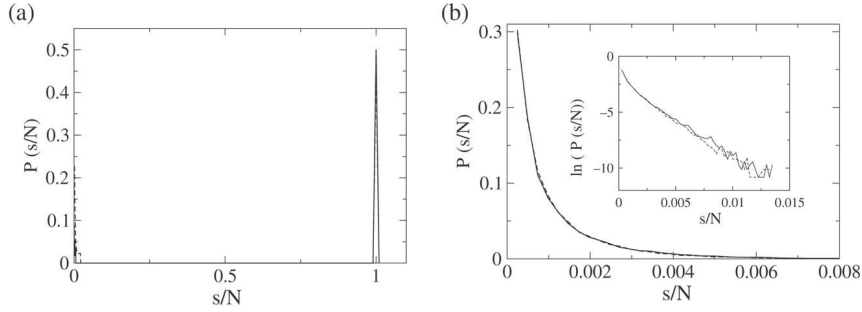

Fig. 53. The distribution of avalanche sizes $P(s/N)$ at (a) $v = 0.1$ (solid curve) and 0.2 (dotted curve); (b) $v = 3$ (solid curve) and 5 (dotted curve). The inset in (b) is a log-linear plot showing the exponential dependence. All data are for PBC with $N = 60 \times 68$, and the same parameters as in Fig. 52.

At $v \gtrsim 1$, the model shows a "smooth" sliding and behaves similarly to the OFC model. The difference is that, due to the randomness of the junctions' distribution, $\Delta r \neq 0$, the function $f(t)$ shows a complicated, non-periodic behavior even for PBC. The distribution of avalanche sizes is exponential, $P(s) \propto \exp(-s/\bar{s})$, both for PBC and OBC as shown in Fig. 53(b) (the power-law distribution is observed for $\Delta r = 0$ with OBC only). The average size of the avalanches can be estimated analytically [182]. For example, for the parameters used in Fig. 52 we have $\bar{s} \approx 4$ for the $v = 3$ case. The fluctuations of the total frictional force scale as $\langle f(t) - \langle f(t) \rangle \rangle \propto N^{-1/2}$ with the number of junctions.

When $v \lesssim 1$, the model exhibits stick–slip behavior (see Fig. 52(a)). The distribution of avalanche sizes possesses two peaks (Fig. 53(a)), the first at $s = 0$ with an exponential distribution as above, and the second at $s \sim N$, i.e., now an avalanche can occupy the whole system. Thus, at low velocities, when the time dependence of the static frictional force is important, the slipping of junctions becomes synchronized. Such a behavior can also be explained analytically [182].

Finally, *the transition is smooth* (see Fig. 52(b)), it is neither discontinuous (first-order) nor continuous (second-order) contrary to predictions of the phenomenological models of Section 2.3.

Thus, the proposed version of the earthquakelike model, which combines features of the OFC model and the phenomenological approach, resolves the disagreement between experimentally observed $v_c \sim 1$ μm/s and MD results of $v_c \sim 1$ m/s. A single junction itself has to behave according to MD predictions, i.e., it should exhibit hysteresis and atomic-scale stick–slip motion. *The experimentally observed smooth sliding corresponds to atomic-scale stick–slip motion of many junctions.* This statement is in agreement with recent experimental results [193] (see Section 7). *The macroscopic-scale stick–slip behavior emerges because of the concerted motion of many junctions due to their interaction, and the transition itself is smooth.* This prediction should be checked experimentally: first, the fluctuations of f in the "smooth" sliding regime should scale as $N^{-1/2} \propto 1/\sqrt{A}$ with the total area A of the contact, and second, a careful analysis of $f(t)$ should show a continuous spectrum for atomic-scale stick–slip, while for steady sliding the spectrum should exhibit characteristic peaks at the washboard frequencies. However, some questions still remain unclear as will be discussed below in Section 7.

Note that the described model with the exponential dependence (39) at $v \ll 1$ again reduces to the OFC model with the threshold force f_{sm}, and the stick–slip motion disappears. It is interesting that the inverse transition from smooth sliding to stick–slip with v increasing was indeed observed in the SFA experiment [181] for the double-chained surfactant DHDA$^+$ [(C$_{16}$H$_{32}$)$_2$ − (C$_2$H$_6$N$^+$)] between two mica surfaces. In this system the positively charged headgroups of the DHDA$^+$ molecules are strongly coupled to the negatively charged mica surfaces and form two monolayers, so that the sliding should occur at the interface separating these monolayers. The authors of Ref. [181] observed the first transition from the static state to smooth sliding at $v_c \ll 0.1$ μm/s. Then, at $v_c' > 0.3$ μm/s the smooth sliding was changed to stick–slip.

However, this is a special case emerging due to simple dependence (39), which achieves a plateau at $t \gg \tau$. If $f_s(t)$ continues to grow at $t \gg 1$, although may be slower and with another law, then the stick–slip regime survives at low velocities. For example, if we take $f_s(t) = c_1 + c_2(t + c_3)^{1/2}$, where the parameters $c_{1,2,3}$ are adjusted to show a behavior similar to the dependence (39) at short times, then we get stick–slip for any $v \ll 1$. Note also that at $t \gg 1$ the number of junctions has to decrease due to coalescence of nearest junctions, resulting in stick–slip motion too.

One should mention also several attempts to develop an analytical theory of macroscopic friction, for example, the approach used by Caroli and Nozieres [194,146] and the one due to Bocquet and Jensen [195].

The mechanism of stick–slip described above can be applied to the contact of two macroscopically flat surfaces as, e.g., in micromachines or in SFA experiments. The slip distance in this case is $\propto (f_s - f_b)/k_{spring}$ and takes mesoscopic values, e.g., of order of microns [18,196]. However, the situation is different in tip-based experiments, where the contact consists of a single or few atoms only. If the contact is formed by one atom only, then the slip distance must be equal to the substrate lattice constant — the tip simply reproduces the surface topography (in the underdamped case the slips may proceed over several lattice constants, but this regime usually does not emerge in FFM experiments). When the contact is due to several atoms, the substrate potential is averaged over these atoms, and the stick–slip may correspond to microslips by distances less than the substrate periodicity [151,197].

7. Conclusion

Let us summarize the main results obtained with the help of MD simulations.

1. First of all, modelling of the friction processes can be done and leads to many new interesting and important results. Visualization of atomic trajectories helps to study such details of processes within the lubricant that are not accessible by experimental methods. However, Langevin equations with the realistic damping $\eta_{\text{ext}}(z, v)$ should be used in simulation.

2. The melting temperature of a thin lubricant film confined between two crystalline surfaces is higher than the corresponding bulk value. Therefore, a very thin confined film is typically in a solid state. This results in a nonzero static frictional force f_s. The dynamics of the film is significantly affected by the substrate, both in the solid and in the molten phases. The solid phase, able to sustain shear stress, shows large diffusional motions of the atoms; the molten phase shows a layered structure.

3. Behavior of the lubricant is determined by the relationship between the interaction within the lubricant, V_{ll}, and the interaction of the lubricant atoms with the substrates, V_{sl}. In the case of the hard lubricant, $V_{ll} > V_{sl}$, the lubricant remains in the solid state during sliding, while in the opposite case of the soft lubricant, $V_{ll} \ll V_{sl}$, the lubricant film is melted at the beginning of sliding.

4. In both cases of the soft and hard lubricants, the function $v_{\text{top}}(f)$ exhibits hysteresis. However, physical mechanisms of the hysteresis are different for these two cases: in the case of the hard lubricant, $V_{ll} > V_{sl}$, the hysteresis is due to an inertia mechanism, while for the soft lubricant, $V_{ll} \ll V_{sl}$, it is due to the melting–freezing mechanism. The hysteresis of the $v_{\text{top}}(f)$ dependence leads to the inequality $f_k < f_s$. The latter, together with the condition $f_s \neq 0$, leads to the stick–slip motion at low driving velocities.

5. In the case of the soft lubricant of three or more layers wide, the simulations show that:

    (a) The operation of the Amontons' law $f_s = f_{s0} + \alpha_s f_{\text{load}}$ for the static frictional force is determined by the interatomic interaction within the lubricant, which leads to the coefficient $\alpha_s \sim 0.5$. The value of the static frictional force depends on a particular structure of the frozen metastable lubricant film. The value of f_s slowly grows with the time of stationary contact and reaches its maximum for the annealed configuration.

    (b) During smooth sliding, the kinetic frictional force is approximately independent of the driving velocity. However, the lubricant effective temperature (the heating of the lubricant due to sliding) as well as the thickness of the film are proportional to the driving velocity. The Amontons' law for the kinetic frictional force, $f_k = f_{k0} + \alpha_k f_{\text{load}}$, operates as well, but with a much lower proportionality coefficient, $\alpha_k \sim 0.05$–0.1.

6. The behavior of a thin soft lubricant film, $N_l \leq 2$, when all lubricant atoms directly interact with the substrates, differs from the case of thicker films. The static frictional force is relatively high and does not change essentially with the time of stationary contact. The threshold velocity of the transition to the smooth sliding regime is also much higher than that for thicker lubricant films. The one-layer film does not melt during sliding, and the stick–slip motion is due to an inertia mechanism similar to the hard-lubricant system. The reason is that the melting temperature of the very thin film is very high.

7. In the case of the hard lubricant, when the lubricant is crystalline without defects and is in contact with the atomically smooth flat substrate surfaces, both static and kinetic frictional forces are very small. This is just the ideal case of negligible friction predicted for the contact of two incommensurate solid surfaces. The static force f_s depends linearly on the load according to the Amontons' law, but the proportionality coefficient α_s is very small. The static frictional force exponentially decreases with the film width. Also, it does not change with the time of stationary contact. Due to so small values of f_s, the threshold velocity of the transition from stick–slip to

smooth sliding is also rather small, $v_c \sim 0.03$–0.1. The kinetic frictional force in the perfect-sliding regime is very small too, $f_k \sim 10^{-3}$–10^{-4}, and essentially depends on the driving velocity. The main losses are due to excitation of vibrations in the lubricant with the washboard frequency.

8. Thus, the frictional force is mainly determined by the lubricant structure: the solid lubricant with a crystalline structure leads to the lowest friction (the perfect sliding), the lubricant with an "amorphous" structure, to a high friction, and the liquid lubricant leads to intermediate values of the friction (and $f_s = 0$). The perfect-sliding mechanism naturally explains the excellent lubrication of layered materials such as graphite, MoS_2 and Ti_3SiC_2: the sliding in these cases occurs between the solid layers rotated relatively to each other and, therefore, most contacts are incommensurate. The perfect-sliding regime of the hard-lubricant system, however, can hardly be realized experimentally. Even specially prepared surfaces are not perfectly smooth on a mesoscopic scale, and the lubricant has typically numerous structural defects. As a result, the static frictional force f_s is large, and the solid lubricant is melted at the onset of sliding. Then, at stick, the film solidifies back, but again into a state with many defects. However, the lubricant structure may self-order due to sliding, which results in almost perfect sliding. There exists an optimal value of the strength of interatomic interaction V_{ll} within the lubricant that leads to the minimization of the kinetic friction. The optimal value of V_{ll} should be high enough (relative to the amplitude V_{sl} of the interaction of lubricant atoms with the substrates) so that the lubricant remains in a solid state during sliding. At the same time, the value of V_{ll} should not be too high, in order to allow annealing of the structural defects in the lubricant.

9. When the driving force decreases, the transition from the sliding regime to the locked state takes place at $f = f_b$ when the average velocity of the top block is nonzero, $v_b > 0$. The threshold values f_b and v_b do not depend on the total mass of the sliding block, but depend on the elasticity of the block — the stiffer is the substrate, the lower are both threshold values. The minimal velocity v_b as well as the critical velocity of the transition from stick–slip to smooth sliding v_c are on the atomic-scale, $v_b \sim v_c \sim 10^{-2} c$, where c is the sound speed.

10. The experimentally observed values of $v_c \sim 1$–10 μm/s of the transition from stick–slip to smooth sliding can be explained with the help of the earthquakelike model. This model demonstrates stick–slip behavior at low velocities which changes to "smooth" sliding at high v. The "transition" takes place at $v_c \sim a/\tau$, where a is the average distance between junctions and τ is an "aging" time of a single junction. The model predicts that experimentally observed smooth sliding actually corresponds to atomic-scale stick–slip motion of individual junctions, and that the "transition" itself is a smooth one.

However, there are still a large number of open questions in the problem of friction. In particular, we would like to mention the following questions:

- What is the mechanism of $f_s(t)$ growing and how can one calculate the "aging" time τ? The macroscopic-scale values of τ are determined, most probably, by plastic deformations, so that τ hardly can be calculated with the help of the MD technique. Possible mechanisms may be the following:
  - The most natural explanation of the growing of f_s with the time of stationary contact is due to growing of the real contact area because of thermally activated plasticity of the contacts. Experiment [198] and theory [199] predict that the contact area should increase logarithmically with the time of stationary contact, $A(t) - A(0) \propto \ln(1 + t/\tau)$.
  - Persson et al. [31,32] discussed the process of relaxation of shear stress at the interface immediately after the sliding stops, which also leads to growing of $f_s(t)$.

- If the lubricant is composed of long-chain polymer molecules, their interdiffusion may result in growing of $f_s(t)$ as well.
- The value of f_s may increase with time due to decreasing the thickness of the lubricant film, e.g., because of squeezing of the lubricant out from the contact area. The theory of squeezing developed by Persson and Tosatti [202] and Persson [203], as well as MD simulation due to Persson and Ballone [158], show that this process is characterized by a low rate too. Recently the squeezing of the OMCTS lubricant was studied experimentally by the SFA technique [176].
- Even before a new contact is formed, a capillary bridge (a "necking") may be formed by filling the space between the surfaces with lubricant (or any other "third-body") molecules. Because this is a thermally activated process (Bocquet et al. [200], Riedo et al. [201]), it is characterized by a low rate and should result in macroscopic-scale values of τ.

• The earthquakelike model (Section 6.2) used to explain the stick–slip to smooth sliding transition, is based on the concept of "pinning contacts". In the case of rough surfaces, they can naturally be associated with real contacts or asperities. But some experiments demonstrate a similar behavior even for atomically smooth surfaces, where one cannot expect any irregularities (however, see Ref. [172], where the question of "atomically smooth surfaces" is critically discussed). Therefore, a question emerges, what is the nature of "pinning contacts" (also called "stress domains" or "stress blocks") in this case? In a series of papers [1,2,77–79] Persson conjectured that the contacts appear due to nucleation of "solid islands" in the molten lubricant, so that the lubricant state corresponds to a "granular 2D fluid" (see also [50]).

• What is a scenario of the onset of sliding? Is it due to cracking of the lubricant or just due to its smooth plastic deformation (e.g., in the case of the soft lubricant)? Is it due to emerging of moving islands or channels as low-dimensional FK-type models predict, again because of plastic deformation of the lubricant? Or it is due to dislocations created at the open boundary of the contact? For example, Sørensen et al. [141] in MD simulations of "dry" friction of a Cu tip over the Cu(111) crystal surface observed tip motion via a dislocation mechanism: dislocations were nucleated at the corner of the contact and then moved rapidly through the contact area.

• What is the noise spectrum during stick–slip and smooth sliding? Does it corresponds to discontinuous jumps, to cascade or concerted jumps due to the elastic interaction between the contacts, or to separate peaks coupled with washboard frequencies? A detailed experimental measuring of the noise spectrum may strongly help in understanding of dynamical processes in the confined film.

In solution of these as well as many other problems essential help could come from surface science physicists. Indeed, the fact that properties of a thin adsorbed film are far from the corresponding bulk properties is trivial from the surface science point of view. Adsorbed films demonstrate a great variety of structures and phase transitions, including commensurate–incommensurate transitions; as we showed above, the structure of the lubricant film plays the key role in its frictional characteristics. Different mechanisms of surface diffusion could find their analogs in lubricant sliding, especially at the onset of motion. And experimental techniques of surface science should certainly be useful (and are widely used already) in tribology.

Finally, we must note that in the present survey we strongly oversimplified the real problem of friction as it appears in experiments as well as in machines. Most of the simulation results described above, were obtained for a simple model of the lubricant consisting of single atoms and interacting via the LJ potential. The reason is that this is a standard approach in physics: in order to understand a complex phenomenon, one has first of all to start with a simplified ("minimal") model, and only

after that, can other more complicated details of the phenomenon be incorporated. Nevertheless, these simple simulations lead to correct qualitative and often even quantitative results, as compared with more complicated simulations based on realistic potentials (as one of the examples of large scale MD simulation of real systems, we may mention, e.g., the study of diamond surfaces coated with amorphous carbon films by Gao et al. [204,205]). In the result of such an approach, however, some important questions have been left out of our discussion. In what follows we briefly mention some of them.

As is well known, the coefficients of *rolling friction* are generally 10^2–10^3 times lower than those of sliding friction for corresponding materials. The main source of friction in rolling is dissipation of energy involved in deformation of the objects. In this context the following intriguing question emerges [206–209]: may a similar mechanism work at a microscopic scale, i.e., may a ball-shape molecules such as almost spherical C_{60} molecules (fullerenes) work as a "molecular bearing"? It could be very promising for realization in nano- and micromachines. Unfortunately, these anticipations have not been confirmed yet in experiments. The C_{60} molecules may form close-packed layers, e.g., on the graphite substrate [206–213]. According to experimental results of Miura et al. [215], two layers of C_{60} molecules are stick but one (close-packed) monolayer may exhibit rolling. However, the lowest friction coefficient between two C_{60} films was found to be of order $\mu \sim 0.15$ [210–213]. Simulations indicate that the smooth rolling is destroyed at high concentrations of the lubricant because of the jamming effect [214]. In the case of rolling friction the jamming is much more dramatic than in the case of sliding friction with conventional lubricants. When two nearest neighboring rolling molecules come in close contact, they hinder mutual rolling, because the two sides of the colliding molecules roll in opposite directions. In the result both molecules stop to roll. Then the jam grows in size and totally destroys the smooth rolling regime. Therefore, the microscopic rolling with very low friction could be expected in systems where (i) the substrates are more rigid than the lubricant, (ii) the lubricant is incommensurate with the substrates, and (iii) the lubricant concentration is lower than some critical value, e.g., lower than the close-packed C_{60} layer. Note that the increase of temperature or the introduction of an additional repulsion between the lubricant molecules may strongly improve the frictional properties of fullerene-like lubricants [216–219,179].

Kinetic friction and wear. Starting from Bowden and Tabor [3], a common opinion in macrotribology is that the pinning of the surfaces is due to forming of cold-welded junctions, so that the sliding corresponds to shearing of these junctions, which may be followed by ploughing the surface of the softer material by the asperities of the harder one. A MD simulation of these effects is rather complicated and requires some special tricks [148]. The experiments due to Budakian and Putterman [220] showed that when two macroscopic metal surfaces are brought into a direct (dry) contact (the authors studied Au–Au and Au–Pt pairs), a nanometer size junction spontaneously forms over a long time scale. The initial Angström-sized radius grows by a factor of 50 in $\sim$1 min. The parameters of junction rupture match the observed dynamics of stick–slip friction, which suggests that stick–slip friction has its origins in the formation and rupture of junctions that form between metal surfaces in contact. This process evidently should result in a wear of the surfaces. However, MD simulations of "dry" friction of a Cu tip over the Cu(111) crystal surface due to Sørensen et al. [141] have shown no wear for sliding velocities up to 5 m/s. This fact may be explained, if we recall that (111) surfaces are the preferred slip planes in fcc metals. But when the tip-substrate structure corresponded to contact of two commensurate (100) surfaces, wear did occur, so that the moving tip left a trail of atoms in its wake. Of course, one of the most important roles of lubricants is to avoid or at least reduce the wear and surface damage.

A very important task is to *control frictional properties* in a desired way. Traditionally, such a control is achieved by chemical means, supplementing base lubricants by so-called friction modifier additives. Recently a detailed microscopic investigation of molecular mixtures was begun with the same accuracy as pure (one-component) lubricants. As an example, we may mention the recent SFA rheological study of a complex system with well defined and controlled friction modifier additives by Zhu et al. [223]. An example of theoretical study of mixed monolayers can be found in Ref. [224]. An idea of the theoretical approach is to play with the concentration of additives and their interaction with the bare lubricant molecules in order to achieve an incommensurate structure, thus lowering the static friction and the stick–slip regime.

The role of chemical additives may be even more involved and active, when the extreme conditions at the contact area (huge local pressure and high temperature) stimulate an irreversible chemical reaction, as was demonstrated recently by Mosey et al. [225]. Using ab initio Car-Parrinello MD technique (a classical MD is not appropriate in this case), the authors showed that at the pressure $P \geq 17$ GPa the zinc phosphate additives $(Zn[S_2P(OR)_2]_2$, where R is an alkyl group) undergo a chemical transformation and form a cross-linked network of zinc phosphate chains. The resulting film covers the asperities, protecting them from wearing and providing smooth sliding. These results also explain why zinc phosphates are effective for protecting steel surfaces and not aluminium ones: the yield threshold of steel is $P \approx 21$ GPa, while it is only ≈ 7 GPa for Al alloys.

Another way to control and manipulate friction is by mechanical means, e.g., by applying small perturbations to accessible elements of the system. The experimental SFA investigation by Heuberger et al. [226] showed that friction in a lubricated junction at low driving velocity ($\sim 10^{-7}$ m/s) can be strongly reduced by small amplitude (of order $\lesssim 1$ Å) normal oscillations of the sliding substrate with frequency $\sim 10^3$ Hz. At low loads (<5 mN) the friction coefficient changed from $\mu = 0.48$ (without oscillations) down to $\mu < 0.01$; for higher loads the effect is smaller, but still essential. The experimental investigation of the effect of tapping on friction between slider and disk in a hard-disk drive with the help of the AFM technique at high sliding velocity (0.6 m/s) was also done by Su et al. [227]. It was found that the tapping can reduce friction, especially when the surface is smooth and the load is light. The observed effect, however, was rather small, the friction may be reduced only by a factor of two or less. A strong reduction of friction (by more than one order of magnitude) due to small amplitude normal oscillations was found in GCMD simulation by Gao et al. [228] where, however, the sliding and oscillating velocities were of order $\gtrsim 1$ m/s as is typical for MD simulations. Different theoretical methods to control friction by mechanical methods, based on simplified FK-like models, were also proposed by Rozman et al. [229], Zaloj et al. [64], and Braiman et al. [230]. In particular, recently Tshiprut et al. [231] have demonstrated that *lateral* vibrations of a substrate with a frequency $\gtrsim 10^5$ Hz and amplitude of the order of the lattice constant can dramatically reduce the friction due to abrupt dilatancy transition (the increase of the separation between sliding surfaces).

Throughout this review paper we had in mind mainly the problem of minimization of friction coefficients. But, as we have mentioned already in the Introduction, the question of how to maximize the friction is also very important in some situations. This question is especially important for the friction between the road and the tyres, and it is typically connected with the *rubber friction*. However, the mechanisms of the rubber friction are essentially different from those discussed in the present paper, because of the very low elastic modulus of rubber and its high internal friction. The rubber friction is first of all determined by the internal friction [221], so that it is mainly a bulk property of the rubber [222] rather than connected with the processes at the interface.

Thus, friction is a complex multidisciplinary problem. Therefore, an essential progress can be achieved only by the concerted approach of scientists from mechanics, material science, physics, chemistry, computer modelling, etc. Moreover, from a theoretical side, the friction is a multiscale problem, e.g., it incorporates time scales from picoseconds (for elementary atomic jumps) to seconds and hours (in junction aging) or even centuries (in earthquakes), so that friction cannot be explained by one "general" model. And any theoretical approach must be strongly based on and supported by experiments. However, as we already noted at the beginning of Section 2, the serious problem of many experiments such as those with the SFA technique, is that they measure a single characteristic only, the time dependence of the spring force. In the result, the attempts to extract detailed information about the frictional mechanisms are often essentially speculative. Of course, it is not simple to study in detail the structure and dynamics of the interface which is closed from both sides by the solid macroscopic substrates, so great experimental artistry is needed here. But this is the necessary step to achieve further progress, and we would like to mention in this context a few experimental works.

When the substrates are transparent, the sliding interface can be studied by optical methods. In a recent work due to Rubinstein et al. [232], the experimental system was designed to allow light to pass through the interface only at actual points of contact, while at all other points the incident light undergoes total internal reflection at the interface. This allows real-time visualization of the net contact and study of the onset of frictional slip. The experiments showed that the onset of sliding is governed by three different types of coherent crack-like fronts. Two of these fronts propagate at subsonic and intersonic velocities, while the third type of front, which propagates an order of magnitude slower, is the dominant mechanism for the rupture of the interface: no overall motion of the blocks occurs until the slower front traverses the entire interface.

The technique developed in Granick's group [166,233] was already mentioned in Section 5.2, where we discussed the melting of the confined film. This technique is based on the fluorescence correlation spectroscopy and allows measuring the diffusivity of molecules in the lubricant within the SFA. The idea is to measure the fluctuations of the fluorescence intensity at a submicron-size spot of a laser beam. In turn, the intensity of fluorescence is directly coupled with the atomic concentration at the small area of the spot. This allows one to find the rate of diffusion of atoms into and out of this area. Note that measuring of the autocorrelation function is a well-known technique in diffusion studies in surface physics (see Section 3), where the fluctuations of the electron current are measured.

Another original technique was developed by Budakian and Putterman [193]. It may be applied to a metal–insulator interface, where the isolator must have surface electronic states (e.g., the authors used a gold ball of 1 mm in diameter sliding over polymethylmethacrylate or quartz). The main idea is that when the metal comes in direct contact with the insulator (i.e., at asperities), the surface states of the insulator at the contact area are discharged (the electrons from the donor surface states move into the metal) leaving the contact area positively charged. These places can be then imaged using the liquid crystal apparatus. It was found that the static frictional force (i.e., the maximum force during stick in the stick–slip regime) is directly proportional to the charge transfer. Thus, the charge transfer is a marker for the number of bonds ruptured at a particular slip event. The important result of this experiment is that in the "smooth sliding" regime (for the velocity 5 μm/s for the gold/quartz pair), when the frictional force is approximately constant, the charge transfer grows linearly with distance with the same proportionality coefficient as for the stick–slip regime. This indicates that the "smooth sliding" corresponds in fact to uncorrelated small-amplitude stick–slip events, which simply are not resolved at SFA experiments, in agreement with the earthquakelike model of Section 6.2.

As has been noted above, one of the main difficulties of tribological experiments is that the contact region is hardly accessible to a direct study, because it is "closed" by two solids. In this context we would like to mention also a recently developed "levitation" experimental setup (Kulik et al. [121]). In this case a slider "levitates" in a magnetic field over the surface and can be easily removed, so that the surface and the lubrication film can be tested before as well as just after the sliding, e.g., with the help of STM technique.

To conclude, the understanding the atomic processes occurring at the interface of two interacting materials in relative motion is central to a number of pure and applied scientific areas as well as to many technological problems, such as friction, adhesion, contact formation, wear, fracture, lubrication, etc. Presently, the tribology is shifting from empirical material science to rigorous physical science. Therefore, we may expect soon many new interesting discoveries in this old problem which has entered its renaissance.

Acknowledgements

References

[1] B.N.J. Persson, Sliding Friction: Physical Principles and Applications, Springer-Verlag, Berlin, 1998.
[2] B.N.J. Persson, Surf. Sci. Rep. 33 (1999) 83.
[3] F.P. Bowden, D. Tabor, Friction and Lubrication of Solids, Clarendon, Oxford, 1950.
[4] B. Bhusham, J.N. Israelachvili, U. Landman, Nature 374 (1995) 607.
[5] C.M. Mate, Atomic scale friction, in: B. Bhushan (Ed.), Handbook of Micro/Nano Tribology, CRC Press, Boca Raton, 1995, p. 167.
[6] S.B. Sinnott, Theory of atomic-scale friction, in: H.S. Nalwa (Ed.), in: Handbook of Nanostructured Materials and Nanotechnology, vol. 2, Academic, 1999 (Chapter 12).
[7] M.O. Robbins, Jamming, friction and unsteady rheology, in: A.J. Liu, S.R. Nagel (Eds.), Jamming and Rheology: Constrained Dynamics on Microscopic and Macroscopic Scales, Taylor and Francis, London, 2000.
[8] M.O. Robbins, M.H. Müser, Computer simulation of friction, lubrication and wear, in: B. Bhushan (Ed.), Handbook of Modern Tribology, CRC Press, Boca Raton, 2000.
[9] G.V. Dedkov, Physics – Uspekhi 43 (2000) 585.
[10] M.H. Müser, M. Urbakh, M.O. Robbins, Adv. Chem. Phys. 126 (2003) 187.
[11] C. Zhang, Tribol. Int. 38 (2005) 443.
[12] J. Krim, Physics World (February) (2005) 31.
[13] R. Bennewitz, Materials Today (May) (2005) 42.
[14] E. Rabinowicz, Friction and Wear of Materials, Wiley, New York, 1965.
[15] F. Heslot, T. Baumberger, B. Perrin, B. Caroli, C. Caroli, Phys. Rev. E 49 (1994) 4973.
[16] J.N. Israelachvili, D. Tabor, Wear 24 (1973) 386.
[17] J.N. Israelachvili, P.M. McGuiggan, A.M. Homola, Science 240 (1988) 189.
[18] M.L. Gee, P.M. McGuiggan, J.N. Israelachvili, A.M. Homola, J. Chem. Phys. 93 (1990) 1895.
[19] J. Van Alsten, S. Granick, Phys. Rev. Lett. 61 (1988) 2570.
[20] J. Peachey, J. Van Alsten, S. Granick, Rev. Sci. Instrum. 62 (1991) 463.
[21] S. Granick, Science 253 (1991) 1374.
[22] A. Widom, J. Krim, Phys. Rev. B 34 (1986) R3.
[23] J. Krim, A. Widom, Phys. Rev. B 38 (1988) 12184.

[24] J. Krim, Sci. Am. 275 (1996) 74;   Langmuir 12 (1996) 4564.
[25] G. Binnig, H. Rohrer, C. Gerber, E. Weibel, Phys. Rev. Lett. 49 (1982) 57.
[26] G. Binnig, C.F. Quate, C. Gerber, Phys. Rev. Lett. 56 (1986) 930.
[27] C.M. Mate, G.M. McClelland, R. Erlandsson, S. Chang, Phys. Rev. Lett. 59 (1987) 1942.
[28] R.W. Carpick, D.F. Ogletree, M. Salmeron, Appl. Phys. Lett. 70 (1997) 1548.
[29] M.A. Lantz, S.J. O'Shea, M.E. Welland, K.L. Johnson, Phys. Rev. B 55 (1997) 10776.
[30] E. Riedo, E. Gnecco, R. Bennewitz, E. Meyer, H. Brune, Phys. Rev. Lett. 91 (2003) 84502.
[31] B.N.J. Persson, Phys. Rev. B 51 (1995) 13568.
[32] B.N.J. Persson, O. Albohr, F. Mancosu, V. Peveri, V.N. Samoilov, I.M. Sivebaek, Wear 254 (2003) 835.
[33] F.F. Abraham, J. Chem. Phys. 68 (1978) 3713.
[34] S. Toxvaerd, J. Chem. Phys. 74 (1981) 1998.
[35] R.G. Horn, J.N. Israelachvili, J. Chem. Phys. 75 (1981) 1400.
[36] M. Plischke, D. Henderson, J. Chem. Phys. 84 (1986) 2846.
[37] M. Schoen, C.L. Rhykerd, D.J. Diestler, J.H. Cusman, J. Chem. Phys. 87 (1987) 5464.
[38] M. Schoen, J.H. Cusman, D.J. Diestler, C.L. Rhykerd, J. Chem. Phys. 88 (1988) 1394.
[39] M. Schoen, C.L. Rhykerd, D.J. Diestler, J.H. Cusman, Science 245 (1989) 1223.
[40] J. Gao, W.D. Luedtke, U. Landman, J. Chem. Phys. 106 (1997) 4309.
[41] J. Gao, W.D. Luedtke, U. Landman, J. Phys. Chem. B 101 (1997) 4013.
[42] J. Gao, W.D. Luedtke, U. Landman, Phys. Rev. Lett. 79 (1997) 705.
[43] P.A. Thompson, G.S. Grest, M.O. Robbins, Phys. Rev. Lett. 68 (1992) 3448.
[44] P.A. Thompson, M.O. Robbins, G.S. Grest, Israel J. Chem. 35 (1995) 93.
[45] A. Volmer, T. Natterman, Z. Phys. B 104 (1997) 363.
[46] J.A. Greenwood, J.B.P. Williamson, Proc. Roy. Soc. A 295 (1966) 300.
[47] T. Baumberger, F. Heslot, B. Perrin, Nature (London) 367 (1994) 544.
[48] T. Baumberger, C. Caroli, B. Perrin, O. Ronsin, Phys. Rev. E 51 (1995) 4005.
[49] B.N.J. Persson, Phys. Rev. B 55 (1997) 8004.
[50] I.S. Aranson, L.S. Tsimring, V.M. Vinokur, Phys. Rev. B 65 (2002) 125402.
[51] A. Lemaitre, J. Carlson, Phys. Rev. E 69 (2004) 61611.
[52] L. Prandtl, Z. Angew. Math. Mech. 8 (1928) 85.
[53] G.A. Tomlinson, Phil. Mag. 7 (1929) 905.
[54] Ya. Frenkel, T. Kontorova, Phys. Z. Sowietunion 13 (1938) 1.
[55] T.A. Kontorova, Ya.I. Frenkel, Zh. Eksp. Teor. Fiz. 8 (1938) 89.
[56] H. Risken, The Fokker–Planck Equation, Springer, Berlin, 1984 (Chapter 11).
[57] B.N.J. Persson, Phys. Rev. B 50 (1994) 4771.
[58] O.K. Dudko, A.E. Filippov, J. Klafter, M. Urbakh, Chem. Phys. Lett. 352 (2002) 499.
[59] A. Vanossi, J. Röder, A.R. Bishop, V. Bortolani, Phys. Rev. E 63 (2000) 017203.
[60] D. Cule, T. Hwa, Phys. Rev. Lett. 77 (1996) 278.
[61] D. Cule, T. Hwa, Phys. Rev. B 57 (1998) 8235.
[62] M.G. Rozman, M. Urbakh, J. Klafter, Phys. Rev. Lett. 77 (1996) 683.
[63] M.G. Rozman, M. Urbakh, J. Klafter, Phys. Rev. E 54 (1996) 6485.
[64] V. Zaloj, M. Urbakh, J. Klafter, Phys. Rev. Lett. 82 (1999) 4823.
[65] M.H. Müser, Phys. Rev. Lett. 89 (2002) 224301.
[66] T. Strunz, F.-J. Elmer, Phys. Rev. E 58 (1998) 1601, 1612.
[67] M. Weiss, F.-J. Elmer, Phys. Rev. B 53 (1996) 7539.
[68] M. Weiss, F.-J. Elmer, Z. Phys. B 104 (1997) 55.
[69] J. Röder, J.E. Hammerberg, B.L. Holian, A.R. Bishop, Phys. Rev. B 57 (1998) 2759.
[70] M.G. Rozman, M. Urbakh, J. Klafter, Europhys. Lett. 39 (1997) 183.
[71] M.G. Rozman, M. Urbakh, J. Klafter, F.-J. Elmer, J. Phys. Chem. B 102 (1998) 7924.
[72] A.E. Filippov, J. Klafter, M. Urbakh, J. Chem. Phys. 116 (2002) 6871.
[73] O.M. Braun, A. Vanossi, E. Tosatti, Phys. Rev. Lett. 95 (2005) 026102.
[74] T. Gyalog, M. Bammerlin, R. Lüthi, E. Meyer, H. Thomas, Europhys. Lett. 31 (1995) 269.

[75] O.M. Braun, Yu.S. Kivshar, The Frenkel–Kontorova Model: Concepts, Methods, and Applications, Springer-Verlag, Berlin, 2004.

[76] O.M. Braun, Yu.S. Kivshar, Phys. Rep. 306 (1998) 1.

[77] B.N.J. Persson, Phys. Rev. Lett. 71 (1993) 1212.

[78] B.N.J. Persson, Phys. Rev. B 48 (1993) 18140.

[79] B.N.J. Persson, J. Chem. Phys. 103 (1995) 3849.

[80] J.E. Hammerberg, B.L. Holian, J. Röder, A.R. Bishop, S.J. Zhou, Physica D 123 (1998) 330.

[81] R.P. Mikulla, J.E. Hammerberg, P.S. Lomdahl, B.L. Holian, Mat. Res. Soc. Symp. Proc. 522 (1998) 385.

[82] I.F. Lyuksyutov, A.G. Naumovets, V. Pokrovsky, Two-Dimensional Crystals, Academic Press, Boston, 1992.

[83] B.N.J. Persson, Surf. Sci. Rep. 15 (1992) 1.

[84] M. Scheffler, C. Stampfl, in: K. Horn, M. Scheffler (Eds.), Handbook of Surface Science, vol. 2, Elsevier, Amsterdam, 2000, p. 285.

[85] O.M. Braun, V.K. Medvedev, Usp. Fiz. Nauk 157 (1989) 631; Sov. Phys. Usp. 32 (1989) 328.

[86] T.L. Einstein, in: W.N. Unertl (Ed.), Handbook of Surface Science, Elsevier, Amsterdam, 1996, p. 577.

[87] V.A. Shchukin, D. Bimberg, Rev. Modern Phys. 71 (1999) 1125.

[88] L.A. Bolshov, Sov. Phys. Sol. State 13 (1971) 1404.

[89] J. Neugebauer, M. Scheffler, Phys. Rev. Lett. 71 (1993) 577.

[90] A.G. Naumovets, in: D.A. King, D.P. Woodruff (Eds.), The Chemical Physics of Solid Surface, vol. 7, Elsevier, Amsterdam, 1994, p. 163.

[91] R.D. Diehl, R. McGrath, Surf. Sci. Rep. 23 (1996) 43.

[92] O.M. Braun, A.I. Volokitin, V.P. Zhdanov, Usp. Fiz. Nauk 158 (1989) 421; Sov. Phys. Usp. 32 (1989) 605.

[93] O.M. Braun, Surface Sci. 213 (1989) 336.

[94] O.M. Braun, R. Ferrando, Phys. Rev. E 65 (2002) 061107.

[95] J. Philibert, Atom Movements. Diffusion and Mass Transport in Solids, Les Editions de Physique, Les Ulis, 1991.

[96] M. Bowker, D.A. King, Surf. Sci. 71 (1978) 583; Surf. Sci. 72 (1978) 208.

[97] P. Atkins, Physical Chemistry, 6th edition, Oxford University Press, Oxford, 1998, p. 830.

[98] A.G. Naumovets, Yu.S. Vedula, Surf. Sci. Rep. 4 (1985) 365.

[99] M. Zinke-Allmang, L.C. Feldman, M.H. Grabow, Surf. Sci. Rep. 16 (1992) 377.

[100] M. Zinke-Allmang, Thin Solid Films 346 (1999) 1.

[101] G. Kellogg, Surf. Sci. Rep. 21 (1994) 1.

[102] R. Gomer, Rep. Prog. Phys. 53 (1990) 917.

[103] H. Brune, Surf. Sci. Rep. 31 (1998) 121.

[104] T. Ala-Nissila, R. Ferrando, S.C. Ying, Adv. Phys. 51 (2002) 949.

[105] A.G. Naumovets, Z. Zhang, Surf. Sci. 500 (2002) 414.

[106] A.T. Loburets, N.B. Senenko, A.G. Naumovets, Yu.S. Vedula, in: M. Kotrla, N.I. Papanicolau, D.D. Vvedensky, L.T. Wille (Eds.), Atomistic Aspects of Epitaxial Growth, Kluwer, Dordrecht, 2002, p. 1.

[107] A.G. Naumovets, Physica A 357 (2005) 189.

[108] V.N. Shrednik, G.A. Odisharia, Sov. Phys. Sol. State 11 (1970) 1487.

[109] T. Masuda, C.J. Barnes, P. Hu, D.A. King, Surf. Sci. 276 (1992) 122.

[110] B.V. Andryushechkin, K.N. Eltsov, V.M. Shevlyuga, Surf. Sci. 472 (2001) 80.

[111] I.F. Lyuksyutov, A.G. Naumovets, Yu.S. Vedula, in: S.E. Trullinger, V.E. Zakharov, V.L. Pokrovsky (Eds.), Solitons, Elsevier, Amsterdam, 1986, p. 607.

[112] A.T. Loburets, A.G. Naumovets, Yu.S. Vedula, in: M.C. Tringides (Ed.), Surface Diffusion. Atomistic and Collective Processes, Plenum, New York, 1997, p. 509.

[113] A.G. Naumovets, M.V. Paliy, Yu.S. Vedula, in: M. Michailov, I. Gutzov (Eds.), Thin Films and Phase Transitions on Surfaces, Institute of Physical Chemistry, Bulgarian Acad. Sci., Sofia, 1994, p. 177.

[114] Yu.S. Vedula, A.T. Loburets, A.G. Naumovets, Sov. Phys. JETP 50 (1979) 391.

[115] R. Gomer, Field Emission and Field Ionization, Harvard University Press, 1961 (Chapter 4).

[116] A.T. Loburets, A.G. Naumovets, Yu.S. Vedula, Surf. Sci. 120 (1982) 347.

[117] R.D. Tilton, in: M. Malmsten (Ed.), Biopolymers at Interfaces, M. Dekker, New York, 1998, p. 363.

[118] J. Weckesser, J.V. Barth, K. Kern, J. Chem. Phys. 110 (1999) 5351.

[119] V.P. Zhdanov, B. Kasemo, Proteins Struct. Funct. Genetics 39 (2000) 76.

[120] J. De Coninck, N. Fraysse, M.P. Valignat, A.M. Cazabat, Langmuir 9 (1993) 1906.
[121] V.S. Kulik, A.A. Marchenko, A.G. Naumovets, J. Cousty, in: V.E. Gaponenko, V.S. Gurin (Eds.), Physics, Chemistry and Application of Nanostructures, World Scientific, Singapore, 2005, p. 74.
[122] O. Marchenko, J. Cousty, Phys. Rev. Lett. 84 (2000) 5363.
[123] H. Yasunaga, A. Natori, Surf. Sci. Rep. 15 (1992) 205.
[124] Y.N. Yang, E.S. Fu, E.D. Williams, Surf. Sci. 356 (1996) 101.
[125] A.V. Latyshev, S.S. Kosolobov, D.A. Nasimov, V.N. Savenko, A.L. Aseev, in: M. Kotrla, N.I. Papanicolau, D.D. Vvedensky, L.T. Wille (Eds.), Atomistic Aspects of Epitaxial Growth, Kluwer, Dordrecht, 2002, p. 281.
[126] H. Emmerich, C. Misbah, K. Kassner, T. Ihle, J. Phys.: Condens. Matter 11 (1999) 9985.
[127] A.T. Loburets, N.B. Senenko, Yu.S. Vedula, A.G. Naumovets, in: M.C. Tringides, Z. Chvoj (Eds.), Collective Diffusion on Surfaces: Correlation Effects and Adatom Interactions, Kluwer, Dordrecht, 2001, p. 97.
[128] G. He, M.H. Müser, M.O. Robbins, Science 284 (1999) 1650.
[129] M.H. Müser, L. Wenning, M.O. Robbins, Phys. Rev. Lett. 86 (2001) 1295.
[130] G. He, M.O. Robbins, Tribology Letters 10 (2001) 7.
[131] G. He, M.O. Robbins, Phys. Rev. B 64 (2001) 35413.
[132] M. Hirano, K. Shinjo, Phys. Rev. B 41 (1990) 11837.
[133] M.H. Müser, M.O. Robbins, Phys. Rev. B 61 (2000) 2335.
[134] F. Lancon, Europhys. Lett. 57 (2002) 74.
[135] M. Hirano, K. Shinjo, Wear 168 (1993) 121.
[136] M.O. Robbins, E.D. Smith, Langmuir 12 (1996) 4543.
[137] T. Gyalog, H. Thomas, Europhys. Lett. 37 (1997) 195.
[138] M. Hirano, K. Shinjo, R. Kaneko, Y. Murata, Phys. Rev. Lett. 78 (1997) 1448.
[139] M. Dienwiebel, G.S. Verhoeven, N. Pradeep, J.W.M. Frenken, J.A. Heimberg, H.W. Zandbergen, Phys. Rev. Lett. 92 (2004) 126101.
[140] Y. Qi, Y.-T. Cheng, T. Cagin, W.A. Goddard III, Phys. Rev. B 66 (2002) 085420.
[141] M.R. Sørensen, K.W. Jacobsen, P. Stoltze, Phys. Rev. B 53 (1996) 2101.
[142] J.B. Sokoloff, Phys. Rev. Lett. 86 (2001) 3312.
[143] J.B. Sokoloff, Phys. Rev. B 65 (2002) 115415.
[144] A.I. Larkin, Yu.N. Ovchinikov, J. Low Temp. Phys. 34 (1979) 409.
[145] B.N.J. Persson, E. Tosatti, Solid State Commun. 109 (1999) 739.
[146] C. Caroli, P. Nozieres, Eur. Phys. J. B 4 (1998) 233.
[147] J.B. Sokoloff, Phys. Rev. E 71 (2005) 056107.
[148] M.H. Müser, Tribol. Lett. 10 (2001) 15.
[149] J.E. Curry, F. Zhang, J.H. Cushman, M. Schoen, D.J. Diestler, J. Chem. Phys. 101 (1994) 10824.
[150] C. Daly, J. Zhang, J.B. Sokoloff, Phys. Rev. E 68 (2003) 66118.
[151] P.A. Thompson, M.O. Robbins, Science 250 (1990) 792.
[152] M.O. Robbins, P.A. Thompson, Science 253 (1991) 916.
[153] M.J. Stevens, M.O. Robbins, Phys. Rev. E 48 (1993) 3778.
[154] M. Cieplak, E.D. Smith, M.O. Robbins, Science 265 (1994) 1209.
[155] E.D. Smith, M.O. Robbins, M. Cieplak, Phys. Rev. B 54 (1996) 8252.
[156] A. Baljon, M.O. Robbins, MRS Bull. 22 (1997) 22.
[157] O.M. Braun, M. Peyrard, Phys. Rev. E 63 (2001) 46110.
[158] B.N.J. Persson, P. Ballone, J. Chem. Phys. 112 (2000) 9524.
[159] C.W. Gardiner, Handbook of Stochastic Methods, Springer-Verlag, Berlin, 1983.
[160] J. Klein, E. Kumacheva, Science 269 (1995) 816.
[161] J. Klein, E. Kumacheva, J. Chem. Phys. 108 (1998) 6996.
[162] E. Kumacheva, J. Klein, J. Chem. Phys. 108 (1998) 7010.
[163] A. Weinstein, S.A. Safran, Europhys. Lett. 42 (1998) 61.
[164] A.V. Tkachenko, Y. Rabin, Solid State Commun. 103 (1997) 361.
[165] O.M. Braun, M. Peyrard, Phys. Rev. E 68 (2003) 11506.
[166] A. Mukhopadhyay, J. Zhao, S.C. Bae, S. Granick, Phys. Rev. Lett. 89 (2002) 136103.
[167] Ph. Valadon, RasTop: molecular visualization software, version 1.3.1, http://www.geneinfinity.org/rastop/.

[168] J. Tekic, O.M. Braun, B. Hu, Phys. Rev. E 71 (2005) 026104.
[169] W. Humphrey, A. Dalke, K. Schulten, J. Mol. Graphics 14 (1996) 33. http://www.ks.uiuc.edu/Research/vmd/.
[170] O.M. Braun, M. Paliy, S. Consta, Phys. Rev. Lett. 92 (2004) 256103.
[171] A. Jabbarzadeh, P. Harrowell, R.I. Tanner, Phys. Rev. Lett. 94 (2005) 126103.
[172] Y. Zhu, S. Granick, Langmuir 19 (2003) 8148.
[173] Y. Zhu, S. Granick, Phys. Rev. Lett. 93 (2004) 096101.
[174] U. Raviv, P. Laurat, J. Klein, Nature 413 (2001) 51.
[175] U. Raviv, J. Klein, Science 297 (2002) 1540.
[176] T. Becker, F. Mugele, Phys. Rev. Lett. 91 (2003) 166104.
[177] L.D. Landau, E.M. Lifshitz, Statistical Physics, Pergamon Press, Ltd., London, 1958.
[178] A.M. Kosevich, The Crystal Lattice: Phonons, Solitons, Dislocations, Wiley-VCH, Berlin, 1999 (Theory of Crystal Lattice, Vuscha schkola, Kharkov, 1988).
[179] O.M. Braun, M. Peyrard, V. Bortolani, A. Franchini, A. Vanossi, Phys. Rev. E 72 (2005) 056116.
[180] B. Luan, M.O. Robbins, Phys. Rev. Lett. 93 (2004) 036105.
[181] H. Yoshizawa, P. McGuiggan, J. Israelachvili, Science 259 (1993) 1305.
[182] O.M. Braun, J. Röder, Phys. Rev. Lett. 88 (2002) 96102.
[183] R. Burridge, L. Knopoff, Bull. Seismol. Soc. Am. 57 (1967) 341.
[184] Z. Olami, H.J.S. Feder, K. Christensen, Phys. Rev. Lett. 68 (1992) 1244.
[185] L.D. Landau, E.M. Lifshitz, Theory of Elasticity, Pergamon, Oxford, 1970.
[186] K.H. Lau, W. Kohn, Surf. Sci. 65 (1977) 607.
[187] P. Bak, C. Tang, K. Wiesenfeld, Phys. Rev. Lett. 59 (1987) 381.
[188] H. Flyvbjerg, K. Sneppen, P. Bak, Phys. Rev. Lett. 71 (1993) 4087.
[189] M. Paczuski, S. Maslov, P. Bak, Phys. Rev. E 53 (1996) 414.
[190] A. Tanguy, M. Gounelle, S. Roux, Phys. Rev. E 58 (1998) 1577.
[191] A.A. Middleton, C. Tang, Phys. Rev. Lett. 74 (1995) 742.
[192] H.-M. Bröker, P. Grassberger, Phys. Rev. E 56 (1997) 3944.
[193] R. Budakian, S.J. Putterman, Phys. Rev. Lett. 85 (2000) 1000.
[194] C. Caroli, P. Nozieres, in: B.N.J. Persson, E. Tosatti (Eds.), Physics of Sliding Friction, Kluwer, Dordrecht, 1966, p. 27.
[195] L. Bocquet, H.J. Jensen, J. Phys. I 7 (1997) 1603.
[196] H. Yoshizawa, J.N. Israelachvili, J. Phys. Chem. 97 (1993) 11300.
[197] A.R.C. Baljon, M.O. Robbins, Science 271 (1996) 482.
[198] J.H. Dietrich, B.D. Kilgore, Pure Appl. Geophys. 143 (1994) 283.
[199] B.N.J. Persson, Phys. Rev. B 61 (2000) 5949.
[200] L. Bocquet, E. Charlaix, S. Ciliberto, J. Crassous, Nature 396 (1998) 735.
[201] E. Riedo, F. Levy, H. Brune, Phys. Rev. Lett. 88 (2002) 185505.
[202] B.N.J. Persson, E. Tosatti, Phys. Rev. B 50 (1994) 5590.
[203] B.N.J. Persson, Chem. Phys. Lett. 324 (2000) 231.
[204] G.T. Gao, P.T. Mikulski, J.A. Harrison, J. Am. Chem. Soc. 124 (2002) 7202.
[205] G.T. Gao, P.T. Mikulski, G.M. Chateauneuf, J.A. Harrison, J. Phys. Chem. B 107 (2003) 11082.
[206] P.J. Blau, C.E. Haberlin, Thin Solid Films 219 (1992) 129.
[207] B. Bhushan, B.K. Gupta, G.W. Van Cleef, C. Capp, J.V. Coe, Appl. Phys. Lett. 62 (1993) 3253.
[208] T. Thundat, R.J. Warmack, D. Ding, R.N. Compton, Appl. Phys. Lett. 63 (1993) 891.
[209] U.D. Schwarz, W. Allers, Phys. Rev. B 52 (1995) 14976.
[210] C.M. Mate, Wear 168 (1993) 17.
[211] G. Luengo, S.E. Campbell, V.I. Srdanov, F. Wudl, J.N. Israelachvili, Chem. Mater. 9 (1997) 1166.
[212] S. Okita, M. Ishikawa, K. Miura, Surf. Sci. 442 (1999) L959.
[213] H. Nakagawa et al., Wear 238 (2000) 45.
[214] O.M. Braun, Phys. Rev. Lett. 95 (2005) 126104.
[215] K. Miura, S. Kamiya, N. Sasaki, Phys. Rev. Lett. 90 (2003) 55509.
[216] P.A. Heiney, J.E. Fischer, A.R. McGhie, W.J. Romanow, A.M. Denenstein, J.P. McCauley Jr., A.B. Smith, Phys. Rev. Lett. 66 (1991) 2911.
[217] R.D. Johnson et al., Science 255 (1992) 1235.

[218] W.I.F. David et al., Europhys. Lett. 18 (1992) 219.
[219] Q. Liang, O.K.C. Tsui, Y. Xu, H. Li, X. Xiao, Phys. Rev. Lett. 90 (2003) 146102.
[220] R. Budakian, S.J. Putterman, Phys. Rev. B 65 (2002) 235429.
[221] K.A. Grosch, Proc. R. Soc. A 274 (1963) 21.
[222] B.N.J. Persson, J. Chem. Phys. 115 (2001) 3840.
[223] Y. Zhu, H. Ohtani, M.L. Greenfield, M. Ruths, S. Granick, Tribol. Lett. 15 (2003) 127.
[224] O.K. Dudko, A.E. Filippov, J. Klafter, M. Urbakh, Tribol. Lett. 12 (2002) 217.
[225] N.J. Mosey, M.H. Müser, T.K. Woo, Science 307 (2005) 1612.
[226] M. Heuberger, C. Drummond, J. Israelachvili, J. Phys. Chem. B 102 (1998) 5038.
[227] L. Su, J. Xu, M. Kurita, K. Kato, K. Adachi, Tribol. Lett. 15 (2003) 91.
[228] J. Gao, W.D. Luedtke, U. Landman, J. Phys. Chem. B 102 (1998) 5033.
[229] M.G. Rozman, M. Urbakh, J. Klafter, Phys. Rev. E 57 (1998) 7340.
[230] Y. Braiman, J. Barhen, V. Protopopescu, Phys. Rev. Lett. 90 (2003) 94301.
[231] Z. Tshiprut, A.E. Filippov, M. Urbakh, Phys. Rev. Lett. 95 (2005) 016101.
[232] S.M. Rubinstein, G. Cohen, J. Fineberg, Nature 430 (2004) 1005.
[233] A. Mukhopadhyay, S.C. Bae, J. Zhao, S. Granick, Phys. Rev. Lett. 93 (2004) 236105.